The Gene *Tbx5* links Development, Evolution and Adaptation of the Sternum in Terrestrial Vertebrates

Sorrel Ruth Bryony Bickley

Division of Developmental Biology

MRC National Institute for Medical Research,

Mill Hill, London

UCL

Submitted in 2013 for the degree of Doctor of Philosophy

Declaration

I, Sorrel Bickley, confirm that the work presented in this thesis is my own and was performed in the laboratory of Dr. Malcolm Logan at the MRC National Institute for Medical Research. Where information or reagents have been derived from other sources, I confirm that this has been stated within this thesis. This work has been submitted in 2013 for the degree of Doctor of Philosophy.

Acknowledgements

There are many people who have helped me throughout my PhD project. First, I would like to thank my supervisor Malcolm Logan for giving me the opportunity to work on such an interesting project and for his guidance, support and patience. I am also grateful for the advice of my thesis committee.

I am indebted to Marella de Bruijn and Andrew Jarratt for sending me the *Runx1* probe template, and Peter Farlie for providing emu embryos. The staff of LLG and particularly Ania have provided enormous assistance with my mouse work.

A big thank you to all the past and present members of the lab: Ania, Fatima, Jutta, Laurianne, Mandy, Martin, Natalie, Peleg, Satoko, Sue and Vero. You all make this a brilliant place to work.

I would like to thank my family and my friends for their support. In particular, my mum, who always took enormous pride in my achievements. I never imagined she wouldn't be here to see me finish this.

Finally, a special than you to James for always encouraging me, and more importantly, for challenging me.

Abstract

The transition from fins to limbs during the colonisation of land was a key innovation in vertebrate evolution. Changes in the limb and shoulder girdle during this event have been investigated extensively, but little attention has been given to the acquisition of the sternum, a feature considered characteristic of virtually all terrestrial vertebrates, and which is mandatory for tetrapod locomotion.

The sternum is a thin flat bone lying at the ventral midline of the thorax that provides a crucial attachment site for the pectoral muscles, allowing the forelimbs to raise the body up from the ground. I demonstrate that a sternum completely fails to form in conditional *Tbx5* mutant mouse embryos. Consistent with this, sternum defects are a characteristic feature of Holt-Oram syndrome, which is caused by mutations in *TBX5*. While the role of *Tbx5* in the development of the heart and forelimbs has been studied extensively, *Tbx5* function in sternum formation is not understood. Using chick and mouse models systems, I set out to investigate the developmental origin of the sternum, and why it fails to form in the absence of *Tbx5*. Since the function of the sternum is to facilitate forelimb movement, I explored the correlation between forelimb use and sternum morphology by comparing sternum size across different avian species. I then investigated the genetic adaptations that could explain sternum and forelimb reduction in flightless birds, using the emu as a model. I suggest that *Tbx5* represents a common node in the molecular pathways regulating forelimb and sternum development.

Table of Contents

List of Figures

List of Tables

gyg

Chapter One:

Introduction

Chapter One: Introduction

1.1 Sternum Evolution

1.1.1 The Evolutionary Origin of the Sternum

The sternum is a thin flat bone lying at the ventral midline of the thorax. It forms direct connections on either side with the clavicles and the distal tips of the ribs. In so doing it strengthens the ribcage and helps protect the internal organs such as the heart and lungs. However the primary function of the sternum is to provide an attachment site for the pectoral muscle (pectoralis major; Clack 2002). This muscle originates along the length of the sternum and clavicle, and inserts into the intertubular groove of the humerus (Romer *et al.* 1978). The pectoral muscle is found in all major groups of tetrapods, and generates the force used to pull the forelimbs forward and raise the body up from the ground (Abdala *et al.* 2010).

The sternum first arose in vertebrates during the colonisation of land. This was coincidental with the limbs undergoing a dramatic evolutionary change, as fins used for swimming were replaced with arms and legs used for walking on land (Clack 2005). During this transition multiple skeletal adaptations arose, such as the lengthening and thickening of the ribs, which is thought to aid lung ventilation and protect the internal organs (Janis *et al.* 2001). Tetrapod locomotion on land requires increased power for locomotion compared with aquatic life, and this power is in part generated by the pectoral muscle, which is anchored by the sternum.

Considerable attention has been focused on changes in the shape and positioning of the bones of the limb and shoulder girdle during the evolutionary transition from water to land. For example the humerus becomes lengthened and the humoral head becomes flatter, allowing for a greater attachment of the muscles that stabilise the shoulder joint (Shubin *et al.* 2006). However, little attention has been given to the acquisition and evolution of the sternum, despite this structure having a crucial role in tetrapod locomotion.

Sterna are generally poorly preserved in the fossil record due to their often cartilaginous nature and their becoming crushed and lost among the ribs and vertebrae upon compaction of the skeleton (Vickaryous *et al.* 2006). The early tetrapod *Ichthyostega* displays the earliest sternum observed in the fossil record, dating back to the late Devonian period (350-380 million years ago; Pierce *et al.* 2013). *Ichthyostega* had ears that resemble those of fish from the same period, and are thought to have functioned underwater, but also possessed well developed shoulders and forelimbs (Clack 2002). This species is purported to be a 'missing link' between aquatic and land dwelling species, and has been proposed to have moved around on land in a manner similar to that of a seal (Clack 2005). The sternum of *Ichthyostega* was ossified, rod-shaped and extended caudally from the clavicles, although it is unclear whether the ribs attached to it (Ahlberg *et al.* 2005). In summary, it appears that the sternum arose during early tetrapod evolution as an adaptation to terrestrial life.

1.1.2 Adaptations in Sternal Morphology across Tetrapods

The sternum is considered characteristic of virtually all extant terrestrial vertebrates, and is essential for tetrapod locomotion (Seno 1961). However, there is wide variation in sternal morphology exhibited across species using different modes of locomotion. Aquatic amphibians often do not possess an ossified sternum, although some species display a membranous or cartilaginous link between the clavicles. However, homology between this structure and the sternum has not been demonstrated (Gladstone *et al.* 1932). Land-dwelling amphibian species, such as anurans (frogs and toads) possess a shield-shaped condensation of cartilage between the clavicles that is thought to be homologous to the sternum (Havelkova *et al.* 2006). Within the reptiles, most members of the lacertilia (lizards) and crocodilia (crocodiles, alligators and caimans) form an elongated, cartilaginous sternum, which extends from the clavicles and forms attachments to multiple pairs of ribs. Unusually, in some crocodiles the caudal region of the sternum is split into two horns, although the evolutionary advantage of this is not clear (Gladstone *et al.* 1932). The length of the sternum and the number of ribs attaching to it varies greatly among reptiles, from zero attached ribs in the slow worm (*Anguis fragailis*) to nine attached ribs in the gharial crocodile (*Gavialis gangeticus*). The sternum has been completely lost in snakes, along with the limbs and the entire shoulder girdle (Gladstone *et al.* 1932). Turtles also do not possess sterna, and instead have ribs that are integrated into the highly specialised carapacial dermis (Gilbert *et al.* 2001).

In mammals the sternum is generally long and thin and is divided into three regions (Figure 1). Situated most rostrally in the thorax is the manubrium (or sternal head),

which is attached to the clavicles (Romer *et al.* 1978). Further caudal is the sternal body. This is a long thin element to which the pairs of ribs attach, and is often divided into segments known as sternebrae. A segmented sternum is formed when the regions of the sternum immediately adjacent to the ribs, known as the sterno-costal junctions, remain cartilaginous, while the regions in between the sterno-costal junctions ossify. Lying most caudally is the diamond-shaped xiphoid process, or xiphisternum, which remains cartilaginous in many species (Kardong 1998). In the mouse, seven pairs of ribs attach to the sternum, and four separate sternebrae make up the sternal body (Figure 1). However, in adult humans the sternebrae fuse completely during puberty to form one single ossified unit (McCormick *et al.* 1981). The length of the sternum and the number of pairs of ribs that attach to it can vary considerably across mammals, but the overall rod-like shape is conserved across the clade.

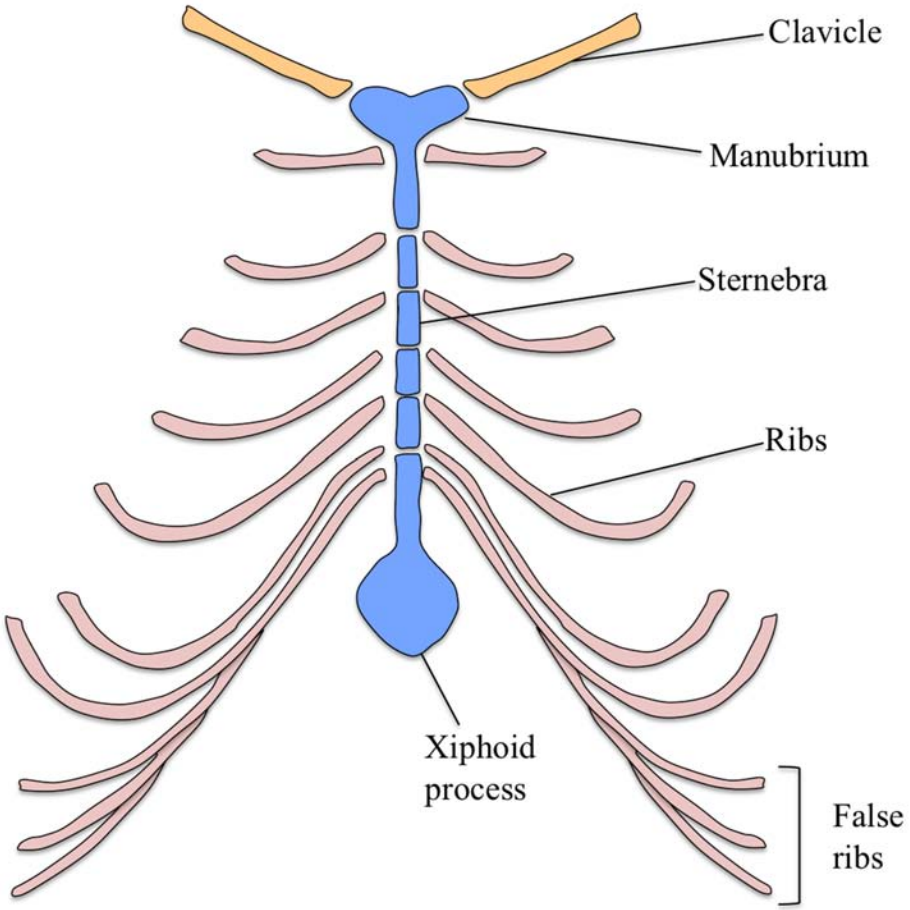

Figure 1. The adult mouse sternum.

Schematic showing the division of the sternum (blue) into the manubrium, sternebrae and xiphoid process, with the ribs (pink) and clavicles (orange) attaching on either side.

1.1.3 Sternum Adaptations in Avians

Perhaps the most dramatic sternum adaptation is exhibited in avians. Species in this clade possess highly adapted forelimbs (wings) that are able to lift the entire body into the air. Flight requires powerful musculature, and in birds the sternum possesses a ventral extension known as the keel, which extends outwards perpendicular to the plane of the ribs and provides an increased surface area for the attachment of these flight muscles (Figure 2). The earliest bird identified in the fossil record, *Archaeopteryx*, is thought not to have been capable of powered flight and did not possess a sternal keel (Ostrom 1970; Olson *et al.* 1979). However, fossil specimens of *Yixianornis garbaui,* a species from the early cretaceous period, display an ossified sternum with a well-projected keel (Clarke *et al.* 2006). This species represents a basal ornithurine (the clade that includes extant birds), and is thought to possess the wing and pectoral girdle adaptations required for powered flight. The sternal keel therefore appears to have arisen as an adaptation that accompanies powered flight in avians (Videler 2005).

Extant birds possess highly adapted flight muscles. The pectoral muscle drives the powerful wing down-stroke that lifts the bird into the air, and often makes up around one quarter of the total weight of the bird (King *et al.* 1975). Avians also possess a supracoracoideus muscle, which drives the wing upstroke (Figure 2A). The supracoracoideus is unique to birds and connects the sternum to the dorsal side of the humerus via a tendon that passes through a canal within the shoulder. This allows the wing to be raised through a pulley-like mechanism, an adaptation that is not seen in any other muscle (Poore *et al.* 1997; Baier *et al.* 2007). The avian furcula (or

wishbone) is a structure that is homologous to the clavicles, with the right and left side connected at the midline (Figure 2B). Often the furcula does not form any physical connection to the sternum, but in many species it fuses directly to the sternal keel (King *et al.* 1975; Kaiser 2007). An additional element known as the coracoid is present in all birds, linking the ventral side of the scapula to the sternum in order to provide additional support for flight (Figure 2B; Bellairs *et al.* 2005). Overall, the body of the sternum in avians is wider that that in mammals, often taking on a shield-like shape, and the sternum is not segmented at any stage of development (Fell 1939; Murillo-Ferrol 1963).

A number of avian species have evolved to become flightless. Flightlessness has arisen multiple times independently, driven by a variety of factors (McCall *et al.* 1998; Harshman *et al.* 2008). For example, flightless species are able to conserve energy through a reduced basal metabolic rate, partly due to forming a smaller pectoral muscle mass (McNab 1994). They also possess smaller, shorter wings than flying species (McCall *et al.* 1998), and it has been observed that they have a reduced sternum (Elzanowski 1988).

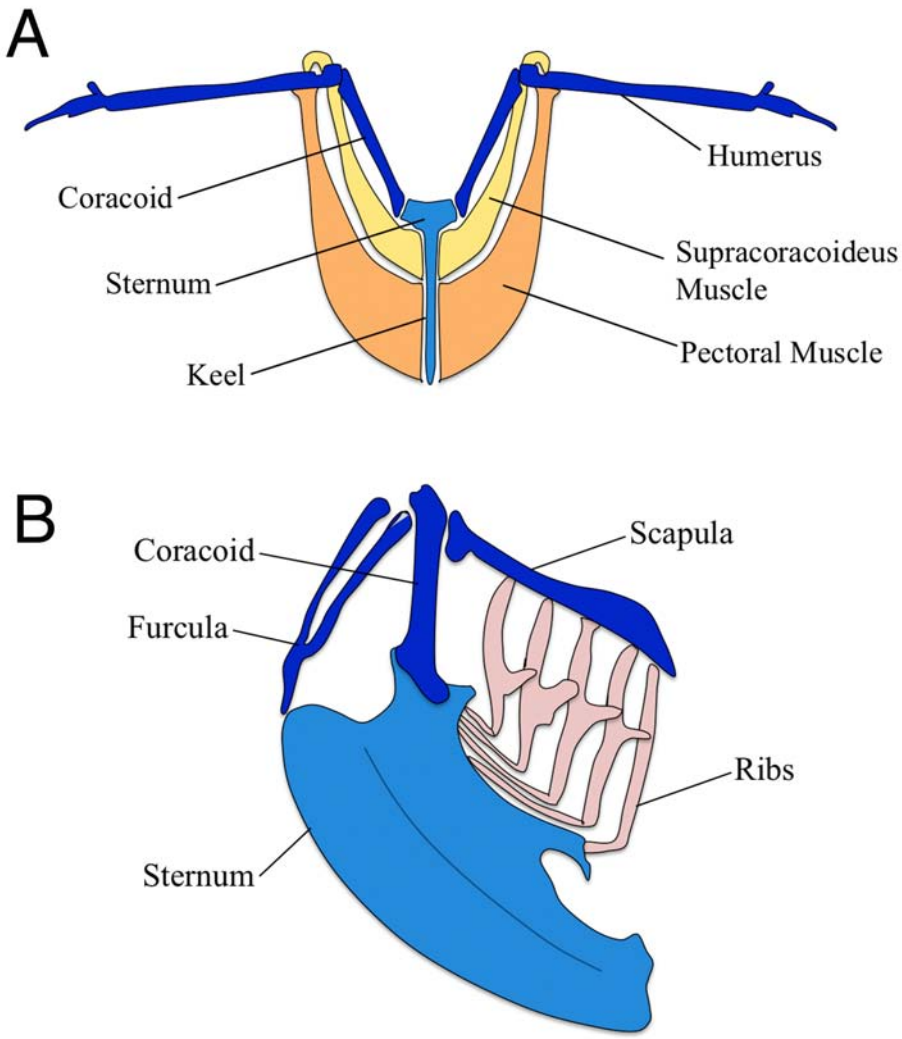

Figure 2. The avian thoracic skeleton and flight musculature.

A, Schematic diagram showing a transverse section through the sternum, illustrating the attachment of the pectoral (orange) and supracoracoideus (yellow) muscles to the sternal keel. **B**, Schematic representation of the avian ribcage from a ventro-lateral perspective, showing the sternum with a large ventral keel (light blue) and associated furcula, coracoid and scapula (dark blue). Five pairs of ribs (pink) attach to either side of the sternal body.

1.2 The Development of the Sternum

1.2.1 Condensation of the Sternal Bands and Sternal Fusion

Much of the work carried out to date on the elucidation of sternal development has been conducted in the mouse. The murine sternum is first visible at around 12 days post coitum (E12.0) as two mesenchymal condensations, or bands, in the ventro-lateral body wall (Chen 1952). These two bands lengthen in a caudal direction and move medially across the thorax towards one another. They begin to form cartilage and then fuse at the ventral midline in a rostral to caudal progression between E13.5 and E16.5 (Chen 1952; Kaufman 1992). While sternum fusion is taking place, the distal tips of the seven anterior-most pairs of ribs attach to either side of the sternum (Gladstone *et al.* 1932). Ossification begins at E16.5, and initiates from the centre of each sternal segment, spreading outwards (Kaufman 1992). The most rostral segment, the manubrium, is first to ossify, followed by the most rostral sternebra and progressing caudally with the xiphoid process ossifying last (Chen 1952).

The process of segmentation in the mammalian sternum is not fully understood. In humans the sternebrae fuse during puberty to form a single ossified element (Kardong 1998), but in most mammalian species the sterno-costal junctions remain cartilaginous. The sternal ends of the ribs often remain cartilaginous as well, which led to the proposal that the sternal ribs may inhibit hypertrophy of cartilage cells both within the ribs themselves and in the sternum (Bryson 1945). In support of this, when regions of the trunk were grown in culture with rib tissue removed, the sternum did not form segments and was ossified along its entire length (Chen 1953). Similarly, in a mutant mouse model in which *Hoxa10* is misexpressed throughout the entire

presomitic mesoderm, embryos completely fail to form ribs (Carapuco *et al.* 2005). These mice display a sternum that is ossified along its entire length and does not form segmented sternebrae. This suggests that the segmentation of the sternum is a secondary process, dependent on the attachment of the ribs.

Despite the differences in their morphology, avian and mammalian sterna have evolved from the same ancestral structure, and therefore the developmental mechanisms guiding sternum formation in these organisms are likely to be shared. In chickens, mesenchymal condensations of sternum precursor cells become visible from day 8 of incubation, or Hamburger-Hamilton (HH) stage 32 (Hamburger *et al.* 1951; Murillo-Ferrol 1963). These condensed bands begin to fuse from day 9 (HH 34) onwards. By day 10 (HH 36) fusion of the sternal bands is complete and the keel begins to form, although ossification does not begin until after hatching (Bellairs *et al.* 2005). Sternum development has also been studied in the budgerigar, revealing similar band-like condensations which move medially to form the sternum (Fell 1939). Ossification of the avian sternum does not initiate in multiple separate regions as observed in the mouse, but occurs gradually in a rostro-caudal progression along the sternal length. However, the rostral and caudal regions of the sternal keel remain cartilaginous in some avian species (Seno 1961). In chickens, five pairs of ribs attach to either side of the sternum, along with the coracoid process and furcula at the rostral most region (Figure 2).

1.2.2 The Embryological Origin of the Sternum

Relatively little is known about the early stages of sternum development, prior to the condensation of the sternum precursor cells to form bands. In contrast, the embryological origins of the other elements of the pectoral girdle have been well-characterised. The postcranial vertebrate skeleton is divided into axial and appendicular components that originate from two distinct mesodermal cell populations (Figure 3; Winslow *et al.* 2007). The axial skeleton comprises the vertebrae and rib cage and is derived from the somites, while the appendicular skeleton is made up of the limbs, pectoral girdle and pelvis and is derived from the lateral plate mesoderm (LPM) (Figure 3, Figure 4; Winslow *et al.* 2007). The LPM can be sub-divided into splanchnic and somatic domains. The somatic mesoderm underlies the ectoderm and goes on to form the appendicular skeleton, while the splanchnic mesoderm overlies the endoderm, and gives rise to the future gut wall (Figure 4B; Kardong 1998). The space between the two layers forms the body cavity, or coelom.

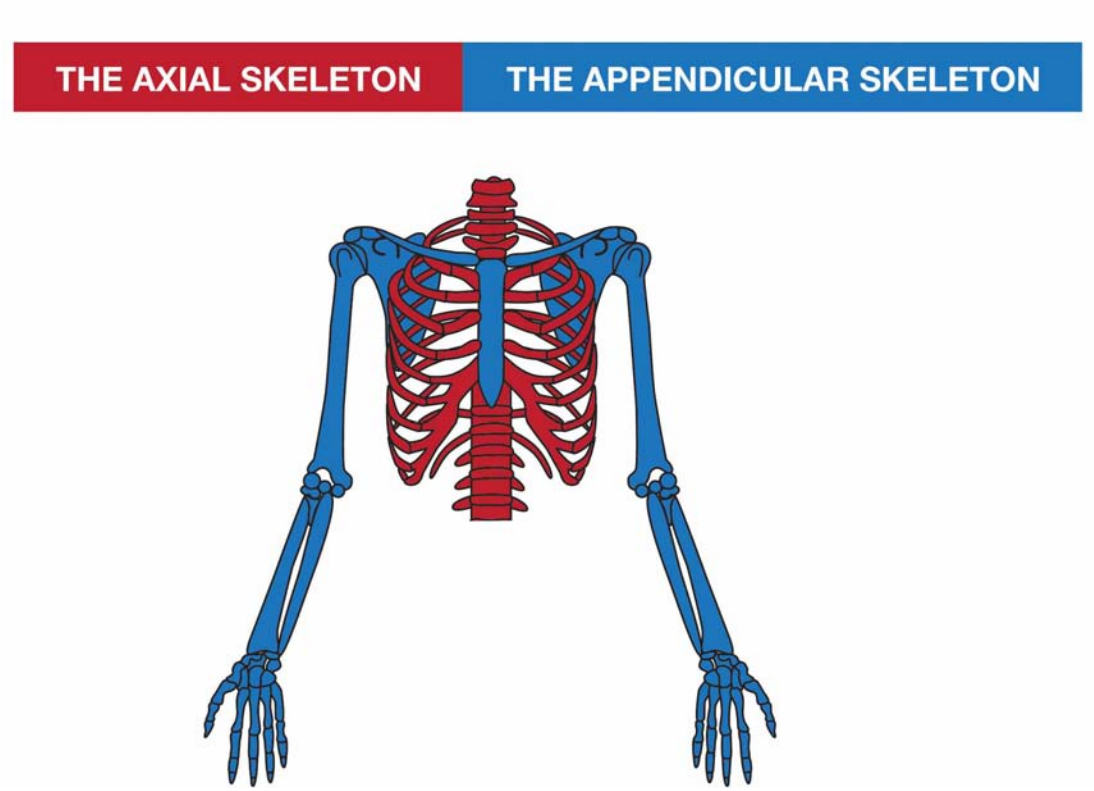

Figure 3. The postcranial skeleton is divided into axial and appendicular components.

The axial skeleton (red) is composed of the ribs and vertebrae and the appendicular skeleton (blue) is made up of the bones of the limbs and pectoral girdle, in addition to the sternum.

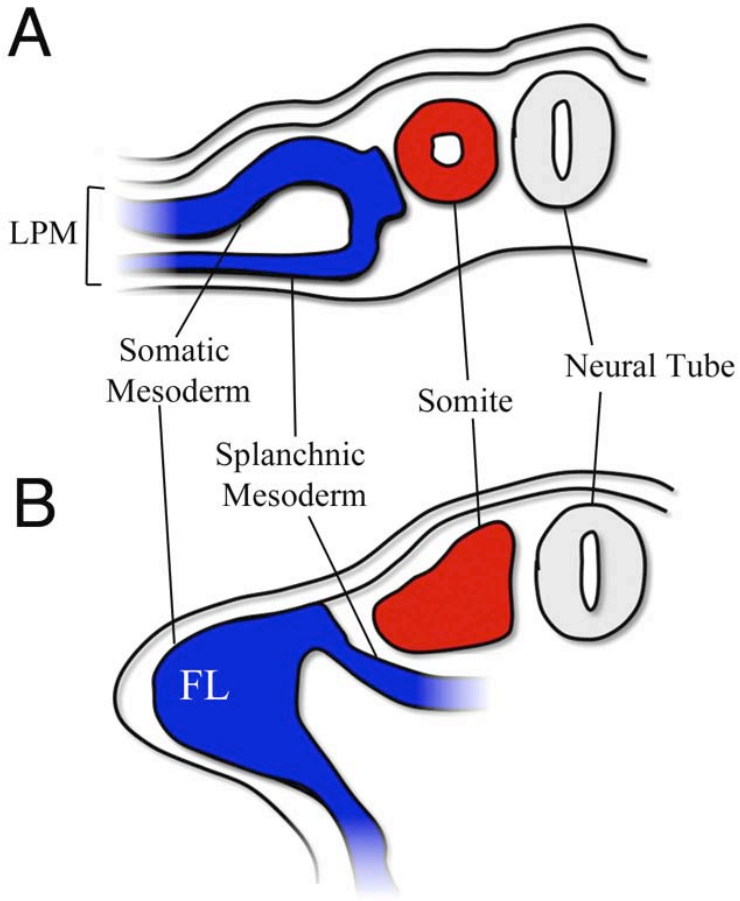

Figure 4. The somites and LPM are distinct embryological compartments.

Schematic representations of transverse sections through the trunk of chick embryos at the level of the forelimbs. **A,** At HH16 the LPM (blue) is subdivided into somatic and splanchnic mesoderm compartments that lie lateral to the somites (red) on either side of the neural tube (grey). **B,** At HH20 the splanchnic LPM domain is positioned ventro-medially, beneath the axial tissue, and a region of the somatic LPM cell population has proliferated to form the forelimb bud (FL) while the most lateral somatic LPM cells become positioned more ventrally and contribute to the ventral body wall.

Grafting experiments in the chick have demonstrated that the clavicle derives from the LPM (Chevallier *et al.* 1977; Hall 2001). In contrast, the scapula has been shown to have a dual embryonic origin, as grafting and lineage tracing experiments demonstrate that the majority of the cells forming the scapula derive from the LPM, while the medial border is instead derived from somitic cells (Huang *et al.* 2000; Valasek *et al.* 2010; Shearman *et al.* 2011). Similarly the pelvis, which braces the hindlimb to the sacral ribs, is also known to be LPM derived. In the chick the LPM region adjacent to somites 26-32 gives rise to the pelvic girdle (Chevallier *et al.* 1977), and in the mouse the chondrocytes making up the bones of the pelvis have also been demonstrated to be LPM derived. The sacral vertebrae however, are derived from the somites (Durland *et al.* 2008).

The ventro-medial position of the sternum within the skeleton and the connections it forms with the ribs (Figure 3) led early researchers to predict that the sternum was formed from the distal ends of the ribs fusing together and elongating (Ruge 1880). Patterson later put forward the idea that the pectoral girdle gives rise to the sternum, based on comparative studies of morphology across a range of species (Patterson 1900). This focused on the interclavicle element observed in amphibians, which connects the clavicles only and does not extend caudally. The theory suggested that the cells from the distal tips of the clavicles spread caudally down the midline to form the sternum. The discovery of a shortened sternum joining the clavicles at the mid-line of the perlon shark *Notidanus indicus* also added support to this theory (Parker 1891).

Considerable evidence has now amassed to suggest that the sternum is not formed from the cells of the ribs or clavicles. Chick-quail somite grafting experiments demonstrated that the sternum is not derived from the somites, unlike the ribs and pectoral muscle (Chevallier *et al.* 1977). A series of explant experiments using different regions of the LPM and somites were carried out in the budgerigar (Fell 1939), the mouse (Chen 1952) and the chick (Murillo-Ferrol 1963). These studies indicate that the presumptive sternal tissue may reside in the LPM, as LPM explants formed sternal band-like condensations, while somitic explants did not. These classical embryological experiments suggest that the sternum is a component of the appendicular skeleton, deriving from the LPM along with the pectoral girdle, scapula, pelvis and bones of the limbs (Figure 3). This would place the sternum in an intriguing situation, arising from a pool of progenitors common to the appendicular skeleton, but migrating medially and fusing with axial skeletal components that have a distinct developmental origin.

1.2.3 The Sternum as a Component of the Ventral Body Wall

When addressing the process of sternum formation, it is important to consider the sternal precursors in the context of a much larger population of cells. A number of different tissues make up the thoracic ventral body wall, including the ribs, sternum, connective tissue and a number of muscles including the pectoral and intercostal muscles. These tissues originate from distinct sources, but move en masse across the ventral thorax during body wall closure. The mechanisms driving body wall closure are unclear, and beyond evidence from a small number of papers, it is not known which tissues may be leading or driving this process.

Explant experiments using mouse trunk tissue have shown that the migration of the sternum precursor tissue is independent of the ribs (Chen 1953; Chevallier 1975). A mutant mouse in which *Hoxa10* is misexpressed throughout the entire presomitic mesoderm completely fails to form ribs (Carapuco *et al.* 2005). These mice are still able to form a sternum, which suggests that the ribs are not required for sternum formation. However, the sternum is ossified along its entire length, suggesting that the ribs play a role in sternum segmentation.

The pectoral muscle attaches to either side of the sternum following body wall closure, but the pectoral muscle precursors originate in the somites (Chen 1952; Chevallier *et al.* 1977). The development of the pectoral muscle has been shown to involve a complex 'in-out' migratory pathway in which the precursors migrate from the somites into the forelimb bud, and then out again into the ventral region of the thorax (Valasek *et al.* 2011). To the best of our knowledge, a mouse lacking pectoral muscle has not been generated, and therefore it is not possible to determine the role of the pectoral muscle in ventral body wall closure or in sternum formation.

1.2.4 Patterning Domains Within the Vertebrate Mesoderm

In addition to the division of the musculoskeletal system into somitic and lateral plate derived domains on the basis of embryonic origin, the dynamics of morphogenesis have led to the use of alternative terminology based on the environment of differentiation of the different tissues (Burke *et al.* 2003). Muscles

and bones that differentiate within an LPM derived connective tissue environment are placed within the abaxial patterning domain. In the thoracic region this domain includes the pectoral muscle, sternum and sternal region of the ribs. On the other hand, elements that differentiate within an environment of exclusively somite-derived tissues belong to the primaxial patterning domain, which includes the vertebrae, proximal ribs and intercostal muscles (Burke *et al.* 2003; Durland *et al.* 2008). The boundary between the primaxial and abaxial domains is known as the lateral somitic frontier (Burke *et al.* 2003; Shearman *et al.* 2009). The lateral somitic frontier is the site of signal exchanges, such as the limb position (abaxial) being determined by the Hox code (primaxial) (Winslow *et al.* 2007). Numerous gene regulatory mechanisms and interactions appear to have a different effect in the abaxial and primaxial domains (Burke *et al.* 2003; Winslow *et al.* 2007). For example *Hoxb6* and *Hoxb9* deficient mice show dramatically disrupted patterning in the abaxial domain including mispatterning of the sternum and aberrant connections between the sternal ribs. However the primaxial domain is affected in a different way, causing homeotic transformations of the vertebrae but beyond this, patterning appears normal (McIntyre *et al.* 2007; Shearman *et al.* 2009). It is thought therefore that the lateral somitic frontier plays an important role in the occurrence of evolutionary modifications, modulating signal exchanges across the frontier and/or enabling adaptations to be made to one domain but not the other (Shearman *et al.* 2009).

1.3 Genetic Regulation of Sternum Development

1.3.1 The Role of *Tbx5* in Sternum Formation

T-box genes encode transcription factor proteins and are named due to the presence of a conserved sequence, the T-box, that codes for the T-domain of the protein which is involved in DNA binding and protein dimerisation. Members of this gene family have been found in all metazoans from diploblasts to humans and mutations in T-box genes in humans have been linked to several congenital syndromes (Minguillon *et al.* 2003).

Tbx5 has an established role in the development of both the heart and the forelimbs (Gibson-Brown *et al.* 1996; Basson *et al.* 1999). *Tbx5* is expressed in both of these tissues, while its paralog *Tbx4* is expressed in the hindlimbs (Logan *et al.* 1998; Rallis *et al.* 2003; Hasson *et al.* 2007). Previous work has indicated that *Tbx5* may also function in sternum development (Rallis and Logan, unpublished). In agreement with this, mutations in *Tbx5* result in the human disorder Holt-Oram syndrome (OMIM142900), (Basson *et al.* 1997; Li *et al.* 1997), which is associated with heart and upper limb abnormalities as well as sternum defects (Newbury-Ecob *et al.* 1996; Basson *et al.* 1999; Bruneau *et al.* 2001). Most mutations in Holt-Oram syndrome patients are predicted to cause *Tbx5* haploinsufficiency (Li *et al.* 1997; Basson *et al.* 1999). It also appears that other human syndromes are caused by mutations in other T-box gene family members. Ulnar-Mammary syndrome is caused by haploinsufficiency of *Tbx3* and Di-George syndrome is the result of *Tbx1* haploinsfficiency (Scambler *et al.* 1991; Bamshad *et al.* 1997).

Murine embryos homozygous mutant for *Tbx5* die early in development due to heart defects, but heterozygous mice survive to birth with some cardiac, forelimb and sternal defects. In particular, the bones of the forelimb are shortened and the digits are malformed, and the sternebrae are shortened and misspatterned, with an asymmetrical appearance (Pizard *et al.* 2005).

The embryonic lethality observed in embryos lacking *Tbx5* can also be bypassed by conditional deletion of *Tbx5* using the *Prx1Cre* transgenic mouse line (Logan *et al.* 2002). These mice lack *Tbx5* exclusively in LPM derived structures (Rallis *et al.* 2003) and survive to birth but die shortly after due to breathing difficulties caused by diaphragm defects. These mice display normal hindlimbs but lack all forelimb elements, demonstrating that *Tbx5* is essential for forelimb development (Rallis *et al.* 2003).

Tbx5 drives the initiation of forelimb outgrowth by activating the expression of the fibroblast growth factor gene *Fgf10* (Ng *et al.* 2002). This establishes an *Fgf* positive feedback loop within the forelimb mesenchyme and ectoderm to drive cell proliferation and enable limb outgrowth (Ohuchi *et al.* 1997). *Fgf10* is the only known direct downstream target of *Tbx5* in the forelimb, and *Fgf10* null mice lack most of the posterior scapula and all other elements of the forelimbs and hindlimbs (Ng *et al.* 2002). *Tbx5* is also known to play a later role in limb development, being required in the connective tissue to pattern the muscles and tendons of the forelimb (Hasson *et al.* 2010). While the role of *Tbx5* in the forelimb has been well studied, its requirement in sternum development has not yet been explored.

1.3.2 A Role for *Cx40* in Sternum Development

Few genes have been directly implicated in sternum development. One gene reported to have a significant function in the sternum is *Connexin 40* (*Cx40),* which encodes an intercellular channel component of gap junctions (Olk *et al.* 2009). Mice deficient in *Cx40* display shortened sterna with aberrant and asymmetric mineralisation of sternebrae and misaligned rib attachments (Pizard *et al.* 2005). It has also been reported that *Cx40* and *Tbx5* are co-expressed in the migrating sternal bands as well as in the sternal perichondrium (Pizard *et al.* 2005). Additionally, the *Cx40* promoter contains T-box binding elements, and haploinsufficiency of *Tbx5* has been shown to result in reduced expression of *Cx40* in the heart (Bruneau et al., 2001). This suggests that *Cx40* may be either a direct or indirect downstream target of *Tbx5* in sternum development (Pizard *et al.* 2005).

1.3.3 *Runx1* Expression Marks the Sternal Bands

Recent work has uncovered a role for the Runt-related transcription factor *Runx1* in sternum development (Kimura *et al.* 2010; Liakhovitskaia *et al.* 2010). The role of *Runx1* in the developing skeleton is not well understood, although is known to be essential for haematopoietic development. Mice deficient in *Runx1* die during early embryogenesis due their failure to form haematopoietic stem cells (Okuda *et al.* 1996; Wang *et al.* 1996). By using a *Runx1* reversible knockout mouse model crossed to a *TIE-2 Cre* deleter line, *Runx1* expression can be selectively rescued in the endothelial and haematopoietic systems. These mice survive to birth and form a

normal skeleton with the exception of the sternum, which completely fails to mineralise (Liakhovitskaia *et al.* 2010).

Runx1 is one of three members of the partially redundant *Runx* gene family (Levanon *et al.* 2004). *Runx2* is considered to be the master switch of osteoblast formation (Lian *et al.* 2006) and mice lacking the gene completely fail to form a bony skeleton (Komori *et al.* 1997; Otto *et al.* 1997). Consistent with this, *Runx1* and *Runx2* are co-expressed in mesenchymal condensations during early skeletal development (Yamashiro *et al.* 2004; Smith *et al.* 2005; Wang *et al.* 2005). *Runx1* is expressed at high levels in the sternal bands at E12.5-13.5 and the sternum at E17.5, which suggests that it may substitute for *Runx2* in regulating sternum ossification (Kimura *et al.* 2010; Liakhovitskaia *et al.* 2010).

1.3.4 Sternum Defects in the Mouse

A wide range of mutant mouse models exhibit sternal defects, ranging from a complete failure of sternum formation to minor defects in the patterning or ossification of the sternebrae. The sternum fails to form in compound transforming growth factor beta (*TGFβ*) mutants (*TGFβ2*$^{-/-}$ *TGFβ3*$^{-/-}$ and *TGFβ2*$^{-/-}$ *TGFβ3*$^{+/-}$), along with other malformations of the heart, blood vessels, palate and eyes. The distal ribs are also absent and the body wall does not close (Dunker *et al.* 2002). Additionally, embryos where *Sox9* has been conditionally deleted in LPM-derived tissues using *Prx1Cre* also fail to form a sternum and all bones of the limbs (Akiyama *et al.* 2002). This is thought be caused by defects in the chondrocyte differentiation pathway.

Incomplete fusion or bifurcation of the sternal bands are common sternal developmental defects, which can arise secondarily as a result of problems in body wall closure. For example, a bifurcated sternum is observed in *TGFβ2* deficient embryos, along with abnormal curvature of the ribs (Baffi *et al.* 2006). *Pax-1* null mice also display an incompletely fused sternum (Wilm *et al.* 1998). Mice lacking the myogenic gene *Myogenin* exhibit a spectrum of sternal phenotypes, from a split sternum to a shortened and excessively ossified sternum (Hasty *et al.* 1993; Vivian *et al.* 1999). Alternatively, sternal bifurcation can be minor and only affect the xiphoid process, as observed in *undulated* mice (*Pax-1* hypomorph mutants) and Glycogen synthase kinase-3β (*GSK-3β*) null mutants (Dietrich *et al.* 1995; Liu *et al.* 2007). Alternatively, the sternal bands can completely fail to fuse, as seen in compound *Hoxb2/Hoxb4* mutants. (Manley *et al.* 2001). Full sternal clefting is also observed in mice deficient for the actin polymerisation gene *Profilin1* (Miyajima *et al.* 2012).

Sternal defects can arise after the fusion of the sternal bands, often involving secondary defects due to aberrant attachment of the ribs to the sternum. For example, mice lacking the *Ephrin B1* ligand or *EphB2/3* receptors have asymmetric sternocostal junctions, fused sternebrae and a shortened sternum (Compagni *et al.* 2003). Similarly, mice deficient for the DNA binding protein *Six-1* exhibit disorganised ossification and defects in the sterno-costal junctions (Laclef *et al.* 2003). Asymmetrical rib attachments and shifted ossification centres are also displayed in a number of other mutant mouse models displaying aberrant rib formation, including *Delta EF1* null mice (Takagi *et al.* 1998), *Mks1* loss of function mutants (Weatherbee *et al.* 2009) and *Follistatin-like 1* conditional mutant mice

(Sylva *et al.* 2011). Rib formation defects can also affect sternum development more severely. For example deregulation of *Hoxc8* expression by deletion of the early enhancer region results in the formation of an additional pair of ribs, which cause an additional sternebra to develop (Belting *et al.* 1998; Juan *et al.* 2006). Also, in mice where *Hoxa10* is misexpressed throughout the entire presomitic mesoderm, the ribs are completely absent, which causes the sternum to ossify along its entire length and fail to form segmented sternebrae (Carapuco *et al.* 2005). The sternum also fails to form segments in screw tail mice, which show retarded development of the ribs (Bryson 1945). Taken together, these mouse models reveal that many sternum defects occur as a secondary effect of problems in rib formation or a failure of ventral body wall closure.

1.3.5 Human Sternum Defects

The sequence of sternum development is similar in the human to that in the mouse (and to a lesser extent, the chick). The human sternal bands are first visible during the sixth week of development, and migrate medially across the thorax from week six to week nine. By the tenth week the bands have fused at the midline, but they do not begin to ossify until the fifth month and the xiphoid process does not ossify until around three years after birth (Engum 2008; van der Merwe *et al.* 2013). During puberty the sternebrae begin to fuse completely to form a single ossified unit (McCormick *et al.* 1981).

The most common sternal defect observed by clinicians is pectus excavatum, or funnel chest, which affects approximately 1 in 250-1000 live births (Kelly 2008).

This condition occurs when the sternum and distal ribs intrude into the thoracic cavity, causing the chest to become sunken, although the pectoral muscle is still able to attach to the sternum. The caudal part of the sternum is most often affected, but the extent of the defect can vary considerably between patients (Mathes *et al.* 2011). It is thought that overgrowth of the rib cartilage may contribute to this condition, although this has yet to be formally demonstrated (Mathes *et al.* 2011). Pectus excavatum is observed in approximately 40% of patients with Holt-Oram Syndrome (Newbury-Ecob *et al.* 1996). The sternum can also protrude out from the chest to cause a condition known as pectus carinatum. This distorts the shape of the ribcage and is also thought to be caused by overgrowth of the costal cartilage (Mathes *et al.* 2011). This condition can affect the entire sternal length, but more often only the more caudal region of the sternum protrudes. Both pectus carinatum and pectus excavatum can be repaired surgically through the implantation of a metal bar wired to the ribs to hold the sternum in place (Kelly 2008; Mathes *et al.* 2011).

A more serious sternal defect arises when the sternal bands fail to fuse properly at the midline, resulting in a cleft or bifid sternum. This condition is rare, with fewer than 100 cases fully described in the literature (Mathes *et al.* 2011). Most often this affects the manubrium and the rostral part of the sternal body with the bands fusing normally in the caudal region, although often the reverse can happen and the caudal region is split (van der Merwe *et al.* 2013). This caudal splitting is known as inferior sternal clefting and is linked to ectopia cordis, a condition in which the heart protrudes from the chest, either covered or uncovered by the skin (Engum 2008).

Many human conditions involve sternal malformations in combination with other defects. For example in patients with Cantrell's Pentalogy, the lower sternum is often clefted or completely absent, accompanied by other ventral body wall defects (Smigiel *et al.* 2011). Pectus excavatum or carinatum are often seen in patients with Marfan syndrome, a disorder of the connective tissue in which patients possess long limbs and hyper-extendable joints (Kotzot *et al.* 2009). In some cases of Monosomy X and in Trisomy 21 (Down syndrome), additional ossification centres have been observed in the manubrium (Mehta *et al.* 1993; Kriss 1999). Finally, both Turner syndrome and Trisomy 18 syndrome are associated with a shortened sternum (Mehta *et al.* 1993; Tucker *et al.* 2007). Many of these defects may arise secondarily as a result of problems in ossification, ventral body wall closure or rib development, as observed in mutant mouse models. Conversely, in conditions affecting the pectoral musculature, the sternum forms completely normally. For example, Poland syndrome includes the unilateral absence or hypoplasia of the pectoral muscles, but the sternum in unaffected (Mathes *et al.* 2011). Overall, these sternal defects arise as a result of aberrant development of a range of tissues including the sternum itself, as well as the ribs, pectoral muscle or the ventral body wall.

1.4 Thesis Aims

As outlined above, the role of *Tbx5* in the development of both the heart and forelimbs has been studied extensively, but *Tbx5* function in sternum formation is not understood. In the following chapters I investigate the developmental origin of the sternum and explore the sternal phenotype in the absence of *Tbx5*. Next, I explore the correlation between forelimb use and sternum morphology by comparing sternum size in avian species with different flight abilities. Finally, I address the genetic adaptations that could explain the reduction in sternum and forelimb size in flightless birds, using the emu as an experimental model. For the first time, I explain *Tbx5* function in sternum formation and suggest how modulation of *Tbx5* may underlie the adaptation of sterna in vertebrates.

Chapter Two:

Materials and Methods

Chapter Two: Materials and Methods

2.1 Source of Eggs and Incubation

Fertile chicken eggs (Winter's Farm) and fertile eggs from a transgenic chicken line that ubiquitously expresses GFP (N. Sherman, Roslin Institute, Edinburgh; McGrew *et al.* 2004) were incubated on their side at 38°C and staged according to Hamburger and Hamilton (HH) (Hamburger *et al.* 1951). Features were identified using an atlas of chick development (Bellairs *et al.* 2005). Chick eggs were opened by making a hole in the rounded end of the egg using forceps and removing 1ml of albumen using a 2ml syringe and needle (Terumo 19G x 2"). This allowed the embryo to sink further from the shell. A circle of approximately 2cm diameter was then cut into the upper-most side of the shell using curved scissors and the circle of shell was discarded. Eggs were re-sealed using clear tape (5 Star Office) to prevent infection and drying-out.

Fertile emu eggs (Denbury Farm and Leicestershire Emus and Rheas) were incubated on their side at 37.5°C, and rotated 90° along their long axis daily. Emu embryos were accessed by making a hole using a Dremel 8000 drill and Dremel 192 High Speed Cutter 4.8mm attachment, and removing 5ml albumin using a 10ml syringe and needle (Terumo 19G x 2"). Eggs were windowed by laying sideways and cutting a circle of approximately 4cm diameter into the upper-most side using a Dremel Cut-Off Wheel 24mm (409) attachment. The circle of shell was removed using forceps and discarded. Eggs were re-sealed using clear tape (5 Star Office).

Since there is no established normal staging system for the emu, embryos were staged according to hindlimb and head morphology, matched with the equivalent chick Hamburger/Hamilton stages and assigned a Hamburger/Hamilton equivalent stage (eqHH).

Chick and emu embryos were harvested from their eggs by cutting through the surrounding membranes using curved scissors, lifting the embryo out of the shell using curved forceps and placing in a petri dish filled with 1X phosphate buffered saline (PBS). PBS solution was made up from 10X PBS stock (800g NaCl, 20g KCl, 115g Na_2HPO_4, 20g KH_2PO_4 in 10L H_2O) by diluting in H_2O. Extra-embryonic membranes were removed and embryos were fixed in 4% paraformaldehyde (PFA), made up by diluting freshly defrosted 20% PFA stock in PBS (20% PFA made up by adding 200g of PFA powder to 1L PBS and heating using a 60°C heat block (Stuart) and magnetic stirrer to dissolve powder before filtering, aliquoting and freezing).

2.2 Grafting of GFP-labelled Tissue

GFP transgenic chicks were incubated to HH20 in parallel with non-transgenic chicks and were stage-matched prior to operating. Embryos were exposed by opening the egg (as described in Chapter 2.1) and the vitelline membrane that lies directly above the embryo was removed using forceps. The forelimb bud of a non-transgenic embryo was removed completely by cutting in line with the flank using a tungsten needle. A corresponding donor limb bud was then removed from a GFP embryo using the same method, and held in place in the non-transgenic host embryo flank using a pin made from 0.08mm mm platinum wire (Goodfellow) bent into an

L-shape. 50μl of penicillin/streptomycin antibiotic (Gembio; 10,000 U/ml penicillin, 10mg/ml streptomycin) was added to the egg before it was re-sealed and incubated at 38°C. Embryos were harvested at HH36, fixed in 4% PFA overnight at 4°C, and photographed using an Leica MZLF III microscope with a Hamamatsu C4742-95 camera and Openlab software.

2.3 DiI Injections

CM-DiI (Molecular Probes) stock solution was made up by dissolving the crystals in 100% ethanol (EtOH) to a concentration of 2mg/ml. Working solutions were made up fresh with each use by diluting stock DiI solution 1/10 in fresh 15% sucrose solution (15g sucrose [BDH] in 100ml PBS, made up fresh and filtered through a 0.45μl syringe filter unit [Sartorius Stedim Biotech]). Embryos were exposed by opening the egg (as described in 2.1) and the vitelline membrane lying directly above the embryo was removed using forceps. DiI solution was administered to the desired location using a hand-held glass capillary needle pulled using a vertical micropipette puller (Kopf model 750). To help prevent infection and reduce mortality rates, 50μl of penicillin/streptomycin antibiotic was added to each egg before it was re-sealed and returned to 38°C. Embryos were harvested at a range of stages from HH22 to HH38, and fixed and photographed as detailed in Chapter 2.2.

2.4 Retrovirus Production and Infection

Chick *Tbx5* cDNA (Logan *et al.* 1998) was cloned into a pSLAX-13 shuttle vector and the Cla fragment from *pSlax-13Tbx5*, containing the *Tbx5* ORF and RCAS

flanking sequences, was then subcloned into the RCAS (BP) A retroviral construct, which was then used to generate retroviral supernatant as described previously (Logan *et al.* 1998). The *Tbx5* construct contains the full-length chick *Tbx5* cDNA (Accession Number AF069396; Rallis *et al.* 2003). The emu forelimb-forming LPM on the right hand side only was injected at eqHH15 with concentrated viral supernatants using a Hamilton syringe (Narishige MN153). 50µl of penicillin/streptomycin antibiotic (Gembio) was added to the egg before it was re-sealed and returned to 37.5°C. Embryos were then left to develop for 14-16 days before harvest and fixation overnight at 4°C in 4% PFA. Production of retroviral constructs, virus production and injection of the virus into emu embryos was carried out by Malcolm Logan.

2.5 Mouse Strain Crosses and Maintenance

Mouse embryos were staged according to Kaufman (Kaufman 1992). Noon on the day a vaginal plug was observed was taken to be E0.5 days of development. To produce mice in which *Tbx5* is conditionally deleted in the limb forming region, $Tbx5^{lox/lox}$ female mice (Bruneau *et al.* 2001) were crossed to $Tbx5^{lox/+}$*; Prx1Cre* male mice as described previously (Rallis *et al.* 2003). The *Prx1Cre* transgene expresses *Cre* recombinase within the rostral somatic LPM (Logan *et al.* 2002). To visualise *Cre* activity in the *Prx1Cre* line, I crossed this line to a ROSA26RlacZ reporter line (Soriano 1999).

Previous work in the laboratory identified a regulatory element responsible for driving *Tbx5* expression in the rostral LPM (Minguillon *et al.* 2012). A series of

constructs were generated using the BGZA vector, resulting in the identification of a 1.5kb fragment containing most of *Tbx5* intron 2 (intron2; Chr5: 120,287,070-120,288,589, Ensembl NCBIM37). This fragment is able to drive *lacZ* expression in the rostral LPM and is sufficient for the earliest onset of *Tbx5* expression in this region (Minguillon *et al.* 2012). The *Intron2lacZ* element was then used to generate a stable transgenic mouse line *Tbx5Intron2lacZ* (Minguillon unpublished data). This line was used to generate transgenic embryos, allowing visualisation of cells in which the *Intron2* enhancer is active, or had been at some point in the past.

The activity of the *Intron2* enhancer was visualised in embryos conditionally lacking *Tbx5* by generating $Tbx5^{lox/lox}$*;Prx1Cre; Tbx5Intron2lacZ* embryos. *Tbx5Intron2lacZ* mice were crossed to the $Tbx5^{lox/+}$*;Prx1Cre* line to generate compound $Tbx5^{lox/+}$*;Prx1Cre; Tbx5Intron2lacZ* mutant male mice. These were then subsequently back-crossed to $Tbx5^{lox/lox}$ female mice to generate $Tbx5^{lox/lox}$*;Prx1Cre; Tbx5Intron2lacZ* progeny. *Fgf10* mutant mice ($Fgf10^{-/-}$; Sekine *et al.* 1999) were also crossed to the *Tbx5Intron2lacZ* line to generate compound $Fgf10^{+/-}$*;Tbx5Intron2lacZ* mutant mice, which were subsequently back-crossed to $Fgf10^{+/-}$ mice to generate $Fgf10^{-/-}$*;Tbx5Intron2lacZ* progeny, allowing us to examine *Intron2* enhancer activity in mice lacking forelimbs but possessing a normal sternum.

2.6 Genotyping

Ear pieces and embryo sacs were digested overnight at 55°C in 200µl lysis buffer (10mM Tris pH7.5, 10mM EDTA, 100mM NaCl, 0.5% Sarkosyl) with 0.1mg/ml proteinase K. 2µl of lysis solution was added to the following reaction mix: 1µl

forward primer, 1µl reverse primer, 0.2µl Taq polymerase, 35.8 µl distilled H_2O (dH_2O) and 10µl 5x genotyping buffer (250ml 1M KCl, 50µl 1M HCl pH 8.4, 12.5µl 1M $MgCl_2$, 10µl 100mM dATP, 10µl 100mM dTTP, 10µl 100mM dGTP, 10µl 100mM dCTP, 85ml BSA 10mg/ml, 562.5ml dH_20).

For the *Tbx5*$^{lox/lox}$ line, a single reaction was carried out using three primers that identify the endogenous *Tbx5* allele, and both the conditional (floxed) and deleted (floxed-out) *Tbx5* allele as described previously (Bruneau *et al.* 2001).

Mouse Strain	Primers 5'-3'	Step	Temp (°C)	Time Min:Sec
Prx1Cre	*Fwd* ATC CGA AAA GAA AAC GTT GA *Rev* ATC CAG GTT ACG GAT ATA GT	1	94	2:00
		2	94	0:30
		3	54	0:30
		4	72	1:30
		Go To 2		
		Cycle x 30		
Tbx5$^{lox/lox}$	*Fwd* GCA GCG CAG TCC TCA CCA G *Fwd* AGC TGC CCT GGG TAT GCC TTA T *Rev* AAA TTC CAA CCC CTT CCA CAG AT	1	94	5:00
		2	85	5:00
		3	94	0:30
		4	65	0:30
		5	72	1:00
		Go To 3		
		Cycle x 30		
Fgf10$^{-/-}$	*Fwd* CACCAAAGAACGGAGCCGGTTG *Rev* ACTCTTTGGCCTCTATCTAG	Same as for *Prx1Cre*		
lacZ	*Fwd* GGT CGG CTT ACG GCG GTG ATT T *Rev* AGC GGC GTC AGC AGT TGT TTT T	1	95	5:00
		2	95	0:30
		3	61	0:30
		4	72	0:45
		Go to 2		
		Cycle x 30		

Table 1. Primer sequences and PCR cycle programs used to genotype mouse strains.

2.7 X-gal Staining

Whole embryos were fixed for 20 minutes in *lacZ* fix solution (0.54ml of 37% formaldehyde, 0.16ml of 25% gluteraldehyde, 0.04ml of 1M $MgCl_2$, 0.2ml of 5mM EGTA, 0.2ml of 2% Igepal, 19ml of PBS), before washing 3 times in PBS and staining for between 1 hour and overnight in X-gal staining solution (0.12ml of 0.5M $K_3Fe(CN)_6$, 0.12ml of 0.5M $K_4Fe(CN)_6$, 0.24ml of 1M $MgCl_2$, 0.12ml of 1% sodium deoxycholate, 0.12ml of 1% Igepal, 0.24ml of 50mg/ml X-gal in dimethylformamide, 12ml of PBS). Embryos were washed a further 3 times in PBS and post-fixed for 1 hour in 4% PFA. When required, embryos were cleared in 1% KOH to reduce background staining and then transferred into glycerol using the following series of glycerol/KOH washes: 20%glycerol/ 1%KOH, 50%glycerol/ 1%KOH, 80%glycerol/ 1%KOH, 100% glycerol, 100%glycerol, 100%glycerol.

X-gal staining on sections was carried out by fixing whole embryos in *lacZ* fix solution as above before embedding and sectioning as described in Chapter 2.12. Frozen slides were allowed to thaw for 2 hours at room temperature and rinsed 3 times for 10 minutes in PBS before X-gal staining was carried out for 10-30 minutes using the solution described above. Slides were post-fixed in 4% PFA for 15 minutes before mounting using DAKO media (DAKO).

2.8 Wholemount *in situ* Hybridisation

Wholemount *in situ* hybridisations were carried out essentially as previously described (Riddle *et al.* 1993). The hindbrain of all embryos was pierced with

forceps or the head was removed completely to prevent probe trapping. In some cases, emu embryos at eqHH23 were bisected along the transverse axis at the torso and the forelimbs and hindlimbs were stained in separate vials in order to test two probes on one embryo. Proteinase K solution at 10μg/ml was used and treatment times were reduced to 6 minutes for emu embryos younger than eqHH20 and 8 minutes for eqHH20-23 emus. For chick embryos older than HH20, proteinase K treatment was extended to 18-20 minutes.

Transcription of DIG-labelled RNA riboprobes was carried out for 2 hours at 37°C using the following reaction mix: 10.5μl dH_2O, 2μl 10x transcription buffer, 2μl 0.1M DTT, 2μl DIG labelled RNA nucleotide mix, 2μl linearised plasmid, 0.5μl RNase inhibitor, 1μl RNA polymerase. A successful *in vitro* transcription was checked by running out 2μl of the reaction mix on a 1% gel. To digest the DNA template, 1μl DNase (Roche) was added and the transcription reaction mixture was incubated at 37°C for a further 15 minutes.

RNA precipitation was conducted by adding 100μl TE-8 (10mM Tris-HCl pH 8 and 0.1mM ETDA pH 8), 10μl LiCl and 300μl 100% EtOH and leaving overnight at -20°C. RNA was then pelleted by centrifuging at 13,000 rpm for 10 minutes, and the resulting pellet was washed in 300μl of 70% EtOH, before being left to air-dry and re-suspending in 50μl TE-8 and 50μl hybridisation buffer. For application to embryos, 10μl of DIG-labelled RNA probe was mixed with 2ml hybridisation buffer.

The following chick and mouse probe templates used have been described previously: *cPitx1* (Logan *et al.* 1998), *cTbx5* (Logan *et al.* 1998), *mRunx1* (Eng *et al.* 2004), *mTbx5* (Rallis *et al.* 2003), *mFgf10* (Hasson *et al.* 2007). A cDNA clone was used for the *mCx40 in situ* probe template (Source BioScience IMAGE Clone 6401526, excised with EcoR1 and Nco1 and RNA transcribed with polymerase T7). Emu probes *eTbx5* and *ePitx1* were both synthesised following ligation of PCR products into a pGem-T vector, linearising with SacII and using Sp6 RNA polymerase for probe transcription.

2.9 Cloning Emu Probes

RNA was extracted from a single, whole limb bud-stage emu embryo (eqHH22) by adding 600µl RNeasy lysis buffer (Qiagen) and breaking up tissues using a plastic pestle in a 1.5ml eppendorf tube. The sample was then pipetted up and down to break the tissues down further, run through a QIAshredder (Qiagen) and centrifuged for 2 minutes at 13,000 rpm. The lysate was centrifuged for 3 minutes at 13,000 rpm and the supernatant was removed and stored at -80°C. An RNeasy mini kit (animal tissues, Qiagen, RNeasy mini kit) was used, adding 1 volume of 70% EtOH to the cell lysate and transferring to a spin column. This was washed and spun down with washing buffers to remove carbohydrates, proteins and fatty acids (buffer RW1), and salts (buffer RPE), and the RNA was then eluted in 60µl dH_2O.

PCR primers were designed based on sequence alignments of chick, turkey, zebrafinch and anole lizard orthologous genes, aligned using the ClustalW alignment program and MegAlign software (Figure 25 and Figure 26), Chick *Tbx5*

ENSGALT00000013434, Turkey *Tbx5* ENSMGAT00000011288, Lizard *Tbx5* ENSACAT00000005130, Chick *Pitx1* ENSGALT00000009427, Turkey *Pitx1* ENSMGAT00000009363, Zebrafinch *Pitx1* ENSTGUT00000001303, Lizard *Pitx1* ENSACAT00000005898). Primer sequences were chosen based on selecting conserved regions that would yield a 3' biased probe template of approximately 400-500 base pairs in length. Primer sequences used are as follows: *Tbx5 Forward* TGT ATG TAC GCC AGC TCT GCT, *Tbx5 Reverse* A GCT GTT CTC GCT CCA CTC TGG, *Pitx1 Forward* AGC CAA GTG GAG AAA GCG GGA, *Pitx1 Reverse* AGC CGG GGC TCT GCA AAC TGC.

A one-step reverse transcription PCR (one step RT-PCR) reaction was carried out, heating the reaction mix to 50°C for 30 minutes (RT reaction) followed by 94°C for 2 minutes, and then run through 40 cycles of 94˚C, 15 seconds; 60˚C, 30 seconds; 68˚C, 1 minute (PCR reaction). PCR products of the expected size (*Tbx5*, 432 nucleotides; *Pitx1*, 496 nucleotides) were gel purified by running on a 1% gel and excising fragments at the desired length using a scalpel. The Qiaquick Gel extraction Kit was used (Qiaspin Handbook, Qiagen), dissolving the agarose in solubilisation buffer, adding isopropanol to increase the yield, and transferring the sample to a QIAquick spin column (Qiagen). This was washed with further solubilisation buffer and wash buffer to remove all traces of agarose. The DNA was then eluted in 50µl of TE-8.

The gel extracted PCR products were cloned using T-vectors (pGEM-T Vector System I, Promega). Ligation reactions were set up as follows: 5µl 2x rapid Ligation

Buffer, 1µl pGEM-T Vector, 3µl insert DNA, 1µl T4 DNA Ligase. After incubation for 1 hour at room temperature, 2µl of each ligation was removed and added to a fresh tube, before adding 50µl XL-10 Gold ultracompetent cells (Agilent Technologies; average transformation efficiency of >5 x 10^9 transformants/µg of DNA), flicking tubes gently to mix and incubating on ice for 20 minutes. A heat shock at 42°C for 45 seconds was then used before returning to ice for 2 minutes. 950µl of TY broth was added to each sample and tubes were incubated at 37°C with shaking for 1.5 hours, before plating 100µl of each transformation onto IPTG/X-gal plates (4µl of 200mg/ml IPTG and 40µl of 50mg/ml X-gal in dimethylformamide spread evenly over an ampicillin plate) and left overnight at 37°C.

Approximately 10 white colonies (indicating disruption of the *lacZ* gene following ligation of insert into vector) were picked per plate and grown up in 4ml LB broth + 4µl ampicillin (Sigma-Aldrich; stock solution diluted 1/1000 to a concentration of 100µg/ml) overnight. Bacterial cultures were spun down and minipreps carried out according to manufacturers' instructions (Qiagen), eluting in 50µl TE-8. Ligation products were checked by running a diagnostic digest of 2µl of each miniprepped sample (NcoI and NotI used to excise insert from pGEM-T vector). Samples were then sent for sequencing (Source Bioscience) using T7 and Sp6 RNA polymerases and contigs were assembled from sequence reads using Seqman and Seqbuilder software (DNASTAR). Emu sequences were then aligned with, and compared to known chick, mouse and human *Tbx5* and *Pitx1* transcript sequences to confirm that the clones contained fragments of the emu *Tbx5* and *Pitx1* genes (Figure 27 and 28).

Both *Tbx5* and *Pitx1* plasmids were linearised by digestion with SacII at 37°C for 1 hour, followed by a phenol-chloroform clean-up. 2µl of DNA (both approximately 300ng/µl) was then used for probe synthesis, as detailed in Chapter 2.9.

2.10 Skeletal Preparations

Embryos were fixed overnight in 4% PFA and washed in PBS for 2 x 5 minutes before undergoing graded dehydration washes and storage in methanol (MeOH) as follows: 25%, 50%, 75% MeOH/PBS, 3 x 100% MeOH. Embryos were skinned and eviscerated in 100% EtOH and the hindlimbs, head and as much muscle as possible was removed. Samples were left overnight at room temperature in glacial acetic acid, before an overnight incubation at 37°C in Alcian Blue/Alizarin Red staining solution (5ml 0.3% Alcian Blue, 5ml 0.1% Alizarin Red, 2.5ml glacial acetic acid, 37.5ml 70% EtOH). Stock solutions were made up as follows: 0.3% Alcian Blue (0.3g Alcian Blue (Sigma-Aldrich) in 100ml 70% EtOH) 0.1% Alizarin Red solution (0.1g Alizarin Red (Sigma-Aldrich) in 100ml 95% EtOH). Skeletons were then washed 3 x 30 minutes in 100% EtOH at room temperature and placed in 1% (w/v) KOH for several days at room temperature until cleared to the desired level, when they were transferred into the following series of 5 minute glycerol/KOH washes: 20% glycerol/1%KOH, 50% glycerol/1% KOH, 80% glycerol/1%KOH, 3 x 100% glycerol. Skeletons were photographed in 100% glycerol using a Leica MZ7S microscope and Leica DFC 320 camera using Leica Firecam software.

2.11 Embryo Embedding and Cryo-sectioning

Embryos were fixed in 4% PFA for 1 hour to overnight at 4°C, before washing in 3 x 5 minutes in PBS and 2 x 30 minutes in 30% sucrose in PBS and then being left overnight at 4°C in 30% sucrose in PBS. An equal volume of OCT compound (VWR Prolab) was added to the sucrose solution and then the embryos were kept at 4°C in OCT for 2-3 days, changing the solution each day. Embryos were transferred to an embedding mold containing OCT and oriented with the rostral end pointing downwards. The molds were then placed on dry ice in order to freeze the OCT, and frozen blocks were wrapped in foil and stored at -80°C. For sectioning, a frozen block was attached to the cryostat chuck of a Leica cryostat (CM3050S), allowing the tissue to equilibrate to the cryostat temperature (-20°C) for 5 minutes. Sections were cut at 10μm, transferred onto Superfrost plus slides (Thermo Scientific) and left to dry for 2 hours at room temperature before storing at -80°C in a sealed box. When required, slides were thawed in a sealed box for 2 hours at room temperature and then rinsed 3 x 10 minutes in PBS. They were stained with DAPI (1:15,000; Vectorlabs) for 1 minute before rinsing a further 2 times in PBS. Slides were mounted using DAKO medium (DAKO) and then photographed using a Zeiss Axioimager M1 microscope with an Axiocam MRc camera and Axiovision software.

2.12 Section Immunohistochemistry

Frozen sections on Superfrost plus slides (Thermoscientific) were thawed for 2 hours at room temperature in a sealed box and then rinsed 3 x 10 minutes in PBS. All blocking and antibody staining steps were performed in a humidified chamber. For Col2 antibody staining, antigen retrieval was performed by washing slides 2 x in

citrate buffer (2mM citric acid, 10mM sodium citrate), before heating using a microwave at full power for 8 minutes, followed by 30% power for 20 minutes. Slides were left in citrate buffer to cool for 2 hours at room temperature before washing 2x in PBS and proceeding to blocking and antibody staining.

For detection of skeletal muscle, cartilage and connective tissue on frozen sections, blocking was performed in 5% sheep serum (Sigma-Aldrich) in PBS for 1 hour, followed by incubation with primary antibody for 2 hours at room temperature or overnight at 4°C. The following primary antibodies were used: mouse anti-my32 for skeletal muscle (1:800; Sigma-Aldrich; M1570), rabbit anti-Col2 for cartilage (1:400; Abcam; ab53047) and mouse anti-tcf4 for connective tissue (1:800; Upstate; 05-511). Slides were rinsed 3 x 10 minutes in PBS before incubating with Alexa Fluor 488 or Alexa Fluor 555 goat anti-mouse or goat anti-rabbit secondary antibodies (1:400; Sigma-Aldrich) for 2 hours at room temperature.

Detection of RCAS transfection of emu tissues was performed by fixing slides for 15 minutes in 4% PFA in PBS, washing 2 x 5 minutes in PBS and blocking in 10% goat serum with 0.2% triton in PBS for 30 minutes. Slides were incubated in 3C2 primary antibody (1:5; DSHB, University Iowa) for 30 minutes at room temperature, before washing 3 x 5 minutes in PBS. Alkaline phosphatase-conjugated anti-mouse IgG secondary antibody (1:1000) was applied for 30 minutes, prior to washing 3 x 5 minutes in PBS and 2 x 5 minutes in fresh NTMT solution (100mM NaCl, 100mM TrisHCl pH. 9.5, 50mM $MgCl_2$, 0.1% Tween-20). Slides were then stained with NBT and BCIP mix (6.75µl NBT, 5.25µl BCIP, 2ml NTMT) for 10-30 minutes at

room temperature. All sections were counter-stained with DAPI nuclear stain (1:15,000; Vectorlabs), mounted using DAKO medium (DAKO) and photographed using a Zeiss Axioimager M1 microscope with an Axiocam MRc camera and Axiovision software.

2.13 Wholemount Immunohistochemistry

For detection of skeletal muscle in wholemount, embryos were heated to 70°C for 1 hour to inactivate any endogenous alkaline phosphatase, before bleaching in 6% hydrogen peroxide (Fisher Scientific) for 1 hour. Blocking was performed for 1 hour in 0.1% Triton (Sigma-Aldrich), 1%BSA (Sigma-Aldrich) and 0.15% glycine (Fisher-Scientific) solution in PBS. Embryos were then incubated overnight with monoclonal anti-myosin (skeletal fast) - alkaline phosphatase conjugated antibody (My32-AP; Sigma-Aldrich 032M4798) made up 1:800 in block solution. 3 x 5 minute washes were carried out in PBT at room temperature, followed by 5 x 1 hour washes in PBT. Embryos were then washed in fresh NTMT solution (see 2.1.3) and incubated at room temperature in the dark with fresh NBT and BCIP (see 2.1.3) for 10-30 minutes, checking regularly for the development of the colour reaction. Stained embryos were post-fixed in 4% PFA, 0.2% gluteraldehyde solution and were stored at 4°C.

2.14 Avian Skeleton Measurements

Adult avian skeletons at The Natural History Museum at Tring and the University Museum of Zoology, Cambridge were measured using vernier calipers.

Measurements of sternum length, width, keel height and thorax length (the distance from the first to the final thoracic vertebra) were taken. Where possible, up to four samples were measured per species and the standard error was calculated.

Chapter Three:

Fate Mapping the Sternal Precursors

Chapter Three: Fate Mapping the Sternal Precursors

Chapter Summary

In this chapter, I investigate the embryological origin of the sternum precursor cells and their spatio-temporal movements during development. A clearer understanding of the events of normal sternum development can help to provide an insight into the causes of sternal abnormalities.

The sternal precursors have been suggested to originate in the LPM (Chen 1952; Murillo-Ferrol 1963; Chevallier 1975). This tissue is divided into two layers: the somatic mesoderm, which gives rise to the bones of the limbs, and the splanchnic mesoderm, which forms the future gut wall and the smooth muscle and connective tissue of the digestive organs (Kardong 1998). The precise location of the sternal precursors within the LPM is not known, and prior to the condensation of the sternal precursors into bands, the movements of these cells have not been described. Here, I describe the use of two fate-mapping techniques to build a picture of the precise location and time-course of the migration of the sternum precursor cells to their final position at the ventral midline.

3.1 The LPM adjacent to Somites 14-21 gives rise to the Sternum

Exploiting the chick model system, I used a lipophillic lineage tracing dye (DiI) to label embryos at HH20. This stage was chosen because at younger stages it is difficult to target specific sites within the LPM, and at later stages the sternum precursor cells may have already begun to move across the thorax, so DiI labelling

may not target them. DiI stains cell membranes and allows the movements of cells and their descendants to be observed over time. It also has the advantage of targeting a small population of cells, although it does become diluted as cells divide. A strategy was designed in which different sites within the LPM in and around the forelimb bud were designated with a number, as shown in Figure 5A (bold numbering). Multiple embryos were injected with DiI at each site and were left to develop until the point of sternal band fusion (HH36). Surviving embryos were then harvested and the distribution of DiI-positive cells was analysed (Figure 5, Table 2).

Labelling cells at the distal extremes of the forelimb bud (sites 11, 13 and 14) resulted in DiI-positive cells within the distal most half of the limb (data not shown), but not within the thorax (Figure 5K). This indicates that, as expected, there is no migration of cells out of the limb bud from this distal position. However, labelling cells in more proximal regions of the forelimb bud (sites 8-10 and 12) led to DiI-positive cells within the ventral body wall and the forelimb, but not at the midline. This indicates that the sternum precursor cells are not present within the limb bud proper at HH20. The DiI-positive cells visible in the ventral body wall of these harvested embryos (Figure 5I, J) are likely to contribute to the pectoral muscle. Pectoral muscle precursor cells follow an 'in-out' mechanism, migrating into the forelimb bud, and then out again into the ventral region of the thorax (Valasek *et al.* 2011). It is likely that DiI labelling at HH20 targets some of these cells during this migration process, leading to the thoracic labelling observed.

DiI-labelling the region of the LPM ventral to the limb bud resulted DiI-positive cells accumulating at the ventral midline (Figure 5A, shaded area, and Figure 5C-G). This suggests that the sternal precursors reside within this region, which encompasses injection sites 2 to 6 (adjacent to somites 14 to 21). Other injection sites situated rostral or caudal to this region (sites 1 and 7, adjacent to somites 13 and 22 respectively), resulted in no detectable DiI at the midline of harvested embryos (Figure 5A,B,H). These embryos did show DiI-positive cells within the lateral embryonic flank, but no medial migration was observed. This demonstrates that the rostro-caudal boundaries of the sternal precursor population within the LPM at HH20 are adjacent to somites 13/14 and 21/22.

In harvested embryos showing DiI-positive cells at the midline (Figure 5C-G), there are virtually no other DiI-positive cells visible elsewhere within the thorax. As such, it appears that at HH20, the territory of cells fated to form the sternum are present as a uniform population that migrate collectively from their origin in the LPM to the ventral midline.

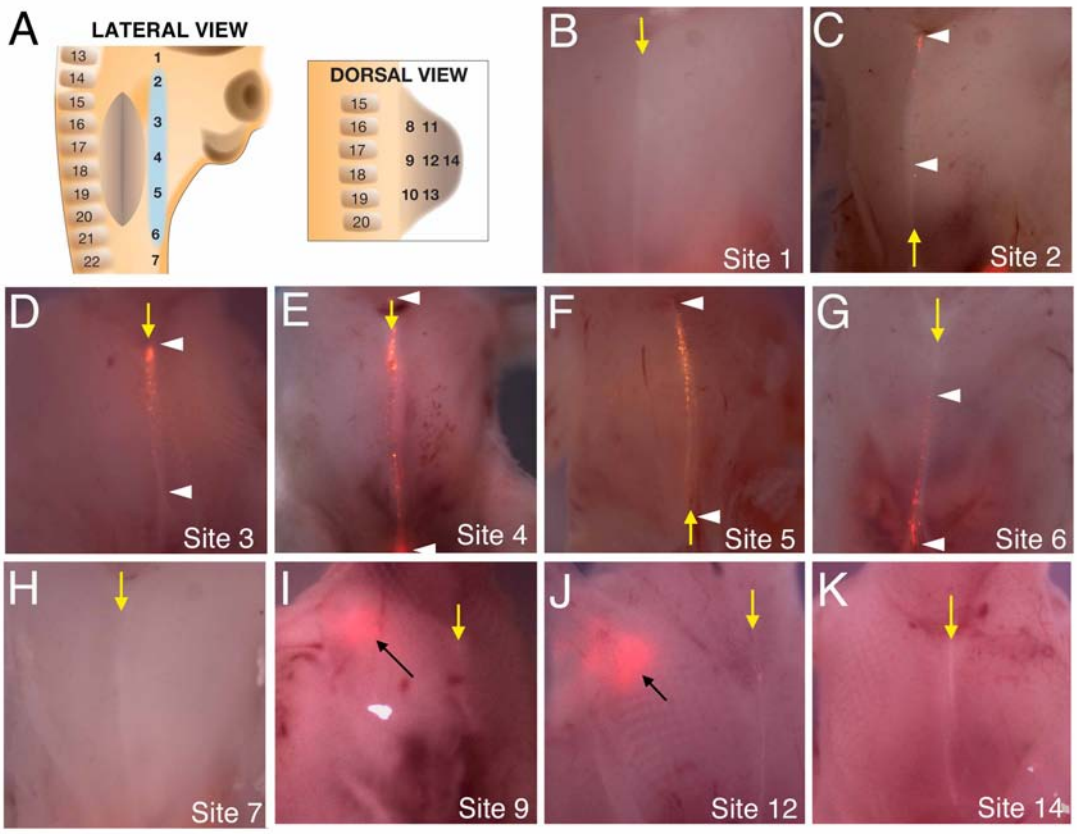

Figure 5. The sternum precursor cells reside in the LPM, ventral to the forelimb bud.

A, Schematic of DiI injection sites (numbered in bold) and adjacent somites (numbered 13-22) with the sternum precursor population highlighted (blue). **B-H, K,** Ventral wholemount views and **I, J,** ventrolateral wholemount views of harvested, skinned HH36 embryos showing DiI-labelled cells (red) at the midline (**B-K,** ventral midline shown by yellow arrows, **C-G**, boundaries of population shown by white arrowheads), and in the thorax (**I, J,** black arrows) following DiI labelling of cells at sites 1-14 in HH20 chick embryos.

Injection Site	Embryos with DiI visible	DiI visible at ventral midline	Embryos with DiI at midline (%)	Anterior/Posterior Bias to DiI?
1	3	0	0	-
2	3	2	66	Anterior (2/2)
3	5	4	80	Anterior (3/4)
4	3	3	100	No
5	6	6	100	No
6	4	4	100	Posterior (2/4)
7	5	0	0	-
8	8	0	0	-
9	7	0	0	-
10	4	0	0	-
11	5	0	0	-
12	7	0	0	-
13	4	0	0	-
14	3	0	0	-

Table 2. Tabulation of the distribution of DiI-positive cells in harvested embryos.

Summary table showing the number and percentage of HH36 harvested embryos showing DiI labelling within the thorax and/or at the midline following injection at sites 1-14. Any rostral or caudal bias in the distribution of the DiI-positive cells along the midline is also represented.

For the injection sites resulting in DiI accumulation at the midline, a number of embryos were harvested immediately following labelling and were cryo-sectioned to confirm precisely which region of the LPM was labelled (Figure 6A,B, N=4). In section, DiI labelling is visible exclusively within the somatic mesoderm and does not extend into the splanchnic mesoderm layer, internal organs or limb bud (Figure 6B). This demonstrates that the DiI labelled sternal precursors at HH20 originate from the somatic mesoderm layer.

Harvested embryos at HH36 were sectioned to confirm whether the cells observed at the ventral midline were located within the sternum (Figure 6C). In section, DiI was visible within the sternum itself, as well as in the tissues immediately ventral and dorsal. It is not clear which tissues these DiI labelled cells outside of the sternum contribute to. The labelled cells ventral to the sternum may make up part of the connective tissue, and on the dorsal side they may contribute to the parietal pleura, the lining of the inner surface of the chest wall. These cells migrate with the sternal precursors with a considerable degree of co-ordination, which suggests they may be guided by the same mechanism. The labelled cells within the sternum extend as far as the sternal midline, but do not cross over it, suggesting that cells from each of the left and right sternal bands do not mix following sternal band fusion (Figure 6C). These embryos were harvested soon after sternal band fusion, so it remains is possible that the cells mix across the midline at later stages. Together, these results confirm that at HH20, the sternal precursors reside within a region of the somatic lateral plate mesoderm ventral to the forelimb bud and adjacent to somites 14-21.

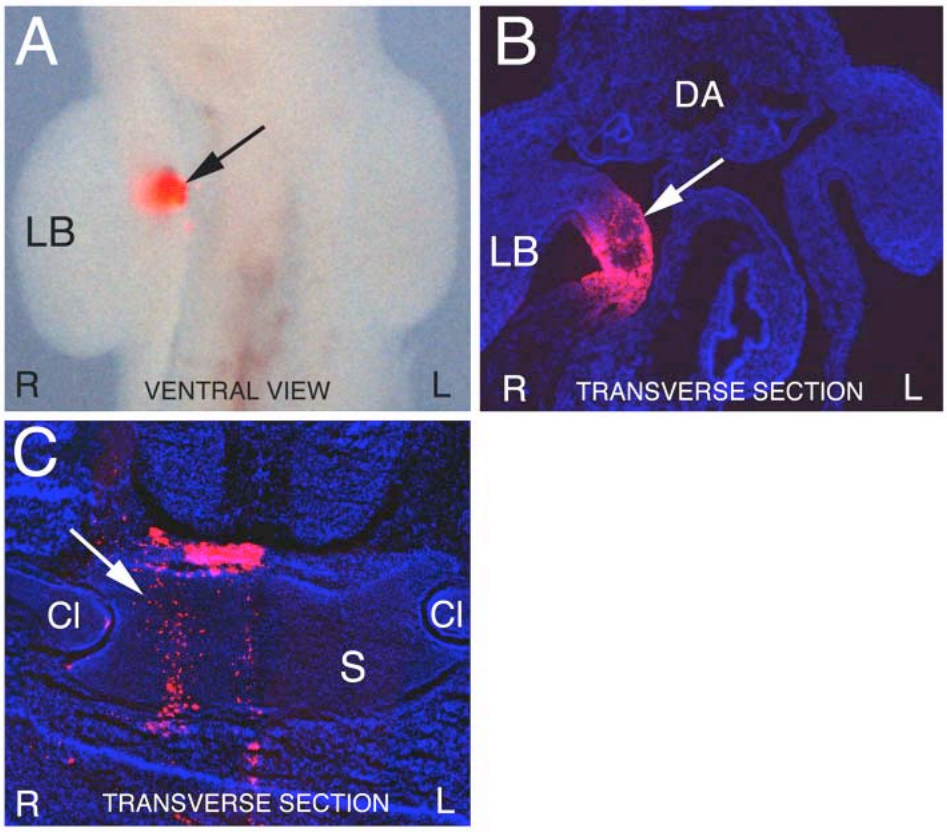

Figure 6. DiI injection site labelling and DiI-positive cells within the sternum at HH36.

A, Ventral wholemount view and **B**, transverse section of HH20 embryos showing DiI-labelling (red, indicated by arrows) following injection into site 4. Internal organs have been removed for clarity in A. **C**, Section through a harvested embryo at HH36 following injection into site 4, showing DiI-labelled cells (red) within the sternum (S; white arrow), and the surrounding tissues. Sections are counterstained with DAPI (blue). Limb bud (LB), dorsal aorta (DA), clavicle (Cl), right and left (R and L).

3.2 The Sternal Precursors do not reside within the Limb Bud

A potential caveat to the interpretation of DiI labelling experiments is that only a small population of cells can be labelled at once, so it is not possible to follow the lineage of all of the limb bud cells and definitively state that none go on to contribute to the sternum. Therefore grafting experiments were conducted to follow the lineage of all the cells within the forelimb bud and directly assess any contribution to the sternum.

Forelimb bud grafting experiments were carried out using fertile eggs from a chicken line that ubiquitously expresses Green Fluorescent Protein (GFP) (McGrew *et al.* 2004). GFP-expressing chicks were incubated alongside non-transgenic chicks until HH20, at which point stage-matched pairs were selected and the entire right forelimb buds of both embryos were completely removed. The GFP donor embryo limb bud was then grafted into place in the non-transgenic host and secured with platinum wire, as shown in Figure 7. Operated embryos were left to develop until HH36, by which time the sternal bands have fused. This strategy allows cells derived from grafted tissue to be distinguished from host tissues, and the GFP signal will not weaken or become diluted over time. Operations were carried out at HH20 to maintain consistency with the timing of DiI labelling experiments. However, a potential caveat to this approach is the possibility that the precursors may be present within the limb bud earlier than HH20 and could migrate out prior to this stage.

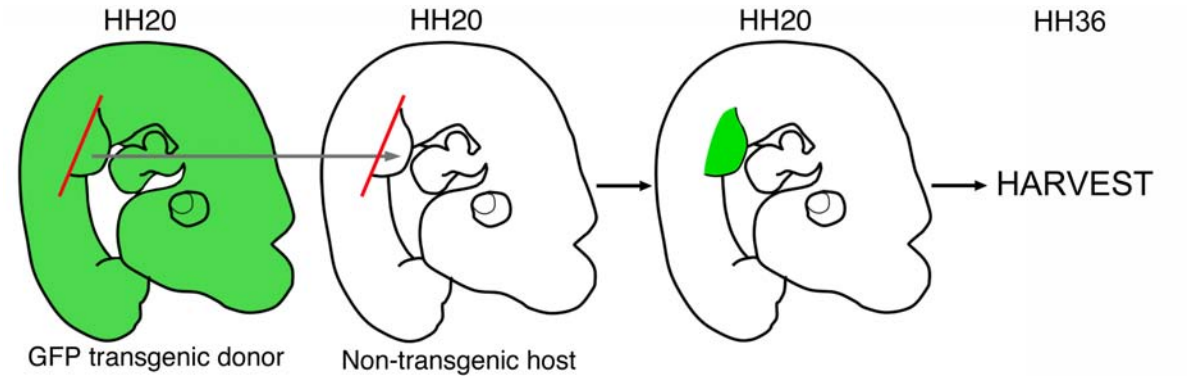

Figure 7. Schematic showing the strategy for grafting GFP-expressing limb buds.

Whole HH20 GFP-expressing transgenic limb buds were grafted into stage-matched non-transgenic host embryos and left to develop, before harvesting at HH36.

In a number of harvested embryos, the grafted forelimb buds were able to heal successfully and continue to develop to form a limb, although the grafted limbs are reduced in size compared to contralateral control (left) forelimbs (Figure 8A, N=5/11). GFP-positive cells are visible throughout the grafted limb and also within the ventral body wall, extending as far as the ventral midline (Figure 8A, N=5/5). Dorsal views also reveal that GFP-positive cells have migrated medially into the dorsal thorax, apparently contributing to the dorsal musculature (Figure 8A, inset).

Grafted embryos were sectioned to determine the tissue layer in which the GFP donor cells are residing and particularly whether they are found in the sternum. Sections were also stained using an anti-muscle myosin antibody (My32), which detects skeletal muscle. Figure 8B shows that the sternum forms normally in grafted embryos and is not composed of any GFP expressing cells, confirming that the sternum precursor cells do not reside within the limb bud proper. Immunostaining with the anti-muscle myosin antibody demonstrates that the GFP-positive cells within the thorax of grafted embryos contribute to the pectoral muscle (Figure 8B). At HH20 (at least some of) the pectoral muscle precursors are located within the limb bud, and following grafting they migrate out across the thorax of the host embryo. However none of the cells within the forelimb bud at HH20 contribute to the sternum.

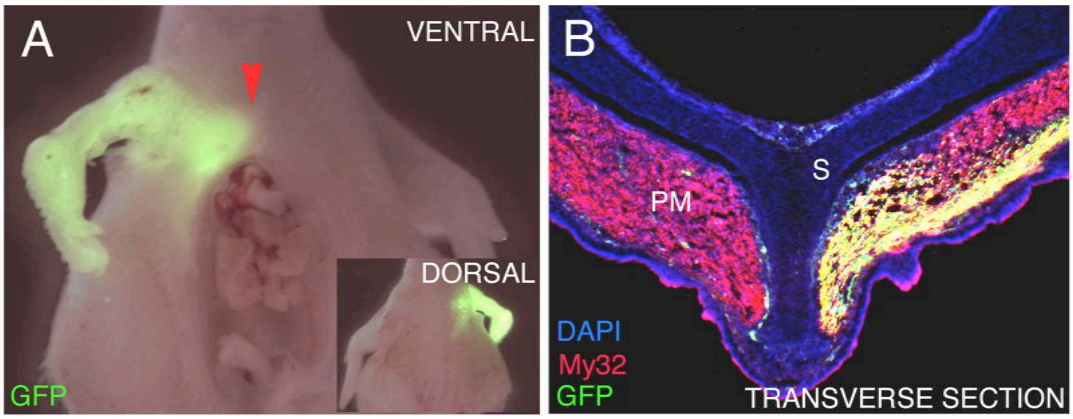

Figure 8. Grafted GFP chick limb bud tissue does not contribute to the sternum.

A, Wholemount HH36 embryo in ventral and dorsal (inset) view showing GFP expressing cells in the thorax and extending towards the ventral midline (red arrowhead) and dorsal midline (inset), (N=5)**. B,** Transverse section with immunohistochemical staining for GFP (green), skeletal muscle (My32, red) and nuclei (DAPI, blue) shows that the GFP labelled tissue does not contribute to the sternum (S), but does contribute to the pectoral muscle (PM).

3.3 Mapping the Time-Course of Sternum Precursor Migration

I set out to establish the spatio-temporal movements of the sternum precursor cells in their path from the somatic lateral plate mesoderm to the ventral midline. Embryos were DiI labelled within the region known to encompass the sternal precursors (sites 2-6) and were harvested at a range of stages prior to HH36 (Figure 9). Since the sternal bands have not yet fused at these stages, it is difficult to distinguish the sternum precursor cells from any other cell types.

The migratory path of the DiI-positive cells observed in HH26 and HH30 embryos appears to be directly medial, with cells forming a streak extending from just ventral to the proximal end of the limb, to the medial edge of the ventral body wall (Figure 9A-B,E-F,I-J). By HH34 the DiI labelled cells have spread rostrally and caudally in addition to moving medially at the leading edge of the body wall as it closes (Figure 9C,G,K). In some cases, a subset of the labelled cells have formed a band-like pattern at the medial extent of the body wall (Figure 9K), reminiscent of the sternal bands. The DiI labelled cells reach the ventral midline by HH36 and form a straight rostro-caudally oriented line (Figure 9D,H,L).

At all observed stages, DiI labelled cells are situated at the most medial edge of the body wall as it closes. This was also suggested by Chen in the mouse (Chen 1952) and Murillo-Ferrol in the chick (Murillo-Ferrol 1963). The movement of the sternal precursors across the thorax is not a migration through a static, fixed substrate, but rather a movement ‘en bloc’ alongside the other tissues of the ventral body wall, such as the ribs and pectoral muscle precursors. The closing body wall is comprised

of a mixed lineage of cells, deriving from the LPM, as well as the somites, and it is not clear which cells are driving this movement.

Examining the distribution of DiI-positive cells throughout the rostro-caudal length of the midline suggests that not all injection sites contribute equally to the sternum (Table 2, far right column, Figure 5C-G, Figure 9D,H,L). Although there is clearly movement of cells along the rostro-caudal axis of the sternal precursor population as they migrate, it appears that cells situated in the most rostral region of the sternum precursor population (sites 2 and 3) tend to show a rostral bias in their contribution to the sternum (Figure 5C-D, Figure 9D, Table 2, N=3/4). Similarly, cells in the caudal most region of the sternal precursor population (site 6) tend to show a caudal bias to their contribution to the sternum (Figure 5G, Table 2, N=2/4). Cells in the middle of the precursor domain do not appear show any bias and contribute to the entire length of the sternum.

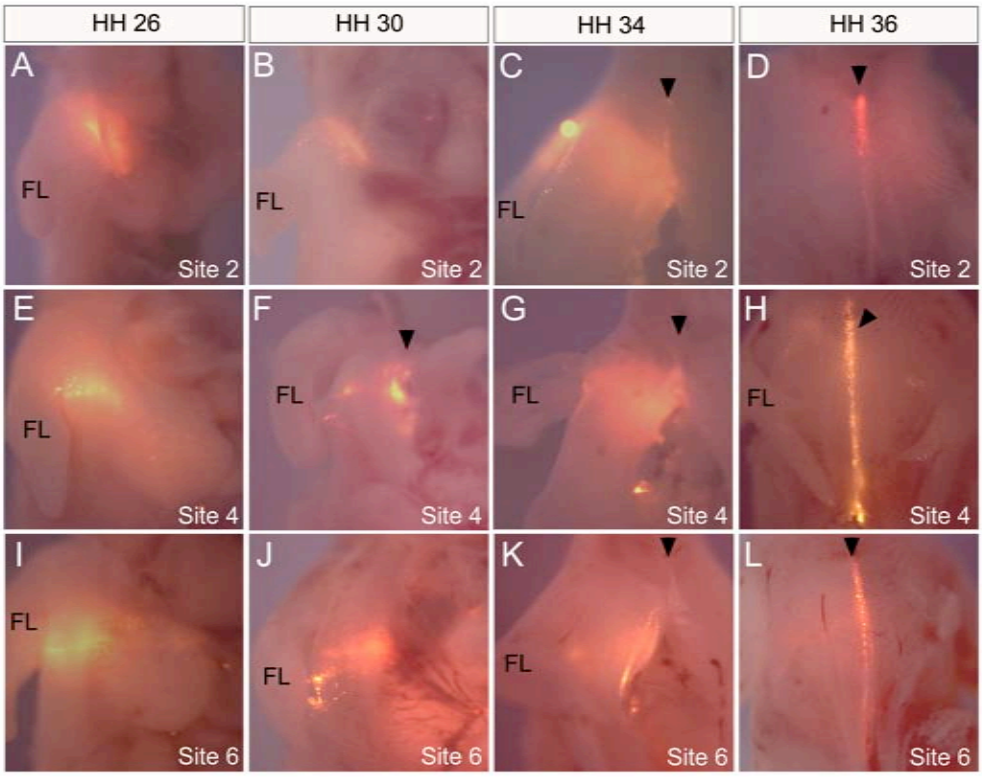

Figure 9. Time-course of the migration of DiI labelled cells toward the ventral midline.

Ventrolateral views of embryos injected at site 2 (**A-D**), site 4 (**E-H**) and site 6 (**I-L**) and harvested at HH24 (**A,E,I**), HH30 (**B,F,J**), HH34 (**C,G,K**) and HH36 (**D,H,L**). Harvested embryos show the distribution of DiI-positive cells as they move medially across the thorax. The right forelimb (FL) and midline (black arrowhead) are indicated.

Overall, fate mapping work using DiI injections and GFP limb grafting has shown that the sternum precursor cells do not reside within the limb bud proper at HH20. Instead they are located in an area of the somatic LPM situated ventral to the forelimb bud, adjacent to somites 14 to 21. Other cell types, such as pectoral muscle precursor cells also migrate from the limb bud into the thorax, but do not accumulate at the midline. It appears that the sternal precursors migrate initially as a loose stream of cells. Between HH30 and HH34, they aggregate to form bands of cells that complete the medial movement to ultimately fuse with an equivalent band of cells that has migrated from the opposite flank of the embryo.

Chapter Four:

The Role of *Tbx5* in Sternum Formation

Chapter Four: The Role of *Tbx5* in Sternum Formation

Chapter Summary

In Chapter four I address the genetic regulation of sternum formation, and particularly the role played by *Tbx5* in this process. Holt-Oram syndrome is caused by mutations in *TBX5* and results in aberrant development of the upper limbs, heart and sternum (Newbury-Ecob *et al.* 1996; Basson *et al.* 1997). While *Tbx5* function in forelimb and heart development have been well studied, its requirement in sternum formation is not yet understood.

In this chapter, a combination of gene expression and mutant phenotype analysis are used to gain an insight into the role of *Tbx5* in sternum development. I begin by detailing the sternal phenotype of mice where *Tbx5* is deleted in the postcranial LPM. The expression pattern of *Tbx5* in the ventral body wall of chick and mouse embryos is analysed using *in situ* hybridisation in addition to a *Tbx5* reporter transgene. I also use *Runx1* expression to mark the position of the sternum precursor cells in control and *Tbx5* conditional mutant mice to elucidate the nature of the role played by *Tbx5* in sternum development. Finally, *Fgf10* and *Cx40* are explored as potential downstream targets of *Tbx5* in the sternum.

4.1 *Tbx5* is Required for Forelimb and Sternum Formation

Tbx5 deficient murine embryos die early during development due to heart defects (Basson *et al.* 1999), but this can be bypassed by conditional deletion of *Tbx5* exclusively in LPM derived structures using the *Prx1Cre* transgene (Logan *et al.*

2002). These mice survive to birth but completely fail to form forelimbs. (Rallis *et al.* 2003). *Prx1Cre* activity in the forelimbs has been characterised previously (Logan *et al.* 2002), but the extent to which this domain extends into the ventral body wall has not been studied in any detail.

The *Prx1Cre* mouse line was crossed to a *Rosa26lacZ* reporter line to establish the region of *Tbx5* deletion in the ventral body wall of $Tbx5^{lox/lox}$*;Prx1Cre* mice. *Rosa26lacZ; Prx1Cre* embryos were harvested from E10.5 to E13.5 and stained with X-gal to visualise the *lacZ* expression pattern (Figure 10). At E10.5, *lacZ* activity is visible throughout the limb bud and extends a short distance into the body wall in rostral, caudal and ventral directions (Figure 10A,E). By E11.5, *lacZ* expression in the body wall extends a short distance rostral to the forelimb, and is continuous between the forelimb and hindlimb. The ventral domain of *lacZ* staining has expanded across the thorax, with a scattering of *lacZ* positive cells visible even further ventral to this region (Figure 10B,F). The forelimbs and entire ventral body wall are covered by weak *lacZ* staining by E12.5 and E13.5 (Figure 10C-D,G-H). However, the *lacZ* expression domain extends only a very short distance dorsal to the limbs. This staining pattern shows that the *Prx1Cre* transgene is active in the ventral body wall in the region that encompasses the sternal precursors, as established in fate mapping experiments in Chapter 3.

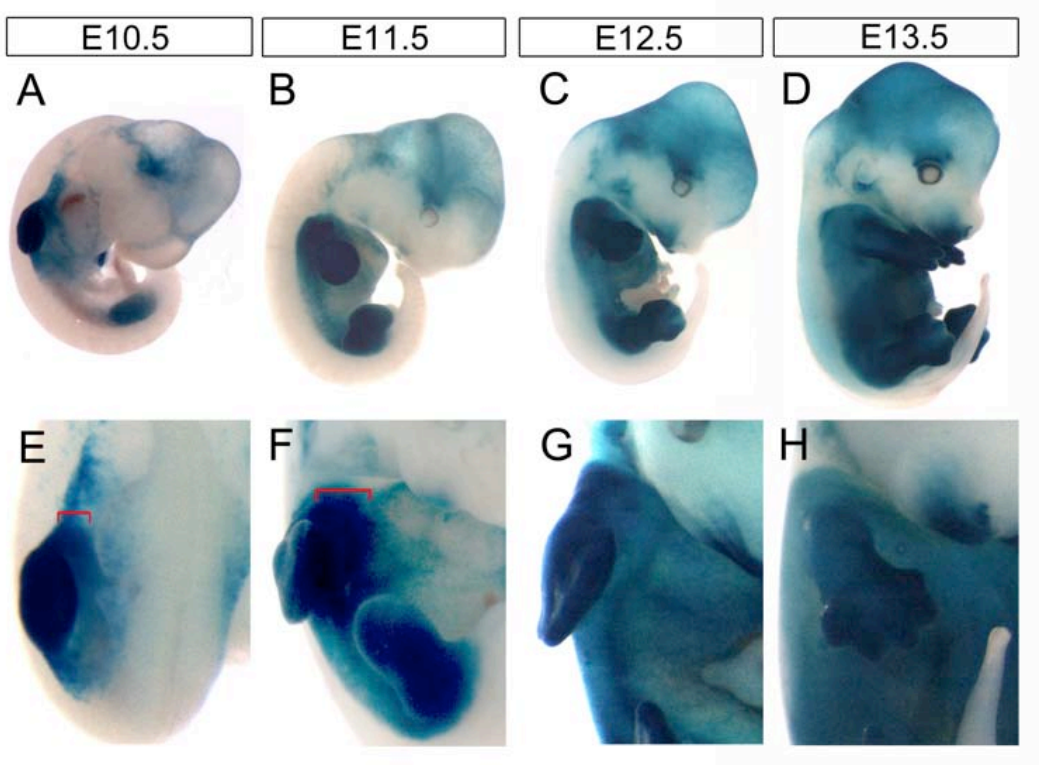

Figure 10. *Cre* activity is visible throughout the limbs and extends into the ventral body wall of *Rosa26lacZ; Prx1Cre* embryos.

X-gal stained transgenic mice at E10.5 (**A,E**), E11.5 (**B,F**), E12.5 (**C,G**) and E13.5 (**D,H**) are shown in lateral (**A-D**) and ventro-lateral views (**E-H**). The domain of *lacZ* staining in the ventral body wall is highlighted (red bracket).

I conditionally deleted *Tbx5* using the *Prx1Cre* transgene, generating *Tbx5*$^{lox/lox}$*;Prx1Cre* mice, which die shortly after birth due to breathing difficulties (Rallis *et al.* 2003). *Tbx5*$^{lox/lox}$*;Prx1Cre* mice fail to form forelimbs (Rallis *et al.* 2003) and also completely lack a sternum (Figure 11A-B,D-E). In the absence of a sternum the distal ribs have no medial attachment sites and the ribcage fails to close, often with ribs fusing together at their distal tips. In some cases this is also associated with failure of abdominal body wall closure and herniation of internal organs (discussed in Chapter 6.1.4), but in many embryos, the ventral body wall is able to close, despite the absence of a sternum (Figure 11B, E). This striking phenotype demonstrates that although the sternum and forelimbs occupy distant final positions within the skeleton, *Tbx5* plays an essential role in both sternum and forelimb development.

The only known downstream target of *Tbx5* in the forelimb is *Fgf10* (Ng *et al.* 2002). *Fgf10* plays a crucial role in limb development, and both the forelimbs and hindlimbs are completely absent in *Fgf10*$^{-/-}$ mice, with the exception of the scapula and a rudimentary pelvic girdle (Sekine *et al.* 1999). However, the sternum forms almost completely normally in the absence of *Fgf10* (Figure 11C,F). The sternal bands reach the midline and fuse, but ossification of the sternebrae appears slightly misspatterned in some embryos. This may be a result of misaligned attachment of the ribs to the sternum, as the ribcage overall appears narrower, possibly due the absence of lungs in these mice (Sekine *et al.* 1999). Together, these results demonstrate that *Tbx5* plays a crucial role in the developing sternum and forelimbs, but in the sternum this

role is independent of *Fgf10*. *Tbx5* must therefore act through downstream target(s) other than *Fgf10* in its role(s) in sternum formation.

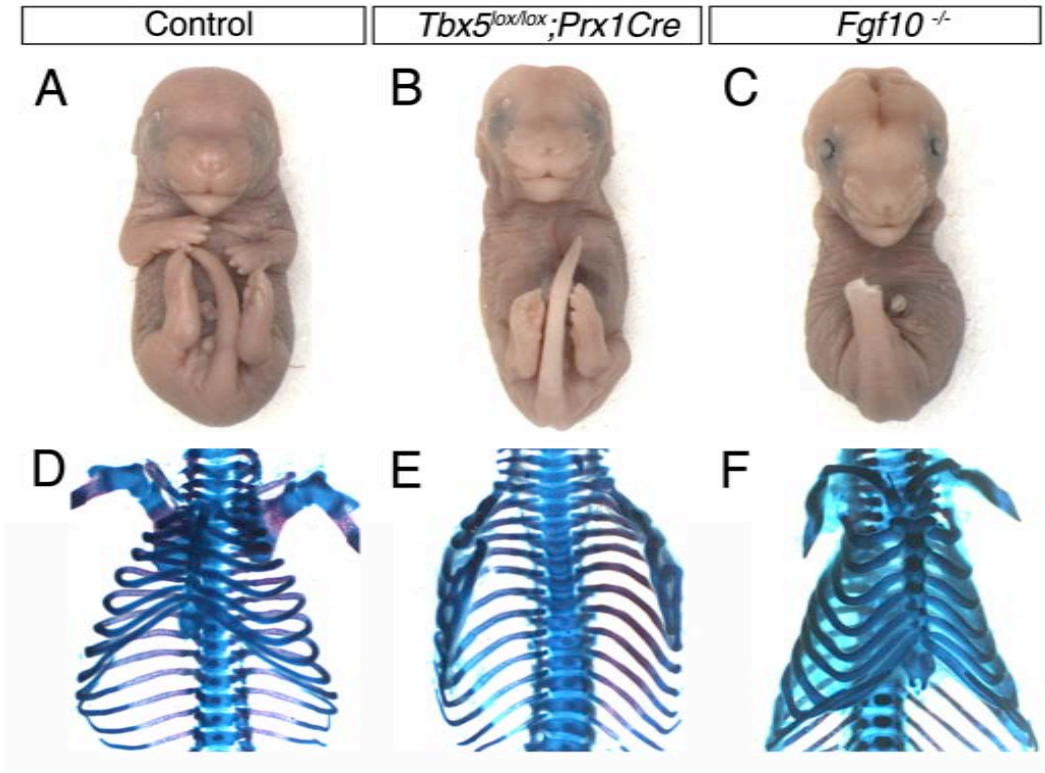

Figure 11. The sternum and forelimbs fail to form in the absence of *Tbx5*.

Ventral views of control (**A,D**), *Tbx5* conditional mutant (*Tbx5*$^{lox/lox}$*;Prx1Cre*) (**B,E**) and *Fgf10* mutant (*Fgf10*$^{-/-}$) (**C,F**) embryos at E17.5. **A,B,C**, in wholemount and **D,E,F,** alcian blue/alizarin red skeletal preparations. The most distal forelimb structures have been cropped in the control panel.

To further characterise the ventral body wall defects arising in *Tbx5*$^{lox/lox}$*;Prx1Cre* mice, embryos were stained in wholemount and in section using an antibody that recognises muscle myosin. According to the 'in-out' model, the precursor cells of the superficial muscles of the pectoral girdle, including the pectoral muscles, migrate from the somites into the proximal forelimb bud, before moving into the trunk and migrating towards the midline. In contrast, the deeper girdle muscle such as the serratus anterior extend directly from the somites (Valasek *et al.* 2011). The behaviour of the pectoral muscle precursors in the absence of forelimbs was analysed in *Tbx5*$^{lox/lox}$*;Prx1Cre* and *Fgf10*$^{-/-}$ mice.

In control embryos, the pectoral muscle is visible in the ventral body wall and can be seen attached to the sternum (Figure 12A,D). In contrast, wholemount *Tbx5*$^{lox/lox}$*;Prx1Cre* embryos display almost no pectoral muscle. The serratus anterior and external oblique muscles form normally, but only a thin layer of muscle cells are visible in the ventral region of the thorax (Figure 12B,E). This suggests that in the absence of *Tbx5*, the vast majority of the pectoral muscle precursor cells are unable to complete their 'in-out' migration.

Fgf10$^{-/-}$ mice provide an interesting comparison for this analysis, as they do not form forelimb buds, but show normal ventral body wall closure and normal sternum development. In these embryos the pectoral muscle develops normally and can be seen attaching to the sternum (Figure 12C,F), suggesting that pectoral muscle precursors are able to migrate to their final position in the absence of forelimbs. These results challenge the 'in-out' migration hypothesis, demonstrating that the

pectoral muscle precursors do not need to migrate into a limb bud proper, but perhaps the *Tbx5* expressing, but not *Fgf10*-expressing cell population provides enough information to allow these cells to migrate to their final position in the thorax.

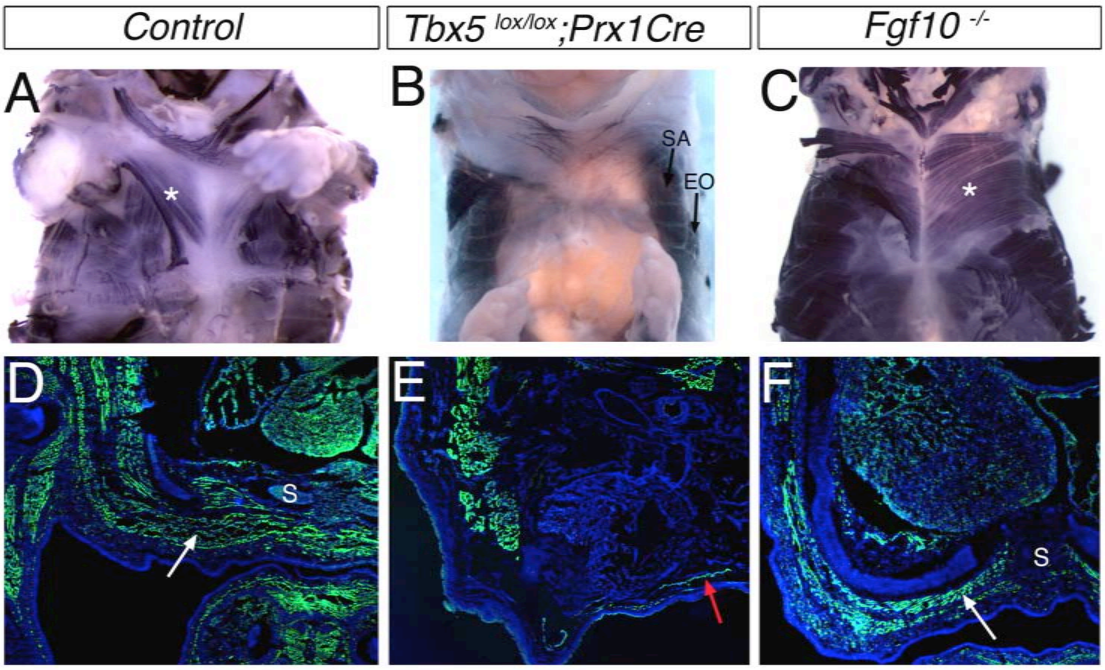

Figure 12. The pectoral muscle is dramatically reduced in the absence of *Tbx5*.

A-C, ventral views of wholemount embryos at E16.5 stained with an alkaline phosphatase conjugated anti-muscle myosin antibody. **D-F**, transverse sections through E16.5 mice stained with an anti-muscle myosin antibody (green) and DAPI (blue). Control (**A,D**) and *Fgf10*$^{-/-}$ (**C,F**) embryos show pectoral muscle throughout the ventral body wall (white asterisks, white arrows) and attaching to the sternum (S), while *Tbx5*$^{lox/lox}$*;Prx1Cre* embryos (**B,E**) show only a very thin layer of pectoral muscle cells (red arrow), although the serratus anterior (SA) and external oblique (EO) muscles are still present.

4.2 Analysing the Expression of *Tbx5* and *Fgf10* in the Body Wall

To determine where and when *Tbx5* may be acting in sternum development, the spatio-temporal expression patterns of *Tbx5* and *Fgf10* in the developing chick embryo were analysed by wholemount *in situ* hybridisation. Stages ranging from HH18 to HH24 were deemed to be the most relevant to the role of *Tbx5* in sternum development, as it is likely that *Tbx5* is required at some stage after the initiation of LPM differentiation to form a forelimb bud at HH16, and prior to the condensation of the sternal bands at HH32 (Bellairs *et al.* 2005). Furthermore, my fate mapping analysis has revealed the location of the sternal precursors at limb bud stages (HH20 onwards) during chick development, which will allow us to determine whether *Tbx5* is expressed in the sternal precursor population.

Tbx5 is expressed throughout the early forelimb bud at HH18 (Figure13A). From HH20 onwards, this expression domain extends ventrally beyond the forelimb bud into the ventral body wall (Figure 13B,C). By HH24 this domain has expanded further both ventrally and caudally within the thorax (Figure 13D). The ventral expansion of *Tbx5* expression overall appears coincident with the migratory path of the sternum precursor cells identified by fate mapping (Chapter 3). In contrast to the expression of *Tbx5* in the ventral body wall, *Fgf10* expression is restricted to the limb buds and does not extend into the thorax at any of the stages studied (Figure 13E-H). This observation is consistent with the role of *Fgf10* in limb development (Sekine *et al.* 1999; Ng *et al.* 2002), confirming that *Fgf10* does not play a role downstream of *Tbx5* in sternum development. The position of the population of *Tbx5* positive, *Fgf10* negative cells, lying just ventral to the limb bud at HH20 (Figure

13B,F), correlates with the population of sternal precursors identified in the fate mapping studies (Figure 5A). This suggests that the sternal precursors reside within a *Tbx5*-positive, *Fgf10*-negative population of cells. Importantly, these results do not distinguish whether the precursors themselves express *Tbx5,* as there are multiple cell types within this population.

There is an area of the flank immediately adjacent to the forelimb that appears to show fewer *Tbx5* positive cells (Figure 13B,C,D). It is possible that there are two separate domains of *Tbx5* expression on either side of the embryo from HH20 onwards, one in the limb and one encompassing the sternum precursor cells. However, it is also possible that the reduced staining is an artefact resulting from poor penetration of the probe in this region, and that the two regions visible have a greater density of *Tbx5*-positive cells. Overall, it is clear that the *Tbx5* expression domain encompasses the sternum precursor cells, while the *Fgf10* expression domain does not.

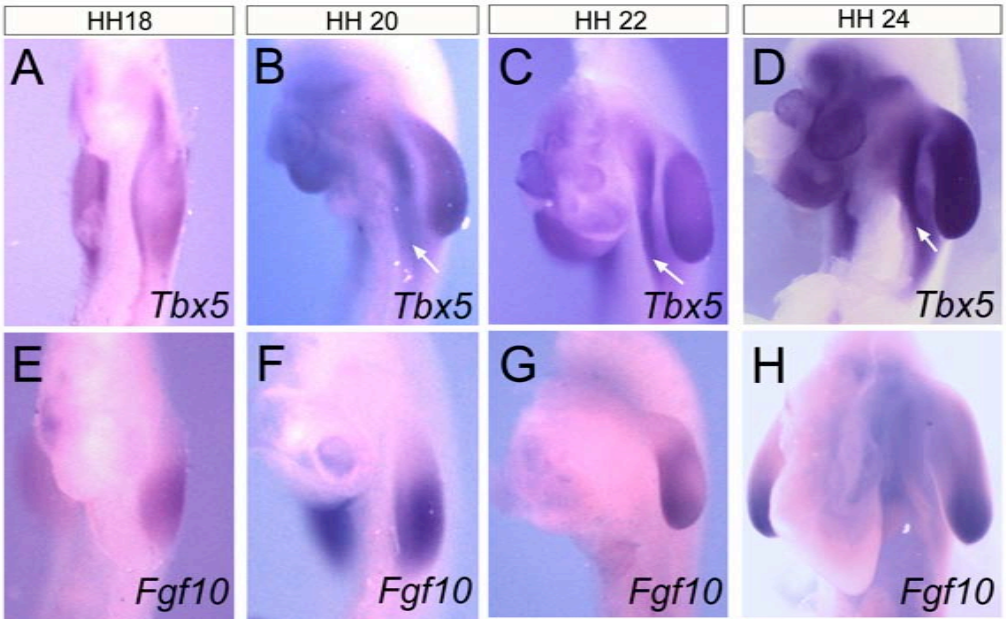

Figure 13. The chick *Tbx5* expression domain extends into the thorax, while *Fgf10* is restricted to the limb bud.

Ventrolateral views showing wholemount *in situ* hybridisation results for *Tbx5* (**A-D**) and *Fgf10* (**E-F**) expression in the forelimb and ventral body wall (white arrows) at HH18 (**A,E**), HH20 (**B,F**), HH22 (**C,G**) and HH24 (**D,H**) chick embryos.

I examined the expression of *Tbx5* in the ventral body wall of developing mouse embryos. Embryos from early limb bud stages (E10.5) up to the point of sternal band fusion (E13.5) were analysed (Figure 14). At E10.5 the expression of *Tbx5* appears to be mostly restricted to the forelimb bud, with faint staining visible in the flank slightly caudal and ventral to the bud (Figure 14A). By E11.5 this expression domain has expanded further both ventrally and caudally into the thorax, and at the medial border of this domain, appears to form a segmented pattern (Figure 14B). This takes the form of two parallel stripes of *Tbx5* positive cells oriented diagonally across each side of the thorax and joined by alternating bands of *Tbx5* positive and *Tbx5* negative cells. At E12.5 and E13.5, the bands have moved further across the thorax, and the segmented pattern is less obvious (Figure 14C, D). The bands of *Tbx5* expression are observed in a position consistent with that of the sternal bands. For example, the *Tbx5* expression domains appear to join at their rostral most ends at the midline at E13.5 (Figure 14D), which is the same stage that the sternal bands also begin to merge at the midline at their rostral tips (Chen 1952). This supports the data in the chick suggesting that the sternal precursors are located within the population of *Tbx5* positive cells.

Chick and mouse *Tbx5* expression patterns show many broad similarities over the stages studied in Figure 13 and Figure 14. The expression domain in both cases extends across the thorax medially and caudally over time, forming band-like structures that run in a rostral to caudal direction. The region displaying fewer *Tbx5*-positive cells immediately adjacent to the limb is also present in both species, becoming more apparent by E13.5 in the mouse. A key difference between the

expression of *Tbx5* in mouse and chick is that the segmented expression pattern is present exclusively in the mouse. In the chick, *Tbx5* expression appears to be completely continuous along the rostro-caudal axis of the expression domain, but in the mouse the ladder-like pattern is clear.

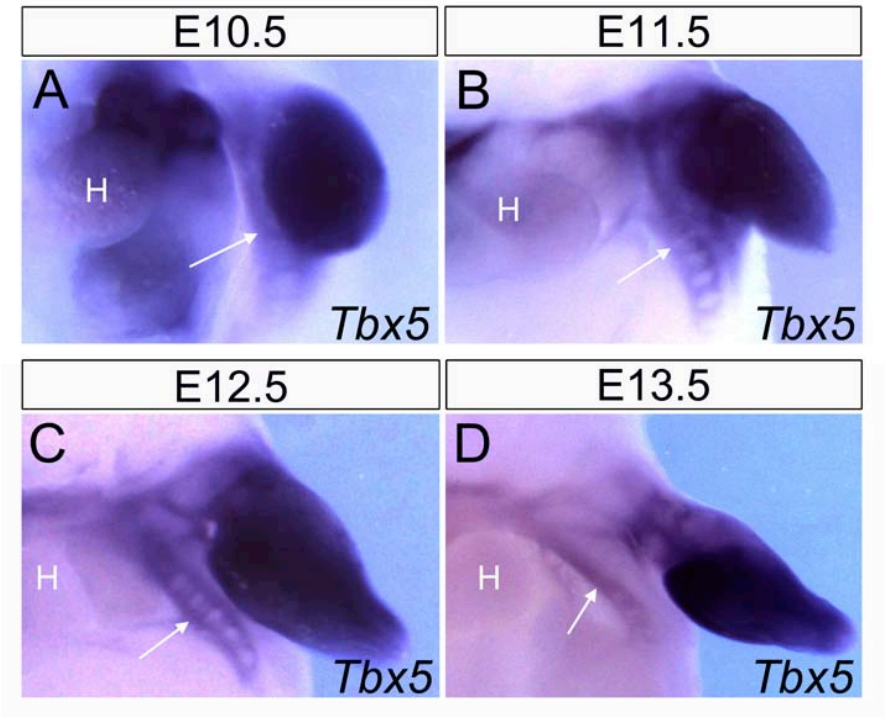

Figure 14. The *Tbx5* expression domain in the mouse extends into the thorax.

A-D, Ventrolateral views showing *Tbx5* expression in the forelimb and ventral body wall detected by *in situ* hybridisation in E10.5-E13.5 mouse embryos. Bands of *Tbx5*-positive cells (arrows) and heart (H).

4.3 Analysis of *Tbx5Intron2lacZ* Reporter Gene Expression

Wholemount *in situ* hybridisation can be unreliable at stages later than E13.5 due to poor penetration of the probe through larger embryos. Therefore to examine the *Tbx5* positive population of cells in the ventral body wall over a wider range of stages, I used a *Tbx5* reporter mouse line. The minimal regulatory element necessary for the earliest forelimb restricted expression of *Tbx5* has been identified (Minguillon *et al.* 2012) and used to produce a stable transgenic *lacZ* reporter mouse line, called *Tbx5Intron2lacZ* (Figure 15A, Minguillon et al., unpublished). This transgenic mouse line provides an opportunity to study the lineage of cells in which the transgene promoter is active. However, it is important to note that *Tbx5Intron2lacZ* expression may not represent the endogenous expression of *Tbx5*, rather it represents a read-out of the activity of a single, isolated regulatory element integrated randomly into the mouse genome. *Tbx5Intron2lacZ* expression data, supported by *in situ* hybridisation results can provide a representation of *Tbx5* expression.

Wholemount X-gal staining of *Tbx5Intron2lacZ* embryos at E10.5 reveals *lacZ* staining throughout the forelimb bud and extending a small distance medially into the ventral body wall (Figure 15B,F). Additionally, the flank lying caudal to the forelimb, and a smaller region lying rostral, is also *lacZ*-positive. By E12.5 the *lacZ*-positive cell population has spread further across the ventral body wall (Figure 15C,G) with the most medial cells in a position reminiscent of mouse *Tbx5* expression detected by *in situ* hybridisation (Figure 14).

The *lacZ*-positive population of cells has reached the midline by E14.5, with just a narrow band of *lacZ* negative cells visible at the midline (Figure 15D,H). This *lacZ*

negative band is still present at E16.5 (Figure 15E,I), which is surprising since the sternal bands have fully fused by this stage, and so it might be expected that the entire sternum would express *lacZ*. On either side of this *lacZ* negative strip, a strong band of staining has accumulated. This corresponds to the position of the sternum precursor cells and indicates that the *Tbx5Intron2lacZ* transgene marks at least a subset of the population of cells within which the sternal precursors reside.

Horizontal stripes of *lacZ* negative cells on either side of the thorax make up the ribs, which have a distinct embryological origin to the sternum, and do not express *Tbx5* at any stage. The remainder of the thorax is *lacZ*-positive, which suggests that the *Tbx5Intron2lacZ* promoter element has been active in many of the cells residing in the ventral body wall. This is surprising, as the pectoral muscle and ribs are known to be *Tbx5*-negative, and will be addressed in further detail in Figure 16 and Figure 17. Examining the autopod of *Tbx5Intron2lacZ* mice from E12.5 onwards reveals that the anterior-most two digits and the anterior half of the third digit are *lacZ* negative (Figure 15C-E). This is not representative of the endogenous *Tbx5* expression pattern, as *Tbx5* expression is ubiquitous throughout the forelimb mesenchyme at later stages (Figure 14; Rallis *et al.* 2003).

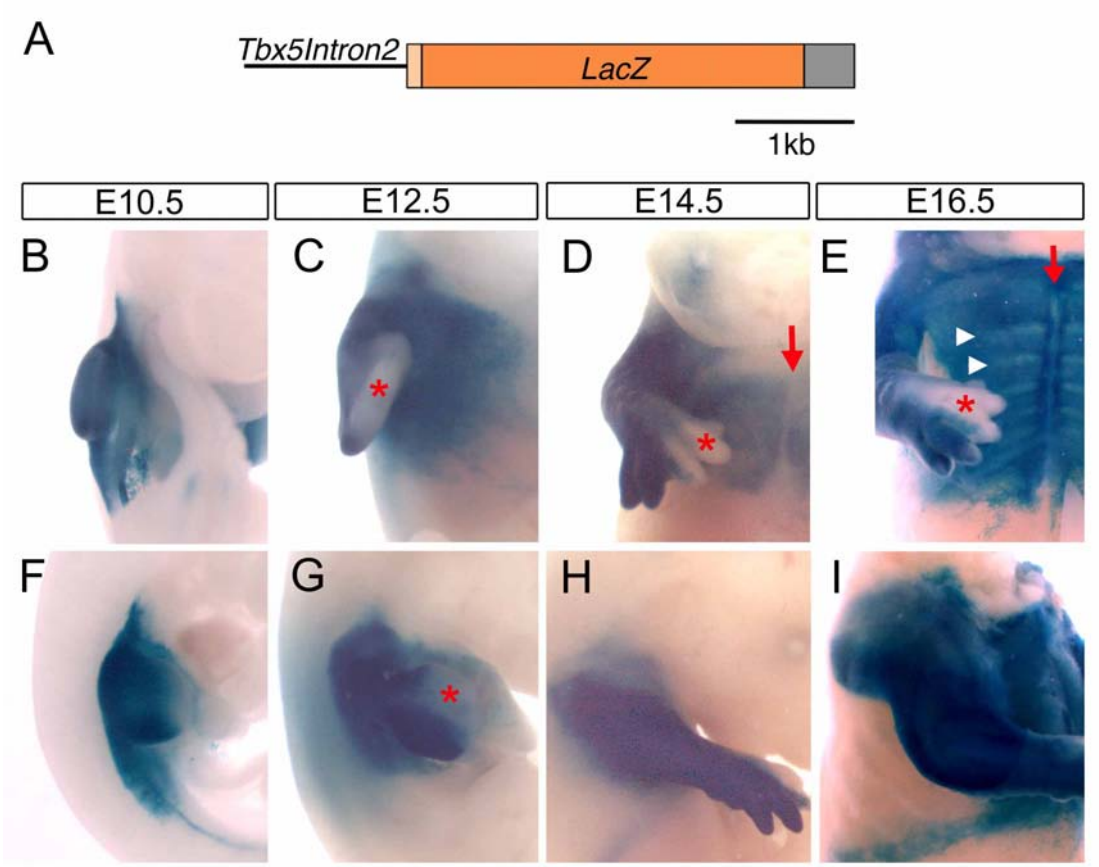

Figure 15. Wholemount X-gal staining of *Tbx5Intron2lacZ* reporter mice.

A, The *Tbx5Intron2lacZ* transgenic construct. The *Intron2* regulatory sequence (thin black line) was cloned into the BGZA reporter vector, which contains the chick β-globin minimal promoter (light orange box), the *lacZ* gene (dark orange box) and an SV40 polyadenylation signal (grey box). Ventral (**B-E**) and lateral (**F-I**) views of the thoracic region of *Tbx5Intron2lacZ* embryos at E10.5 (**B,F**), E12.5 (**C,G**), E14.5 (**D,H**), E16.5 (**E,I**). *LacZ* positive cells make up the limbs and spread across the ventral body wall, with the exception of the ribs (white arrowheads), the anterior region of the autopod (red asterisks) and the midline of the sternum (red arrows). Heads have been removed to allow the entire ventral body wall to be visualised.

The majority of the *lacZ* positive cells are found in embryonic locations that correlate with *Tbx5 in situ* hybridisation analysis (Figure 13,14), and with the location of the sternal bands as established by fate mapping (Chapter 3). Taken together, the *in situ* hybridisation, fate mapping and *Tbx5Intron2lacZ* expression data suggest that it is reasonable to conclude that the sternum precursor cells reside within a population of cells that express the *Tbx5Intron2lacZ* reporter gene. However, the *lacZ* negative cells in the autopod and at the sternal midline and do not correlate with the *in situ* hybridisation or fate mapping data, suggesting that the expression of the reporter gene does not fully recapitulate the endogenous *Tbx5* expression pattern. Therefore there may be caveats to our interpretation of this data. With these limitations in mind, I tentatively pursued the analysis of *lacZ* expression in the ventral body wall further, examining these embryos in transverse section. This made it possible to analyse the distribution of *lacZ*-positive cells within the tissue layers of the ventral body wall.

At E12.5, *lacZ*-positive cells are visible throughout the forelimb bud in *Tbx5Intron2lacZ* embryos. In the body wall streams of cells are visible extending ventrally from the forelimb bud (Figure 16A,A'). These cells appear to be distributed in different layers, separated by a dense region of *lacZ*-negative cells extending ventrally, which are the precursors of the ribs. By E13.5 the body wall has closed further and the streams of *lacZ*-positive cells extend further across the ventral body wall, but do not merge at the midline, appearing to accumulate a short distance from the midline on each side (Figure 16B,B').

At the time of sternal band closure (E14.5) the streams of *lacZ*-positive cells have met at the midline and can be seen to make up the majority of the condensed population of cells making up the sternum (Figure 16C,C'). There is a strip of *lacZ*-negative cells running down the midline of the sternum, consistent with the wholemount data. There is also a strong region of *lacZ* staining immediately ventral of the sternum visible from E14.5, which also does not merge at the midline. If it is assumed that *lacZ* staining is representative of cells that have expressed *Tbx5* at least at some point in the past, this suggests that the cells forming the midline of the sternum have never expressed *Tbx5*. However this is not consistent with chick fate mapping experiments, which showed DiI-positive cells extending as far as the sternal midline (Figure 6).

The ribs can be clearly seen within the ventral body wall as condensed bars of *lacZ*-negative cells lying between the *lacZ*-positive layers. At E12.5 it appears that the *lacZ*-positive cells are migrating ahead of the rib precursors, as they are visible at the leading edge of the ventral body wall at a more ventral position than the tip of the rib tissue (Figure 16A'). By E14.5 the ribs can be seen adjacent to the sternum (Figure 16C').

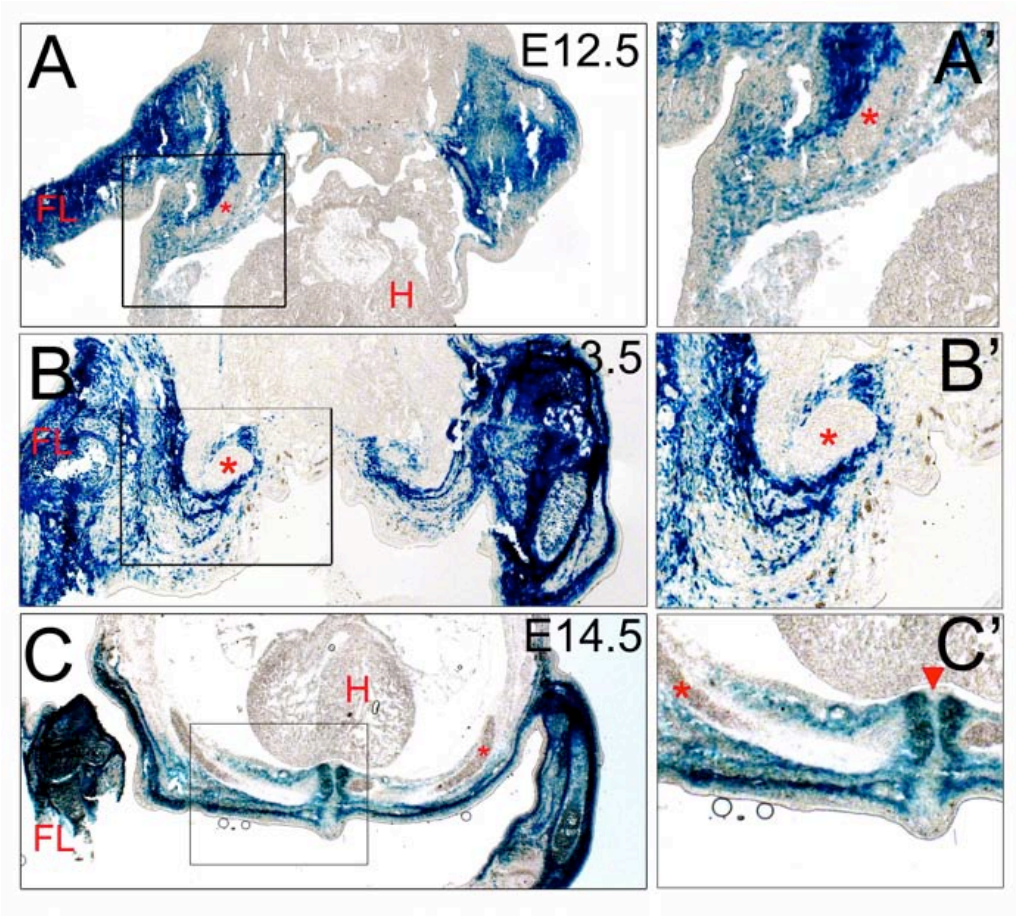

Figure 16. Section X-gal staining of *Tbx5Intron2lacZ* embryos.

Brightfield images of transverse sections showing the ventral body wall of *Tbx5Intron2lacZ* embryos at E12.5 (**A,A'**), E13.5 (**B,B'**), E14.5 (**C,C'**). The region enclosed by black rectangle in A-C is shown in greater detail in A'-C'. Images show *lacZ*-negative cells at the sternal midline (red arrows). The ribs (red asterisk), right forelimb (FL) and heart (H) are labelled.

The contribution of *lacZ*-positive cells to the various tissue layers within the ventral body wall was analysed by staining sections with antibodies specific to skeletal muscle, cartilage, and connective tissue (Figure 17). Examining the expression of Col2, a marker of cartilage, confirms that the *lacZ* transgene is not expressed in the ribs, although streams of *lacZ*-positive cells lie in between and ventral to the ribs. Even within the sternum, *lacZ* and Col2 do not appear to be co-expressed (Figure 17A).

An antibody against skeletal muscle, My32 was used in combination with *lacZ* staining to reveal that the *lacZ*-positive cells are My32-negative and so do not contribute to the skeletal muscle (Figure 17B). The streams of *lacZ*-positive cells lie in between the muscle layers in the ventral body wall, suggesting that they may contribute to the muscle connective tissue. To investigate this, I used an antibody raised against the transcription factor Tcf4, which is known to label a subset of muscle connective tissue cells in the limb (Mathew *et al.* 2011). Although some overlap was observed between Tcf4 expression and My32 expression, Tcf4-positive cells were visible within the ventral body wall and in the sternum at E16.5 (Figure 17C). The Tcf4-positive cells visible are *lacZ* negative, which suggests that the *Tbx5Intron2lacZ* reporter is not expressed in the muscle connective tissue cells, or at least those labelled by Tcf4.

The expression of the *Tbx5Intron2lacZ* reporter gene in the ventral body wall was not found to overlap with markers of muscle connective tissue, collagen or skeletal muscle. Therefore it is not clear in which tissue layer these cells reside, but it is

possible that they contribute to connective tissue cells that are not marked by Tcf4, such as the fascia or tendons. In summary, the *Tbx5Intron2lacZ* reporter gene expression pattern is mostly consistent with wholemount *Tbx5* expression in the mouse and chick. However, the absence of transgene expression within the anterior autopod and at the sternal midline suggests that this line does not fully recapitulate the endogenous *Tbx5* expression pattern. However, this line has proven useful in identifying the contribution of *Tbx5* positive cells to the sternum, as wholemount *in situ* hybridisation cannot be carried out for embryos of this size. Overall this data supports previous work on the timing of sternal band migration. It also provides a strong indication that the sternal precursors themselves express *Tbx5* at some point. However, it is not clear which tissue layer the *lacZ*-positive cells within the ventral body wall contribute to.

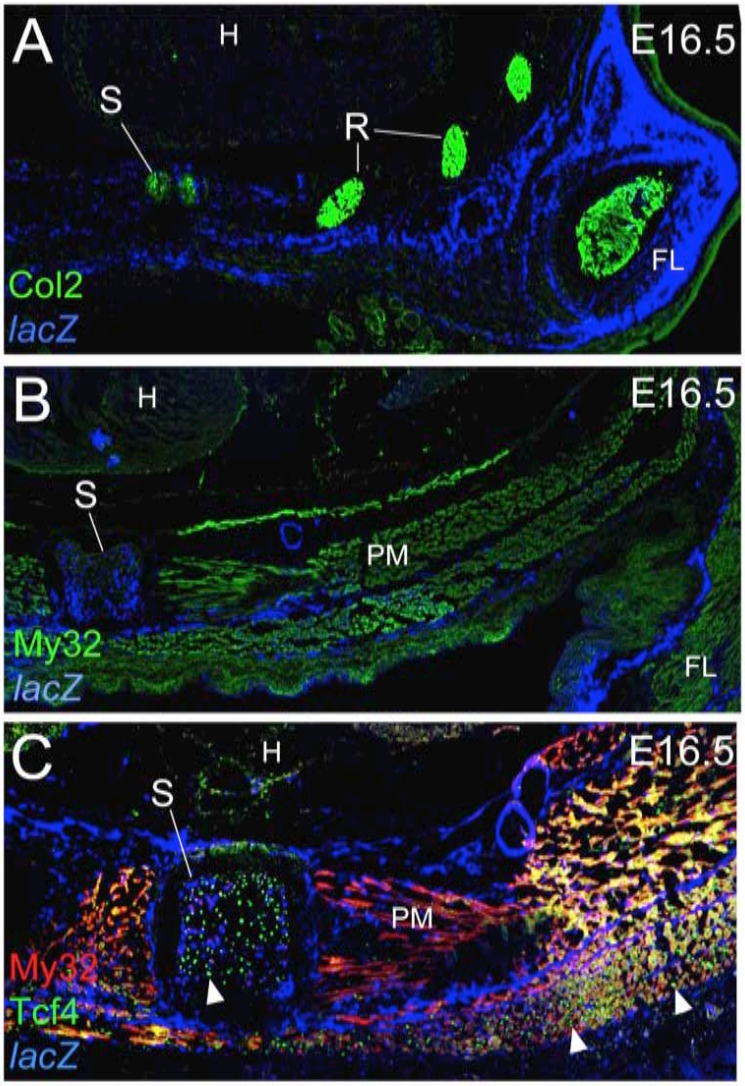

Figure 17. X-gal staining and immunostaining on sections of *Tbx5Intron2lacZ* embryos.

Fluorescence and inverted brightfield images of transverse sections showing the ventral body wall of embryos at E16.5. Sections have been stained with antibodies specific to collagen (Col2, **A**), skeletal muscle (My32, **B**), and connective tissue (Tcf4, **C**). The sternum (S), ribs (R), pectoral muscle (PM), left forelimb (FL) and heart (H) are labelled, and Tcf4-positive, My32-negative cells are shown by white arrowheads.

4.4 *Tbx5Intron2lacZ* Expression in the Absence of *Tbx5* Activity

The *Tbx5Intron2lacZ* analysis was pursued further by generating *Tbx5*$^{lox/lox}$*;Prx1Cre*;*Tbx5Intron2lacZ* mice. This made it possible to examine differences in sternal precursor cell migration under normal and mutant conditions, which could help to further elucidate the role of *Tbx5* in sternum development. *Fgf10*$^{-/-}$*;Tbx5Intron2lacZ* mice were also generated to act as a comparison, representing a situation where *Tbx5* expression is normal, but the embryo does not form limbs.

In *Tbx5*$^{lox/lox}$*;Prx1Cre*;*Tbx5Intron2lacZ* embryos, *lacZ* expression is visible in the most lateral regions of the ventral body wall (Figure 18D-F), but the *lacZ* positive domain does not extend medially, as is the case in the control situation (Figure 18A-C). In particular the rostral half of the thorax of embryos conditionally lacking *Tbx5* shows a much wider domain of *lacZ*-negative cells than control embryos. This demonstrates that the *Tbx5Intron2lacZ* expressing cells do not simply die out in the absence of *Tbx5* activity, but the signals that regulate the *Tbx5* element must still be active in these embryos.

Fgf10$^{-/-}$*;Tbx5Intron2lacZ* embryos show *lacZ* staining consistent with control embryos of the same stage, despite the absence of forelimbs (Figure 18A-C,G-I). This reinforces the argument that *Fgf10* does not play a role in sternum development, and that a different downstream target of *Tbx5* must be required for sternum formation.

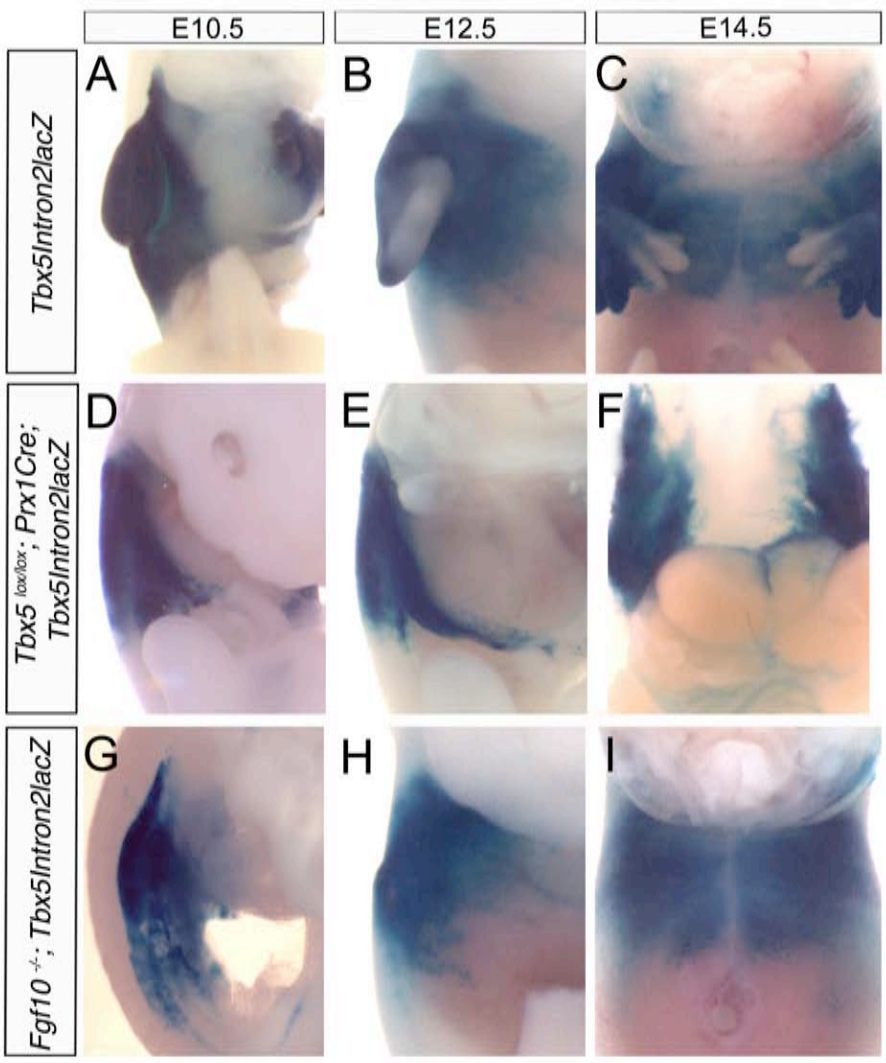

Figure 18. The distribution of *lacZ*-positive cells in the thorax of control and mutant mice.

Wholemount X-gal staining of *Tbx5Intron2lacZ, Tbx5$^{lox/lox}$;Prx1Cre; Tbx5Intron2lacZ* and *Fgf10$^{-/-}$;Tbx5Intron2lacZ* mice is shown in ventro-lateral view at E10.5 (**A,D,G**), and in ventral view at E12.5 (**B,E,H**) and E14.5 (**C,F,I**). Heads have been removed from the majority of embryos for clarity.

4.5 The Sternal Bands Fail to Form in the Absence of *Tbx5*

To understand more fully what happens to the sternum precursor cells in the absence of *Tbx5*, I used *Runx1* as a specific marker of the sternal bands and sternum. *Runx1* is expressed in these tissues but is absent from the ribs, clavicles, limbs and body wall. *Runx1* is required for the ossification of the sternal bands, but not for earlier events in sternum development (Kimura *et al.* 2010; Liakhovitskaia *et al.* 2010).

Wholemount *in situ* hybridisation for *Runx1* in control mouse embryos shows staining in bands on either side of the thorax just ventral to the forelimbs at E12.5 and moving closer towards the midline at E13.5 (Figure 19A,D). The location of these expression domains is consistent with the position of the sternal bands (Figures 9, 13-15; Chen 1952). *Runx1* can therefore be used as a reliable marker of the sternal precursors. Interestingly, at each stage the bands are found at the leading edge of the body wall as it closes, consistent with previous observations in Figure 9,13,14 and 16. Similar to the *Tbx5 in situ* hybridisation data shown in Figure 14, the bands of *Runx1* expression also show signs of segmentation at E13.5 (Figure 19D).

In *Tbx5* conditional mutant embryos (*Tbx5*$^{lox/lox}$*;Prx1Cre*) the bands of *Runx1* positive cells are not present (Figure 19B,E). At E12.5, the *Runx1*-positive cells appear to be restricted to small area of the most rostral region of the body wall (Figure 19B, N=4). suggesting that (at least some of) the sternal precursors are specified and express *Runx1*. However these cells have been unable to form the bands, so it appears that the sternum precursor cells have failed to migrate. By E13.5, no *Runx1*-positive cells are detectable in the ventral body wall, which

indicates that by this stage the sternal precursors have been either lost through cell death or they no longer express *Runx1* (Figure 19E, N=5). *Runx1* is first detectable in the sternal bands at E12.5 and therefore it was not possible to examine the position of the precursors prior to this stage.

Forelimb bud formation is completely blocked in *Fgf10*$^{-/-}$ mutant mice but the sternum is able to form normally. *Runx1* expression appears normal in these embryos despite the absence of forelimbs (Figure 19C, F). *Runx1* expression also appears segmented in *Fgf10*$^{-/-}$ embryos at E13.5 (Figure 19F), similar to the pattern seen in control embryos (Figure 19D). *Runx1* expression in the sternal bands is unaffected in *Fgf10*$^{-/-}$ embryos, which demonstrates that the program controlling sternum formation can operate independently of *Fgf10*.

These results demonstrate that *Tbx5* is required at an early stage of sternum development, as there is a failure of sternal band formation prior to E12.5 in *Tbx5*$^{lox/lox}$*;Prx1Cre* mouse embryos. This is supported by unpublished work from our laboratory using a tamoxifen inducible *Prx1CreErt2* transgenic to delete *Tbx5* in the LPM at different times during embryogenesis. Deletion prior to E10.5 leads to sternal defects, while deletion from E11.5 leads to normal sternum formation, indicating that *Tbx5* is required prior to E11.5 for sternum development (Hasson et al., unpublished). The presence of *Runx1* expressing cells in *Tbx5* conditional mutant mice suggests that (at least some) sternal precursors are initially specified in the absence of *Tbx5*.

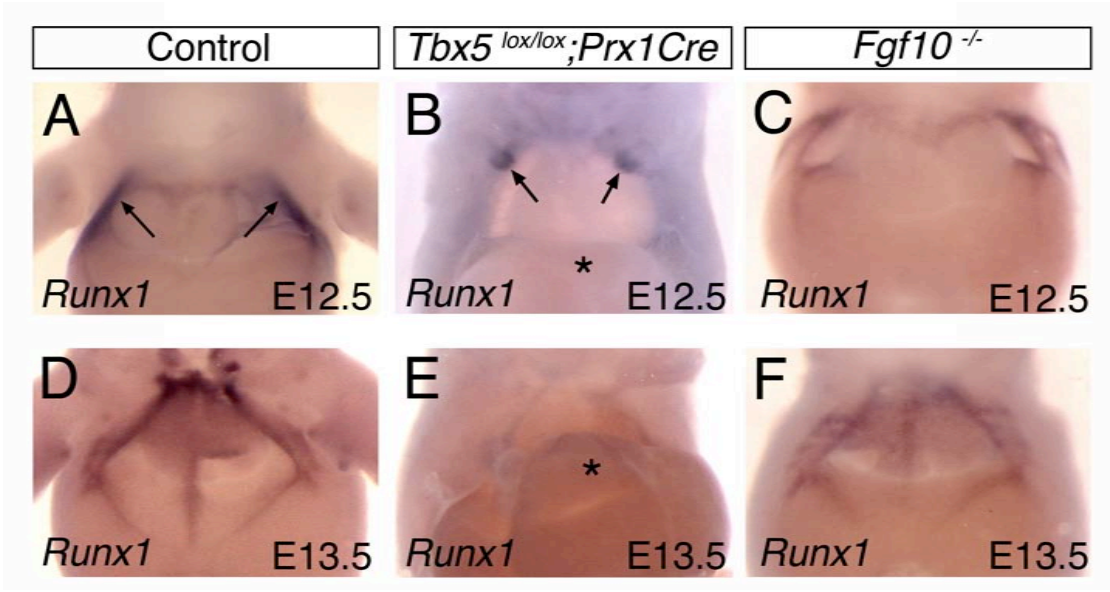

Figure 19. *In situ* hybridisation for *Runx1* in control, *Tbx5$^{lox/lox}$; Prx1Cre* and *Fgf10$^{-/-}$* mice.

Ventral views of embryos at E12.5 (**A-C**) and E13.5 (**D-F**). *Runx1* is expressed in the sternal bands (arrows) in control (**A,D**) and *Fgf10$^{-/-}$* (**C,F**) embryos, but is restricted to a region of the anterior ventral body wall in E12.5 *Tbx5$^{lox/lox}$; Prx1Cre* mice (arrows, **B**) and is not detected in E13.5 *Tbx5$^{lox/lox}$; Prx1Cre* mice (**E**). Herniation of the internal organs following the failure of body wall closure is present in **B** and **E** (asterisk).

4.6 Investigation of *Cx40* as a Potential Target of *Tbx5*

Our data indicate that *Tbx5* is required at the earliest stages of sternum development, and that it is acting through a downstream target other than *Fgf10*. I investigated another potential downstream target of *Tbx5* in the sternum, the gap junction protein Connexin40 (*Cx40)*. It has been suggested that Holt-Oram syndrome defects occur as a result of reduced *Cx40* levels, and mice deficient in *Cx40* show many defects, including shortened sterna and aberrant alignment of the ribs and vertebrae (Pizard *et al.* 2005). *Cx40* and *Tbx5* are co-expressed in the migrating sternal bands, and it has been demonstrated that the *Cx40* promoter contains T-box binding elements (Bruneau *et al.* 2001). It has been suggested that *Tbx5* may regulate *Cx40* expression in either a direct or indirect manner (Pizard *et al.* 2005). However, the exact role of gap junctions in bone development is not understood.

Wholemount *in situ* hybridisations were conducted in the mouse using a probe specific to *Cx40*. In embryos at E10.5, E11.5 and E12.5, *Cx40* expression is visible within the limb bud, but not in the ventral body wall (Figure 20A-C,F-H). At E13.5 and E14.5, *Cx40* expression becomes visible in the sternal bands and also in the distal ribs as both tissues move across the thorax (Figure 20D,I). This result appears to contradict the interpretation of Pizard et al., as the sternal defect in *Tbx5* conditional mutant mice is already apparent by E12.5, prior to the activation of *Cx40* in the sternal precursors (Pizard *et al.* 2005).

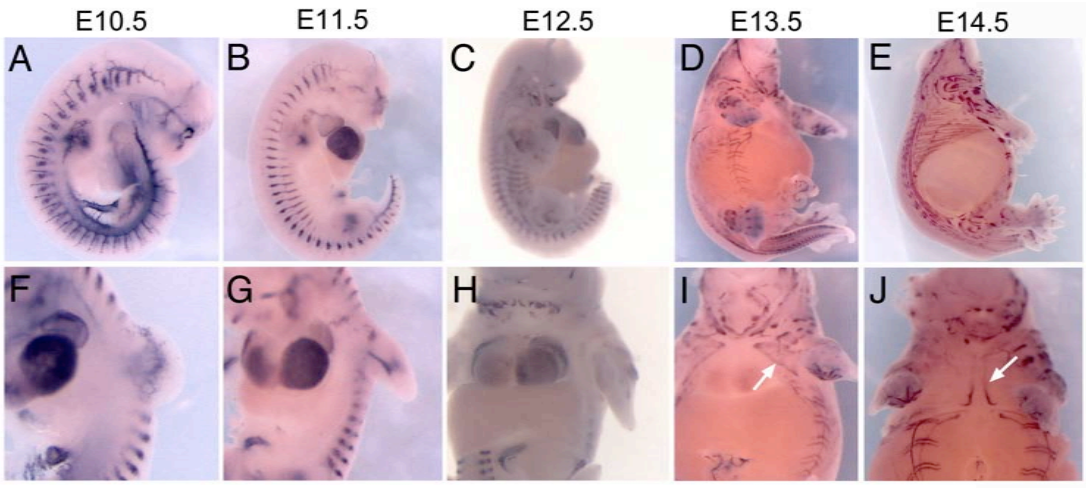

Figure 20. *In situ* hybridisation for *Cx40* in control mouse embryos.

Lateral (**A-E**), latero-ventral (**F,G**) and ventral views (**H-J**) of embryos at E10.5 (**A,F**), E11.5 (**B,G**), E12.5 (**C,H**), E13.5 (**D,I**) and E14.5 (**E,J**). *Cx40* expression is visible in the forelimbs from E10.5 onwards, but does not switch on in the sternal bands until E13.5 onwards (white arrows).

Taken together, these results demonstrate that *Tbx5* is expressed in the population of cells in the ventral body wall which encompasses the sternal precursors, while *Fgf10* is absent from this region. In the absence of *Tbx5,* the sternum does not form. It appears that this defect arises as a result of *Tbx5* playing a crucial role in the migration of the precursor cells to form the sternal bands.

Chapter Five:

Evolution and Adaptation of the Sternum

Chapter Five: Evolution and Adaptation of the Sternum

Chapter Summary

In Chapters 3 and 4, I showed that the forelimbs and sternum share an embryological and genetic connection through their common origin in the LPM and their requirement for *Tbx5*. Chapter 5 investigates the functional link between the forelimbs and sternum, focusing on avian species. The sternum is considered characteristic of virtually all tetrapods (Seno 1961), and plays a crucial role as an attachment site for the pectoral muscles, allowing the body to be raised from the ground. However, in birds the sternum also possesses a large ventral extension known as the keel. This provides an increased attachment area for the pectoral and supracoracoideus muscles that help power the flapping of the wing.

I investigate how sternum dimensions are correlated with forelimb use by comparing the relative dimensions of sterna in birds with different flight abilities. I selected the emu as an experimental model of a flightless bird that has a reduced sternum and forelimbs. I analysed *Tbx5* expression in the emu LPM and compared it to that in the chick to investigate whether changes in *Tbx5* expression may accompany sternum and forelimb adaptation in the emu. Finally I attempted to reverse this reduction in forelimb and sternum size by delivering a precocious dose of *Tbx5* to pre-limb bud stage emu embryos. I propose that *Tbx5* represents a common regulatory node in the molecular pathways controlling forelimb and sternum development, and that modulating its expression enables adaptations to be made specifically to these features.

5.1 Investigating the Correlation between Sternum Size and Forelimb Use

The size and shape of the sternum are connected to the mode of locomotion used by different tetrapod species. For example in kangaroos, which primarily use their hindlimbs in locomotion, the forelimbs are smaller and the sternum is shortened relative to overall body size (Kardong 1998). Another striking example is represented in avians, where the sternum possesses a ventral extension known as the keel. This provides a large surface area, to which the flight muscles attach (King *et al.* 1975). In flightless birds, however, both the wings and sternum are reduced in size and the sternal keel is flattened (King *et al.* 1975). Although this association is often acknowledged, (King *et al.* 1975; Videler 2005), to the best of our knowledge it has not yet been quantitatively analysed.

5.1.1 Selection of Species and Measurements Taken

I examined the relationship between forelimb use and sternum size by measuring sterna in a number of skeletal specimens of avian species that use different forms of locomotion (Table 3). The total length and width of the sternum, and the maximum height of the keel were measured to give an overall representation of the size and shape of the sternum. The bird species measured showed a large range in overall body size, so to normalise for this, sternum measurements were divided by the measurement of thorax length (the distance from the first to the last rib-forming vertebra). Thorax length was chosen as a representation of the overall body size because the total body size could not be measured as many samples were missing heads and/or tails. It was taken to be proportional to the overall bird size, therefore

allowing relative comparisons of sternum size across species with vastly different body sizes. Where possible, up to four specimens were measured per species, and mean values were calculated.

I selected groups of species to include in the analysis by aiming for the greatest variety in flight abilities, and also depending on the availability of skeletons in the archives of the National History Museum at Tring and the Museum of Zoology in Cambridge (species listed in Table 3). I selected the hummingbirds (Trochilidae) as a family of highly adapted and specialised fliers, as they generate incredibly high frequency wing strokes and are the only bird species able to fly backwards. I also measured members of the pigeon family (Columbidae), which are strong fliers that can cover large distances, and the warbler group (Sylvioid and Passeroid warblers), which have a flight behaviour that commonly involves bursts of flight interspersed with perching. A number of flightless land bird skeletons were measured, although many of these species are extinct, such as the dodo (*Raphus cucullatus)* and the moa (*Dinornis sp.)*, meaning that fewer specimens were available for measurement. I also measured diving birds including cormorants (Phalacrocoracidae), which use their legs for underwater propulsion, and auks (Alcidae) which instead move underwater using their wings (King *et al.* 1975). The flightless cormorant (*Phalacrocorax harrisi*) was selected to represent flightless foot-propelled divers, and a number of species of penguin (Spheniscidae) were also measured, to represent flightless wing-propelled divers.

Group	Species	St. length	St. width	Keel height	Th. length	St. length/ Th. length	St. width/ Th. length	Keel height/ Th. length
HUMMINGBIRDS **Flying land birds**	Mean *Phaethornis superciliosus (3)*	17.4	11.5	12.0	9.7	1.78	1.18	1.23
	Mean *Lafresnaya lafresnayi (4)*	17.6	10.7	11.9	9.0	1.97	1.19	1.33
	Mean *Coeligena torguata (4)*	19.4	11.4	12.7	9.9	1.96	1.16	1.28
	Mean *Heliangelus exortis (4)*	16.9	9.7	10.6	7.4	2.28	1.32	1.43
	Mean *Eriocnemis vestitus (4)*	16.8	10.2	10.4	7.4	2.26	1.37	1.40
	Mean *Metallura therasiae (4)*	13.9	8.3	9.3	6.7	2.08	1.25	1.40
	Mean *Archilochus colubris (4)*	14.1	8.0	9.8	6.8	2.09	1.19	1.45
PIGEONS **Flying land birds**	Mean *Columba livia (4)*	65.7	27.3	29.2	29.3	2.24	0.93	0.99
	Mean *Streptopelia turtur (4)*	49.5	19.8	25.0	26.9	1.84	0.74	0.93
	Mean *Streptopelia decaocto (4)*	57.5	21.2	27.7	29.4	1.95	0.72	0.94
	Mean *Goura cristata (4)*	111.8	43.0	53.0	60.3	1.86	0.71	0.88
	Mean *Geopelia striata (4)*	35.9	12.6	17.7	17.1	2.10	0.74	1.03
	Mean *Phaps chalcoptera (2)*	73.8	27.8	35.3	38.7	1.76	0.64	0.82
	Mean *Leptotila rufaxilla (4)*	56.7	20.0	26.6	24.2	2.34	0.83	1.10
	Alectroenas pulcherrima	36.5	19.4	20.9	27.9	1.31	0.70	0.75
	Alectroenas madagascariensis	46.4	20.5	24.7	34.5	1.34	0.59	0.72
	Phaps elegans	61.8	19.5	29.5	27.5	2.25	0.71	1.07
	Gallicolumba luzonica	58.9	18.1	27.9	25.0	2.36	0.72	1.12
WARBLERS **Flying land birds**	Mean *Sylvia atricapilla (4)*	17.3	10.0	6.5	9.7	1.79	1.03	0.67
	Mean *Sylvia comunis (4)*	15.8	7.6	6.1	10.6	1.50	0.72	0.58
	Mean *Sylvia hortensis (4)*	18.6	9.6	6.9	10.4	1.79	0.92	0.67
	Mean *Acrocephalus schoenobaenus (4)*	14.6	7.3	6.2	10.7	1.36	0.68	0.57
	Mean *Phylloscopus trochilus (4)*	14.2	7.3	5.8	9.8	1.44	0.75	0.59
	Mean *Orthotomus sutorius (4)*	13.0	6.8	5.2	8.0	1.64	0.85	0.66
	Locustella naevia	15.7	9.0	5.7	13.6	1.15	0.66	0.42
	Sericornis humil	15.7	8.7	4.3	15.2	1.03	0.57	0.28
	Cettia fortipe	13.5	7.5	3.3	15.5	0.87	0.48	0.21
	Acrocephalus stentoreu	17.4	9.0	4.9	15.7	1.11	0.57	0.31
	Mean *Acanthiza pusilla (4)*	9.0	5.8	2.6	9.2	0.99	0.63	0.29
FLIGHTLESS LAND BIRDS	*Rhea darwinii*	138.0	133.0	4.0	237.0	0.58	0.56	0.02
	Mean *Rhea americana (3)*	140.7	127.0	14.7	211.3	0.67	0.60	0.07
	Dinornis sp.	132.0	122.0	16.0	326.0	0.40	0.37	0.05
	Mean *Pezophaps solitaria (2)*	152.5	109.0	38.0	146.0	1.04	0.75	0.26
	Mean *Struthio camelus (4)*	190.8	180.3	31.0	280.0	0.68	0.64	0.11
	Mean *Raphus cucullatus (2)*	168.5	111.5	24.3	111.0	1.52	1.00	0.22
	Mean *Casuarios casuarius (4)*	182.0	118.3	28.4	230.3	0.79	0.51	0.12
	Mean *Drominaius novaeholandiae (4)*	142.6	109.3	20.9	222.0	0.64	0.49	0.09
	Mean *Apteryx australis (4)*	25.6	41.8	3.0	71.8	0.36	0.58	0.04
	Mean *Apteryx owenii (2)*	18.8	35.5	1.1	65.4	0.29	0.54	0.02
	Mean *Strgops habroptilus (3)*	72.0	45.6	5.6	64.2	1.12	0.71	0.09
	Gallirallus australis	55.4	14.7	10.0	79.6	0.70	0.18	0.13
Flightless foot propelled diver	Mean *Phalacrorax harrissi (3)*	101.7	71.5	11.8	101.2	1.00	0.71	0.12
CORMORANTS Flying foot propelled divers	Mean *Phalacrorax aristotelis (4)*	77.4	52.3	24.9	76.3	1.02	0.69	0.33
	Mean *Phalacrorax carbo (4)*	92.1	62.3	32.9	93.5	0.99	0.67	0.35
	Mean *Phalacrorax albiventer (2)*	86.0	62.0	29.0	93.5	0.92	0.66	0.31
	Mean *Phalacrorax nigrogularis (2)*	85.5	54.5	26.0	96.0	0.89	0.57	0.27
PENGUINS Flightless wing propelled divers	Mean *Eudyptes crestatus (4)*	107.6	55.7	36.2	103.7	1.04	0.54	0.35
	Mean *Aptenodytes patagonicus (2)*	186.0	104.5	49.0	166.5	1.12	0.63	0.29
	Mean *Pygoscellis papua (4)*	169.3	84.0	46.5	144.5	1.17	0.58	0.32
	Sphiniscus magellanicus	125.0	64.0	40.0	142.0	0.88	0.45	0.28
	Mean *Sphiniscus demersus (2)*	95.0	53.0	33.0	108.0	0.88	0.49	0.31
AUKS Flying wing propelled divers	Mean *Alca torda (4)*	102.6	27.2	36.0	66.0	1.56	0.41	0.55
	Mean *Alle alle (4)*	60.6	19.2	21.9	38.8	1.56	0.50	0.56
	Mean *Brachyramphus marmoratus (4)*	70.3	21.8	25.8	51.3	1.37	0.42	0.50
	Mean *Uria aalge (4)*	117.3	35.3	38.3	83.5	1.40	0.42	0.46
	Mean *Fraturcula arctica (4)*	82.8	33.3	31.3	53.0	1.56	0.63	0.59
	Mean *Cepphus grille (4)*	85.3	31.3	29.3	55.8	1.53	0.56	0.52

Table 3. Tabulation of adult avian skeleton sternum measurements.

Table indicating the species measured and their modes of locomotion. Sternum length (St. length), sternum width (St. width) and keel height were measured in centimetres and normalised for overall bird size by dividing by thorax length (Th. length; the distance in centimetres along the spine from the most rostral to the most caudal rib). Where multiple specimens were measured per species, the number of specimens is indicated after the species name, and the means of the measurements are shown. Text colour corresponds to that used in Figure 21 and Figure 22.

5.1.2 The Relationship between Flight Ability and Sternum Size

Normalised skeleton measurements for each species were plotted onto scatter graphs and colour-coded according to their group (Figure 21, Figure 22). The species measured show a strong positive correlation between keel height and sternum length (Figure 21, R^2=0.83), with stronger fliers like pigeons and hummingbirds having larger sterna, while poorer fliers and flightless birds have smaller sterna. I also saw a similar correlation between sternum width and keel height (Figure 22, R^2=0.58), although this was weaker than that seen for sternum length. This may be because sternum length is more important in ultimately determining the surface area available for pectoral muscle attachment. The length of the sternum and the height of the keel (as well as keel shape) determine the total keel surface area, while sternum width does not directly influence keel surface area. Sternum length may therefore be expected to be more evolutionarily constrained and show a stronger correlation with keel height, while sternum width may be less affected by the constraint of muscle attachment area, and may vary more according to other factors such as balance, body shape, or weight.

This data demonstrates that sternum length, and to a lesser extent, sternum width, increase in proportion with keel height in species of varying flight ability. None of the species measured showed very long sterna with a short keel or vice versa, which suggests that these features are evolutionarily constrained to provide the optimum keel size for the attachment of flight muscles. Flightless birds generally have flatter, shorter sterna than flighted birds, occupying the lower left region of the graphs (Figure 21, Figure 22). However three of the flightless birds show relatively larger

sterna than other flightless birds (solitaire, kakapo and dodo; Figure 21 and Figure 22, points labelled). This may reflect the reported use of the wings in display or fighting, which has lead to (or perhaps has been a result of) these species retaining a larger sternum (Strickland *et al.* 1848; Livezey 1992). Solitaires in particular have been reported to use their wings in display and in combat, and skeletons of sexually mature specimens have been found to form a large carpal knob, thought to have been used as a weapon (Hume *et al.* 2013). The correlation between sternum dimensions is generally weaker in flightless birds than in flying birds, with the points on the graphs fitting less closely to the line of best fit (Figure 21, Figure 22). This may reflect the reduced evolutionary constraint placed on sternum dimensions in birds that no longer require flight muscles. The sternum is not required for locomotion in these species, and so is less likely to maintain the optimum proportions for muscle attachment.

Of the diving birds, the auks and cormorants lie on the same trend line as the land birds (Figure 21, Figure 22). Auks generally show longer sterna with a taller keel than cormorants (although the sternum width is similar), which may be due to the use of their wings in the air and underwater, while cormorants use their wings solely in flight and use their feet for underwater propulsion. The flightless cormorant, which does not use its wings in either the air or the water lies closer to the other flightless birds. However, in penguins the sternum is closer in size to other flighted species, such as the warblers. Both the flightless cormorant and penguins are flightless, but penguins may display a much larger sternum because they still require powerful pectoral muscles for swimming. Conversely, the flightless cormorant does not use its

wings in the air or underwater, and has a considerably reduced sternum size. This demonstrates that avian sternum dimensions are linked to the use of the forelimbs, both in flight and in underwater locomotion.

Most of the species studied cluster along a single line of best fit for sternum length and keel height (Figure 21, lower trend line). However the hummingbirds lie on a different trend line, having a taller keel but similar sternum length to pigeons (Figure 21, upper trend line, R^2=0.71). This may reflect an extreme adaptation to facilitate their uniquely high speed wing strokes. Hummingbird flight muscles represent a significantly larger proportion of the total body muscle mass than in other birds. The supracoracoideus muscle is particularly well developed in hummingbirds, being 50% as large as the pectoral muscle, as opposed to 20% as large as the pectoral muscle in most bird species. This allows the hummingbird to generate sufficient force to power the rapid upstroke required for hovering and efficient flight at low speeds (Warrick *et al.* 2012).

The increased muscle mass in hummingbirds requires a larger attachment surface area, generated by a greater sternal keel height. The sternal length is not greatly increased in hummingbirds, which may reflect an upper limit to sternum length, where the sternum has reached the maximum length possible to support the sternum without increasing the size of the ribcage (and therefore the thorax length). Therefore to gain a greater muscle attachment surface area, hummingbirds show an increased keel height relative to their sternum length. However, hummingbird sternum width

does not show the same constraint as sternum length, and hummingbirds have significantly wider sterna than pigeons (Figure 22).

This data quantitatively demonstrates that sternum dimensions are linked with mode of locomotion, and specifically, with the use of the forelimbs. It also suggests that the wing motions and musculature required for flying and for diving may be similar, because the sternum proportions of flightless wing propelled divers (penguins) are similar to that of flying birds.

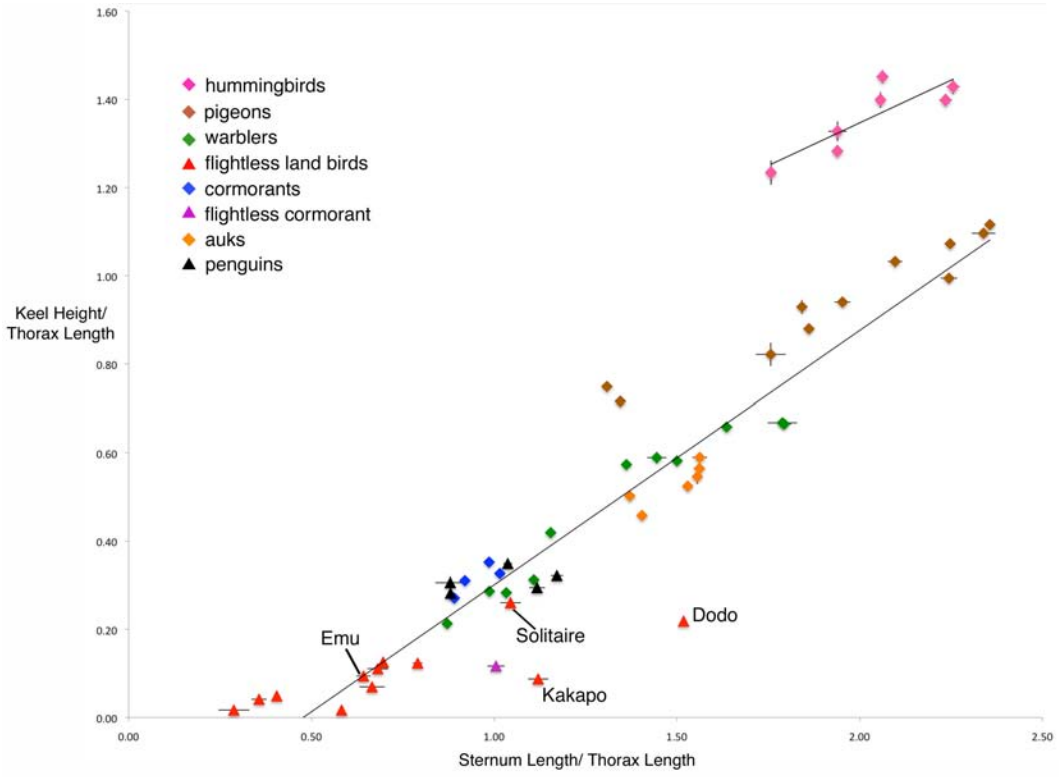

Figure 21. Avian sternum length and keel height are correlated with mode of locomotion.

Scatterplot of measurements for sternum length and keel height for a range of bird groups, normalised for bird size by dividing by thorax length. Each point on the graph represents one species. When possible, multiple specimens were measured per species, and error bars show standard error between multiple specimen measurements. Flying species are represented as diamonds, flightless species as triangles. Plot compiled in Microsoft Excel 2008 for Mac.

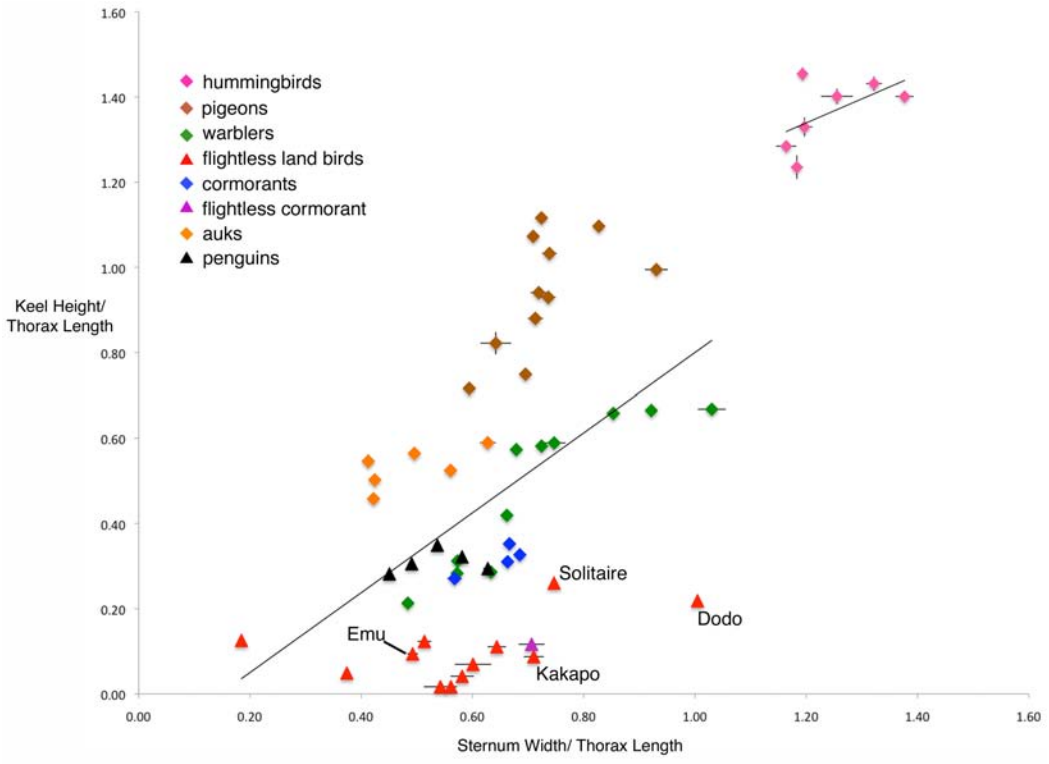

Figure 22. Avian sternum width and keel height are correlated with mode of locomotion.

Scatterplot showing measurements for sternum width and keel height for a range of bird groups, normalised for bird size by diving by thorax length. Each point on the graph represents one species. Where possible, multiple specimens were measured per species, and error bars show standard error between multiple specimen measurements. Flying species are represented as diamonds, flightless species as triangles. Plot compiled in Microsoft Excel 2008 for Mac.

5.2 Modulation of *Tbx5* Expression in the Emu

Birds that have lost the power of flight display reduced size wings compared to flying birds (McCall *et al.* 1998) and, as I demonstrate in Chapter 5.1, they also have a smaller sternum. The molecular mechanisms that drove these changes over the course of evolution are unclear, but it is likely to involve adaptations in regulatory pathways that operate during embryonic development. I set out to investigate the genetic mechanisms that underlie the reduction in forelimb and sternum size, by comparing the expression patterns of selected genes in flightless and flighted bird species. I used the emu, *Dromaius novaehollandiae* as a model flightless bird, because I was able to obtain fertile eggs from commercial sources. A number of published works are available that provide protocols and guidelines regarding emu egg incubation (Deeming 1997; Nagai *et al.* 2011). I also used the chicken, *Gallus gallus*, as a flighted bird for comparison.

5.2.1 Forelimb and Sternum Formation in the Emu

There is no established normal staging system for the emu, so embryos were staged according to hindlimb and head morphology and matched with the equivalent chick Hamburger/Hamilton stages (Hamburger *et al.* 1951) to assign a Hamburger/Hamilton equivalent stage (eqHH). The head and hindlimbs were used as references to determine the developmental stage. These features were chosen because changes in the morphology of the head and hindlimbs over developmental time are clearly identifiable, which allows the developmental stage to be accurately estimated. Somite counting was not considered a useful staging technique due to the development of tissues that obscure the somites by limb bud stages.

Examining limb bud stage emu embryos, it is clear that the forelimb bud is considerably smaller compared to the chick, while the hindlimbs appear similar in size (Figure 23A,B). Skeletal preparations of older embryos also reveal that the emu forelimbs are reduced, and the sternum appears smaller, with very little or no keel visible (Figure 23C,D). To analyse the extent of emu forelimb reduction in greater detail, I made skeletal preparations of chick and emu forelimbs at a range of stages. Only one ossified digit is present in the adult emu (Maxwell *et al.* 2007), while the chicken forms three ossified digits (Bellairs *et al.* 2005). Extant birds evolved from a common theropod ancestor, which possessed three clawed fingers (Xu *et al.* 2013). Therefore digit loss in the emu is an aquired state. At day 11 of chick development (HH37), embryos have formed three digit condensations (Figure 24A), and at day 26 of emu development (eqHH38), one digit is present, with some residual cartilage condensations visible (Figure 24B). Suprisingly, examining younger emu embryos reveals that, at day 19 (eqHH34), three initial digit condensations can be detected (Figure 24B, N=4/4). Therefore three digits are initially specified in both the chick and the emu, but the emu fails to maintain all of these digits.

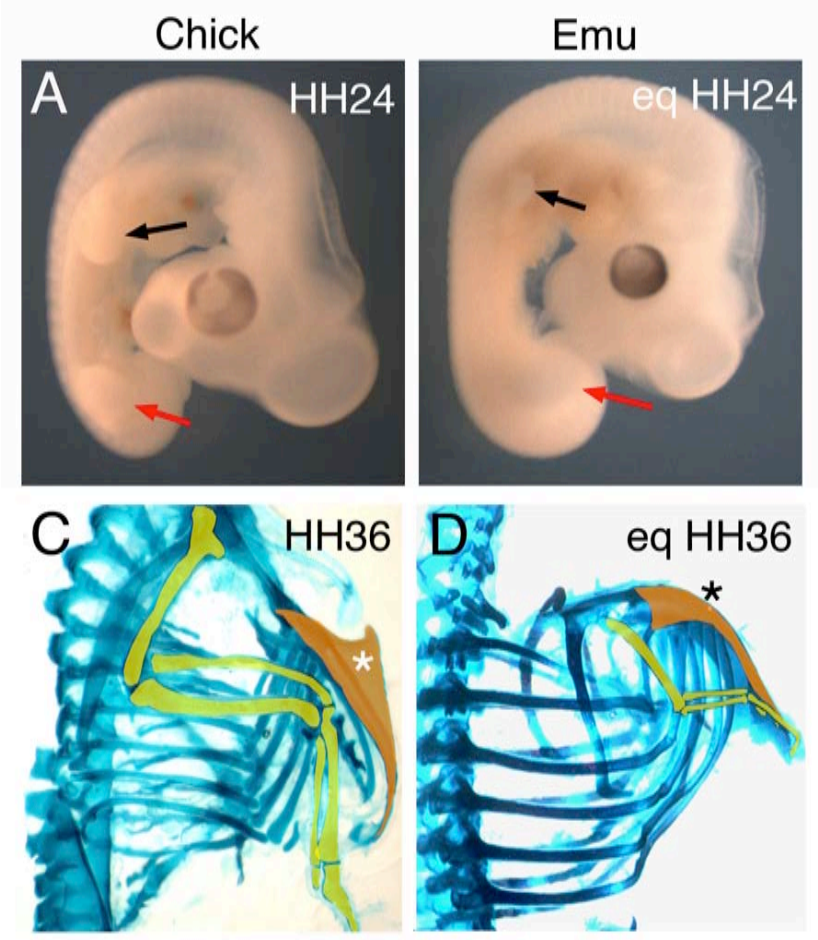

Figure 23. The emu forelimb and sternum are reduced compared to the chick.

A,B Wholemount lateral views of HH24 chick and eqHH24 emu embryos show that the emu forelimb bud is reduced in size compared to the chick (black arrows), while the emu hindlimb is a similar size to the chick (red arrows). **C,D** Lateral views of alcian blue/ alizarin red stained chick and emu skeletons at HH36 (day 10) and eqHH36 (day 27), respectively, showing a size reduction in the emu forelimbs (highlighted yellow), and sternum (highlighted orange). The sternal keel observed in the chick (white asterisk) is absent in the emu (black asterisk).

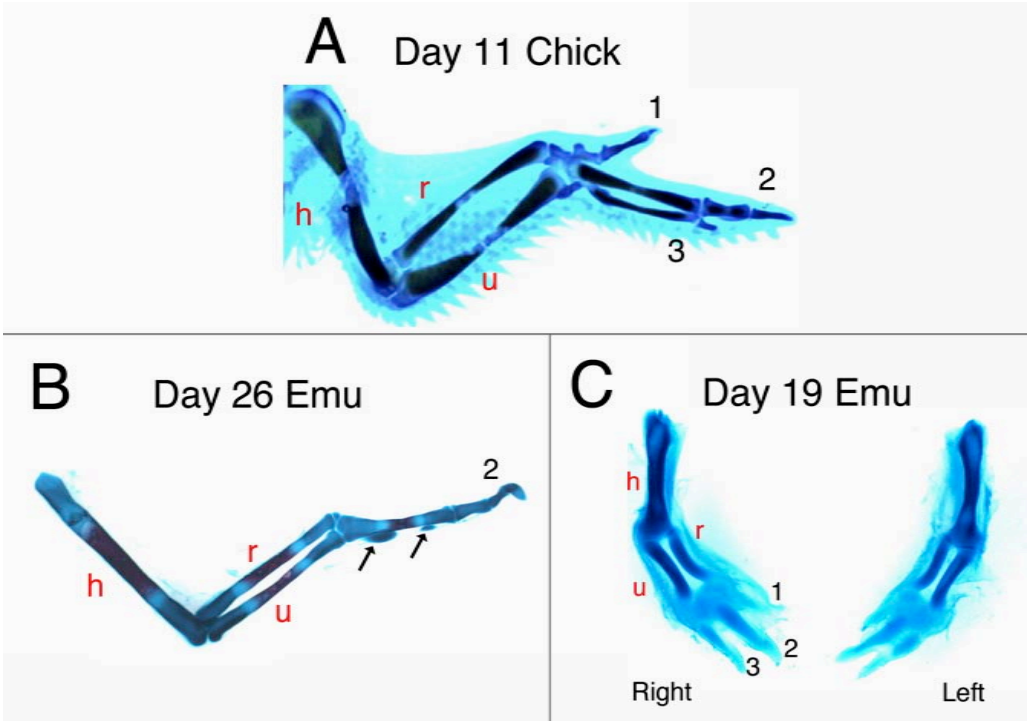

Figure 24. Three digits initially condense in the emu.

Alcian blue/alizarin red staining of chick and emu forelimbs. **A**, Day 11 chick right forelimb showing 3 digits. **B,** Day 26 control right emu forelimb with a single digit (digit 2) and residual cartilage condensations (arrows). **C,** Day 19 emu forelimbs showing three digit condensations (digit 1,2,3). Humerus (h), radius (r) and ulna (u).

5.2.2 Analysing *Tbx5* Expression in the Emu

In the chick, the forelimb emerges slightly ahead of the hindlimb (Hamburger *et al.* 1951). However, in the emu, forelimb budding is delayed and the hindlimb emerges first (Nagai *et al.* 2011). This reversal of heterochrony in limb development suggests that the reduced forelimb observed in the adult emu is caused by embryological adaptations arising prior to limb bud stages. I have shown that *Tbx5* is essential for the formation of both the forelimbs and sternum (Figure 11), and is expressed in the precursors of both tissues (Figure 13, Figure 14). Forelimb and sternum adaptations observed in the emu arise prior to limb bud emergence, which is the stage when *Tbx5* is required in forelimb and sternum development (Figure 19; Rallis *et al.* 2003; Hasson *et al.* 2007). *Tbx5* is so far the only gene known to be involved in both forelimb and sternum development, without affecting the hindlimbs or axial tissues. Therefore, I investigated regulation of *Tbx5* expression as a candidate mechanism responsible for the sternum and forelimb adaptations seen in the emu. For comparison with the development of the hindlimb, I also analysed the expression of *Pitx1* in the emu. *Pitx1* is a marker of hindlimb initiation (Logan *et al.* 1999), and so can be used as a reference for comparison with emu forelimb initiation at a range of stages.

To make antisense probes for RNA *in situ* hybridisation analysis on emu embryos, I cloned cDNA fragments of emu *Tbx5* and *Pitx1*. Total RNA was extracted from a single eqHH22 embryo and one-step reverse transcription PCR reactions were conducted to synthesise emu *Tbx5* and *Pitx1* cDNA fragments. PCR primers for these reactions were designed based on sequence alignments of chick, turkey,

zebrafinch and anole lizard orthologous genes (Figure 25 and Figure 26). Conserved regions that would yield a 3' biased probe template of approximately 400-500 base pairs in length were selected. PCR products were ligated into a pGEM-T vector, transformed into competent cells and amplified. Emu cDNA was then sequenced and contigs were aligned with chick, mouse and human transcript sequences using the ClustalW alignment program and MegAlign software (Figure 27 and Figure 28). Both sequences showed a high level of conservation to those in chick (and to a lesser extent, mouse). At the nucleotide level, the cloned *Tbx5* fragment is 94% identical to the corresponding region of the chicken *Tbx5* transcript, and 77% identical to mouse. Emu *Pitx1* also shows a high level of conservation, with 95% identity to the corresponding region of chick *Pitx1*, and 83% identity to mouse. The emu sequences were translated *in silico* and peptide alignments were performed with the same reference species (Figure 29 and Figure 30). The *Tbx5* peptide alignment reveals that the emu sequence is 99% identical to the corresponding region in chick, and 85% identical to mouse. For *Pitx1*, the translated emu peptide sequence is 94% identical to chick and 84% identical to mouse. Peptide sequences showed higher conservation than nucleotide sequences, demonstrating that that some of the changes in the nucleotide sequence are silent mutations.

It should be noted that the cloned emu *Tbx5* and *Pitx1* sequences do not necessarily represent the true emu transcript sequence. The technique used relies on PCR amplification and although a high fidelity polymerase was used, sequence changes can arise. Also, the primers used were designed based on alignment of other avian species, so these regions will not provide any information about the emu sequence.

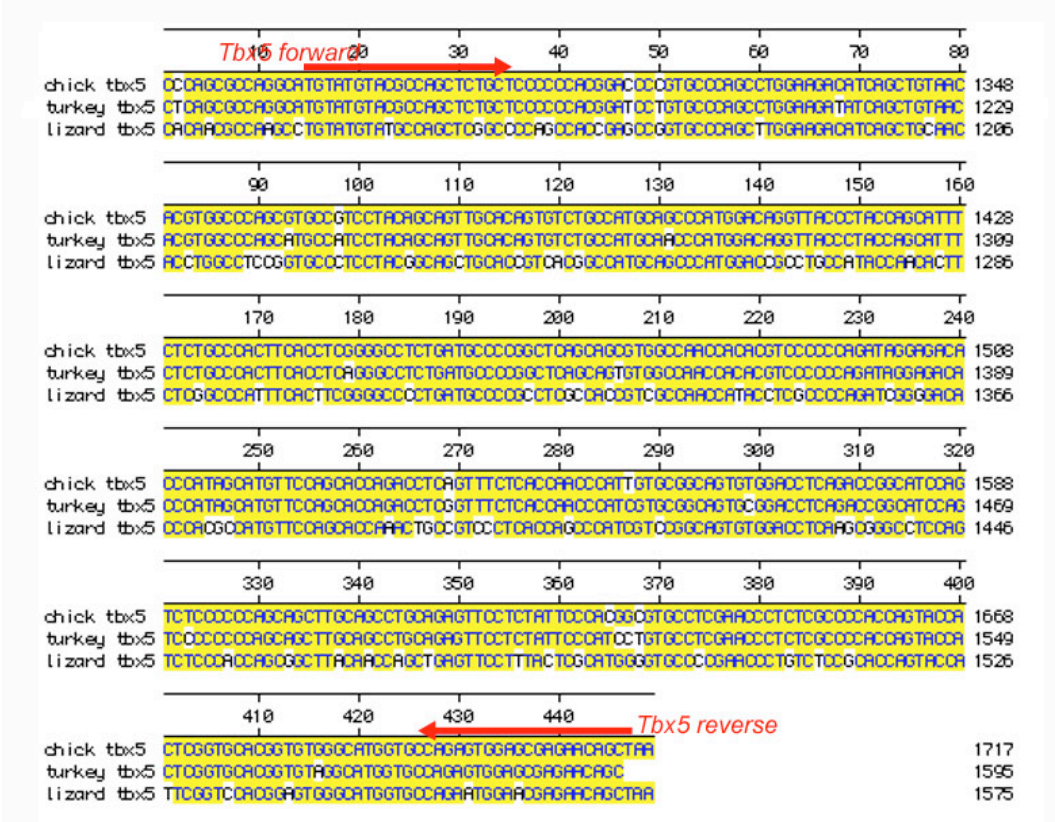

Figure 25. Avian and lizard *Tbx5* cDNA sequence alignments used to design emu primers.

Residues matching the consensus are highlighted in yellow, and forward and reverse primer sequences are indicated by red arrows (*Tbx5 Forward* TGT ATG TAC GCC AGC TCT GCT, *Tbx5 Reverse* A GCT GTT CTC GCT CCA CTC TGG). Sequences aligned using the ClustalW alignment program and MegAlign software.

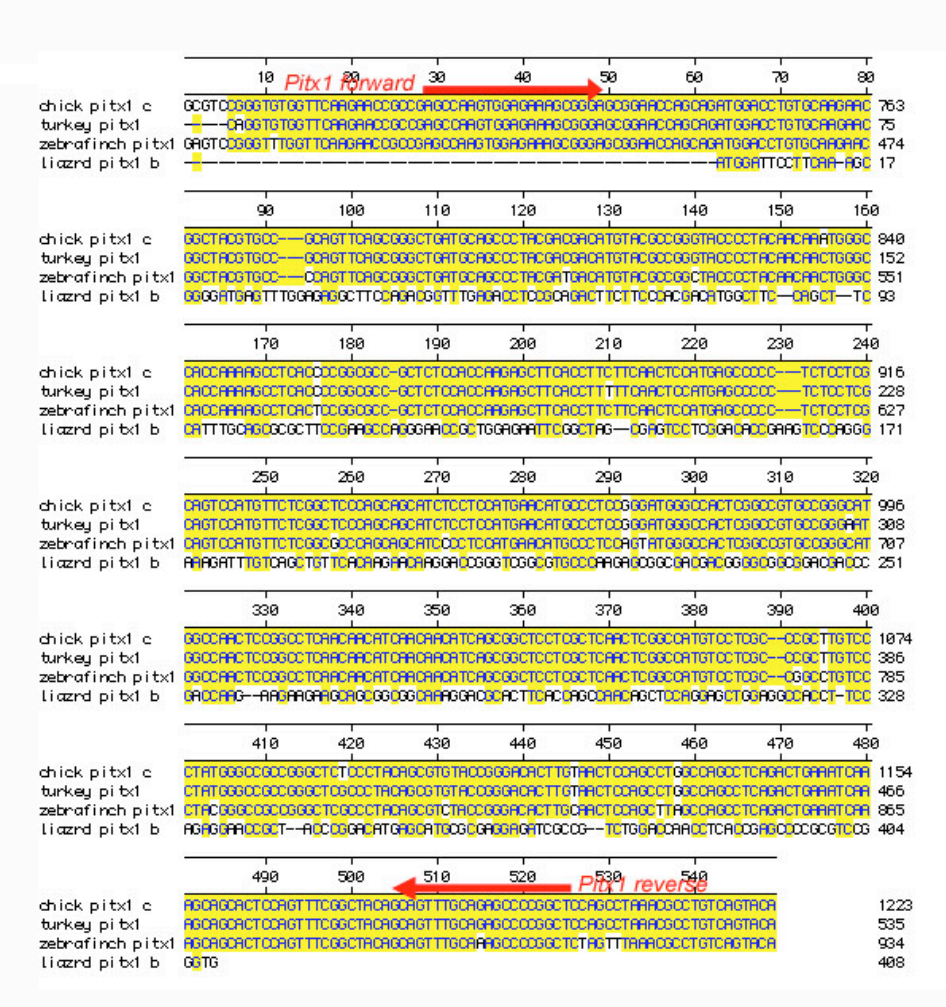

Figure 26. Avian and lizard *Pitx1* cDNA sequence alignments used to design emu primers.

Residues matching the consensus are highlighted in yellow, and forward and reverse primer sequences are indicated by red arrows (*Pitx1 Forward* AGC CAA GTG GAG AAA GCG GGA, *Pitx1 Reverse* AGC CGG GGC TCT GCA AAC TGC). Sequences aligned using the ClustalW alignment program and MegAlign software.

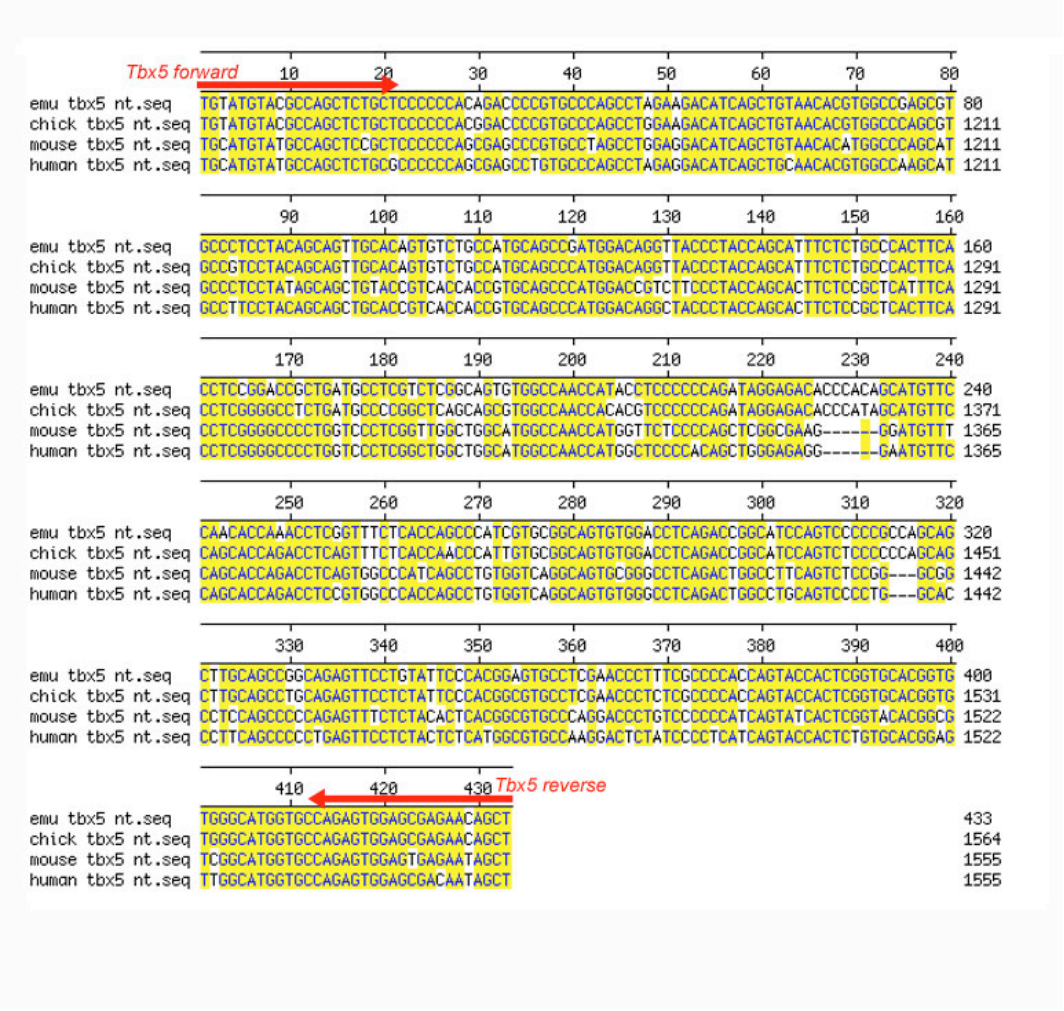

Figure 27. Emu, chick, mouse and human *Tbx5* cDNA sequence alignment.

Matching residues are highlighted in yellow. Sequences aligned using the ClustalW alignment program and MegAlign software.

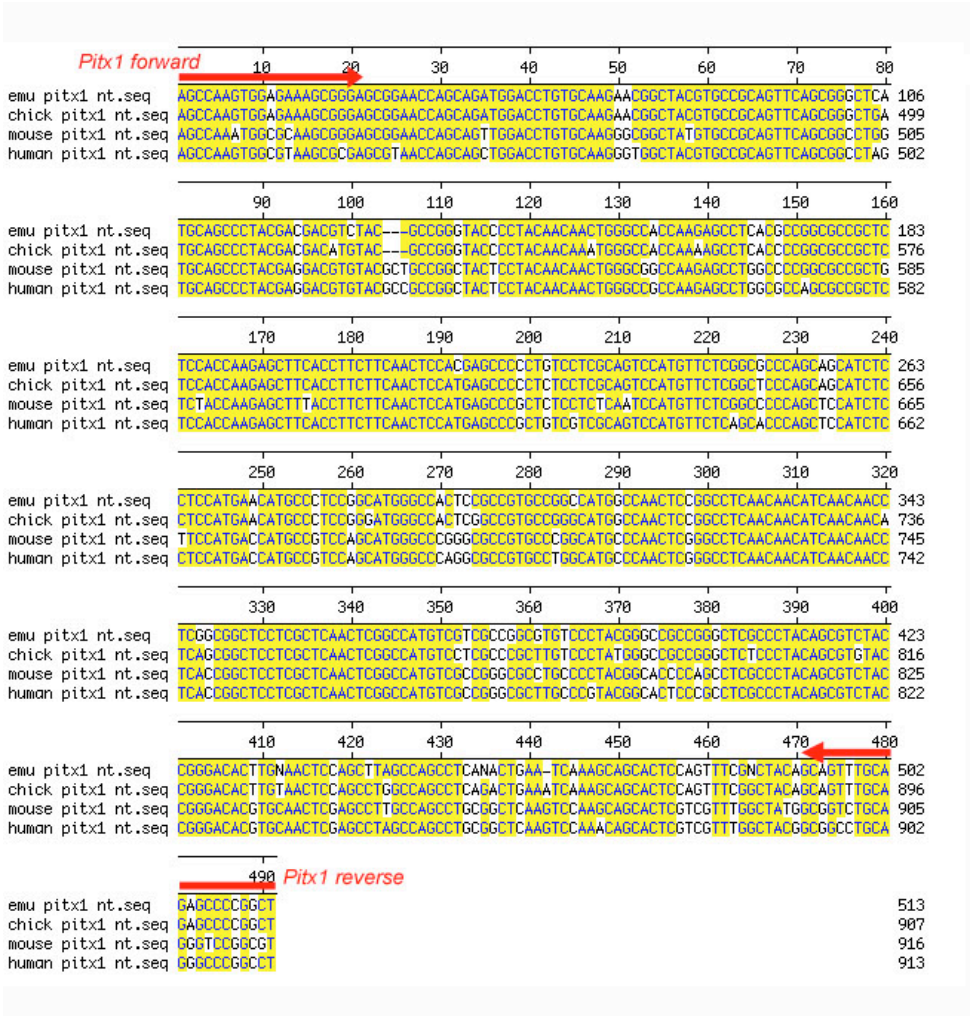

Figure 28. Emu, chick, mouse and human *Pitx1* cDNA sequence alignment.

Matching residues are highlighted in yellow. Sequences aligned using the ClustalW alignment program and MegAlign software.

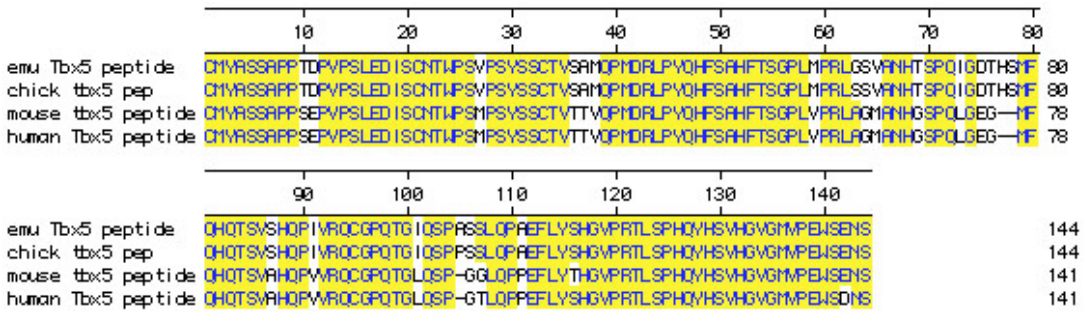

Figure 29. Emu, chick, mouse and human *Tbx5* peptide sequence alignment.

Matching residues are highlighted in yellow. Sequences aligned using the ClustalW alignment program and MegAlign software.

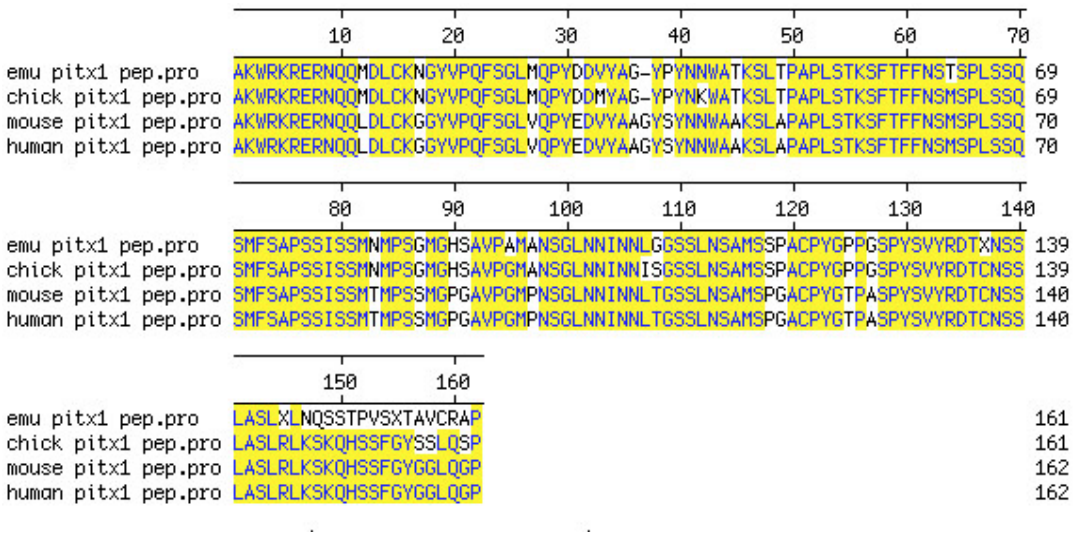

Figure 30. Emu, chick, mouse and human *Pitx1* peptide sequence alignment.

Matching residues are highlighted in yellow. Sequences aligned using the ClustalW alignment program and MegAlign software.

I analysed the spatio-temporal expression of *Tbx5* and *Pitx1* in the emu, and compared this to the expression of orthologous genes in the chick. At HH16, *Tbx5* is already expressed in the chick forelimb-forming LPM (Figure 31A). However, at eqHH16, no *Tbx5* expression is visible in the emu LPM, although *Tbx5* can be detected in the heart (Figure 31E). At the same stage, *Pitx1* is expressed in the emu hindlimb-forming LPM (Figure 31I). This demonstrates that the emu *Tbx5* probe is working correctly, and *Tbx5* expression must be delayed in the emu LPM, compared to the chick. By HH19, *Tbx5* expression is detected throughout the outgrowing chick forelimb bud. However in eqHH19 emu embryos, the forelimb bud has yet to emerge, and *Tbx5* expression is not visible in the LPM (Figure 31B,F), although at the same stage, emu *Pitx1* is expressed throughout the emerging hindlimb (Figure 31J). This shows that the activation of *Tbx5* expression is delayed in the emu, relative to the expression of both *Pitx1* in the hindlimb, and *Tbx5* in the chick forelimb.

Tbx5 expression is first detectable in the emu forelimb-forming LPM at eqHH20 (Figure 31G). This is approximately 2 days after the time at which *Pitx1* expression is first visible in the emu hindlimb-forming region (Figure 31I, G; Nagai *et al.* 2011). Emu *Tbx5* expression at eqHH20 spans a rostro-caudal domain of comparable size to that in a HH16 chick, suggesting that the emu *Tbx5* expression domain is spatially conserved between the chick and the emu. (Figure 31G, H). The emu forelimb bud emerges from eqHH20 onwards, and by eqHH23, *Tbx5* and *Pitx1* are expressed in the emu forelimb and hindlimb respectively (Figure 31H,L). However the emu forelimb bud is reduced in size, spanning only 2.5-3 somites compared to 6 somites

in the chick when the forelimb bud first appears (Figure 31D,H; Hamburger *et al.* 1951). Therefore, although *Tbx5* expression does not appear to be spatially reduced in the emu LPM when it first comes on, by eqHH23 the *Tbx5* expression domain coincides with the (reduced) size of the forelimb.

In the chick, the *Tbx5* expression domain extends ventrally beyond the limb bud into the ventral body wall (Figure 13). I showed that this *Tbx5* positive region encompasses the sternum precursor cells (Figure 5). In eqHH23 emu embryos, the expression of *Tbx5* also extends ventrally into the thorax (Figure 31H). However due to limited embryo numbers, I was not able to examine any stages later than HH23 to determine whether the *Tbx5* domain expands further into the thorax over time, as seen in the chick and mouse (Figure 13, Figure 14). In summary, these results suggest that emu *Tbx5* shows a delayed onset of expression, but not an initial reduction in the size of the expression domain when compared to the chick.

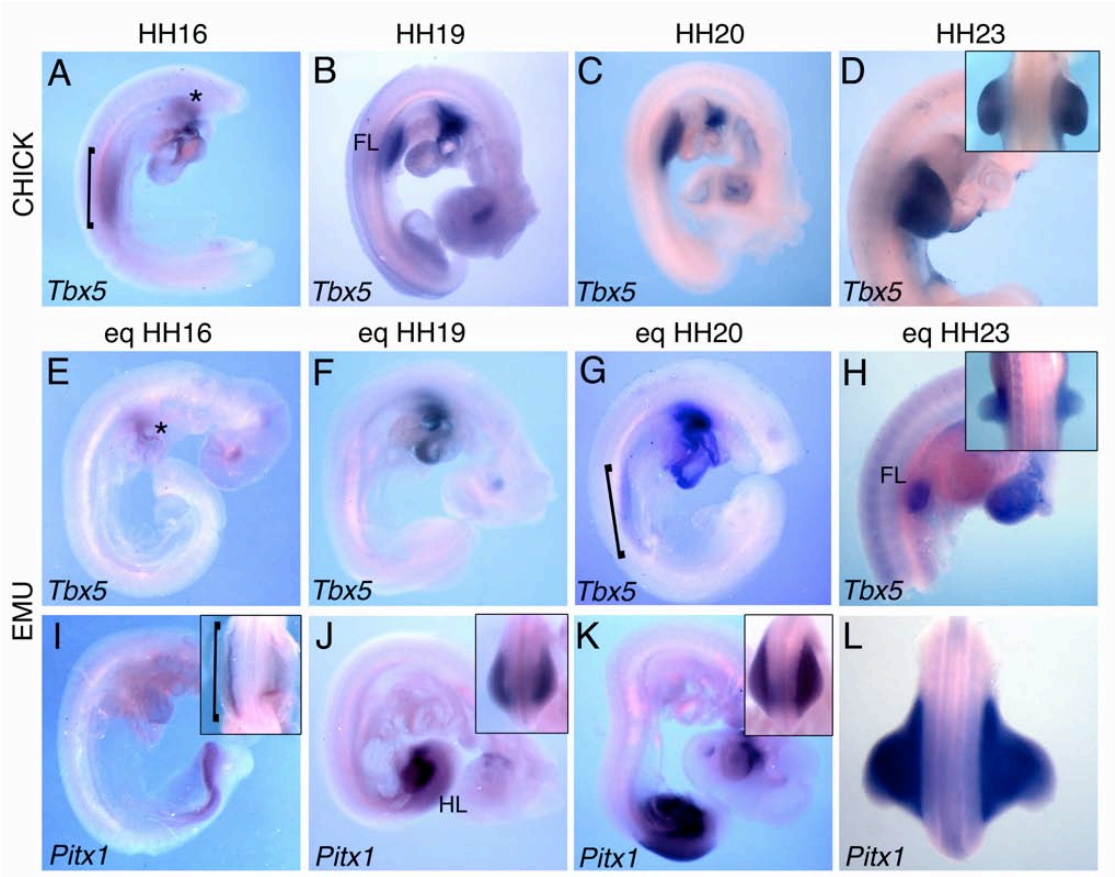

Figure 31. Modulation of *Tbx5* expression accompanies forelimb and sternum reduction in the emu.

A-H, *In situ* hybridisation showing *Tbx5* expression in the forelimb-forming region (bracket), forelimb (FL) and heart (*) of chick (**A-D**) and emu (**E-H**) embryos. **I-L**, *In situ* hybridisation showing *Pitx1* expression in the emu hindlimb-forming region (bracket) and hindlimb (HL). **A-K** lateral views, **L** and inset images dorsal views.

5.2.3 Rescue of Emu Forelimb Reduction

I set out to investigate whether the observed temporal delay in emu *Tbx5* expression underlies the reduction in forelimb and sternum size. Using the replication competent retrovirus system, RCAS, a precocious dose of *Tbx5* was introduced into the emu LPM prior to forelimb budding. RCAS is a retroviral vector system that allows sustained misexpression of genes in avian cells. It has been widely used in chick misexpression experiments (Gordon *et al.* 2009), but has not yet (to our knowledge) been used on emu embryos. The production of retroviral constructs and virus products, and injection of the virus were carried out by Malcolm Logan. An antibody directed against a viral coat protein (3C2) was applied to sections of injected emu embryos harvested a short time after injection. Infected cells, identified by alkaline phosphatase staining, can be seen in the heart, demonstrating that the RCAS virus is able to infect emu cells (Figure 32). However, due to limited numbers of embryos I was not able to demonstrate infection specifically in the emu LPM. Nevertheless this shows that the RCAS system can be used to successfully misexpress *Tbx5* in emu embryos.

The forelimb-forming LPM on the right hand side only of eqHH15 emu embryos was injected with RCAS virus carrying the full-length chick *Tbx5* open reading frame (Logan *et al.* 1998; Rallis *et al.* 2003). This delivers a precocious dose of *Tbx5* into the cells of the forelimb-forming LPM. Embryos were then harvested 14-16 days later and were found to be too young to examine sternal morphology because the sternal bands had not yet fully condensed. However, a longer incubation period

was not used due to the small number of embryos available and considerations of embryonic lethality.

The morphology of the forelimbs was examined by alcian blue/alizarin red staining, and of the five surviving embryos, none displayed any visible difference in the size of the left and right forelimb. However, two of five embryos showed a rescue of the most posterior digit on the right (injected) side of the embryo, while the left (contralateral control) side showed a single digit (Figure 33). One harvested embryo formed an additional full digit-like condensation in the right forelimb (Figure, 33A), while the second formed only a small cartilaginous condensation posterior to digit 2 in the right forelimb (Figure 33B). These additional digits were not observed in any uninjected emu skeletal preparations (8 forelimbs in total). These results indicate that precocious expression of *Tbx5* in the emu can rescue forelimb structures that normally are reduced.

Cells of the interlimb flank have a limited time-window in which they are competent to respond to initiation cues and form a limb (Cohn *et al.* 1995). In the emu the delay in *Tbx5* expression could result in a smaller cohort of limb progenitors being recruited and a smaller sternum and forelimb being formed, which displays normal proximo-distal patterning, but is unable to maintain all three digits. By introducing a precocious dose of *Tbx5*, I was able to rescue the formation of an additional digit, suggesting that a larger pool of forelimb progenitors may have been recruited and so another digit could be maintained. These observations are consistent with a model in

which modulation of *Tbx5* expression underlies forelimb and sternum reduction in the emu.

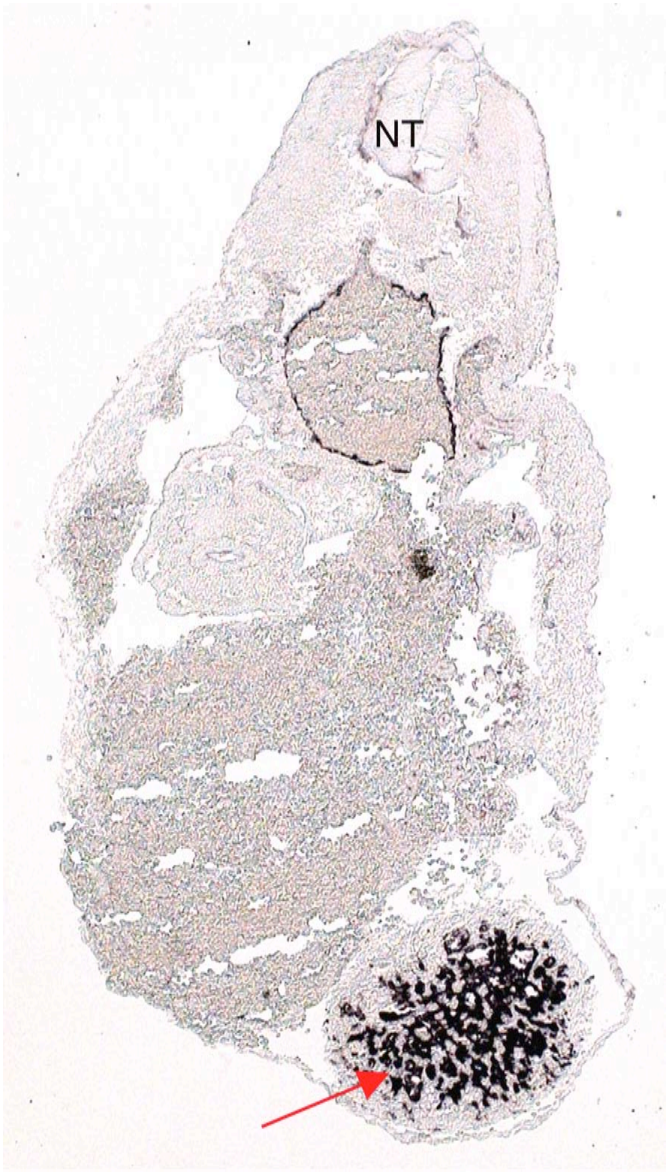

Figure 32. Avian RCAS retrovirus is able to infect emu tissues.

Immunohistochemical staining of a transverse cryosection through an eqHH24 emu embryo using the 3C2 antibody against a viral coat protein. Red arrow indicates alkaline phosphatase staining at site of retroviral infection in the heart. Neural tube, NT.

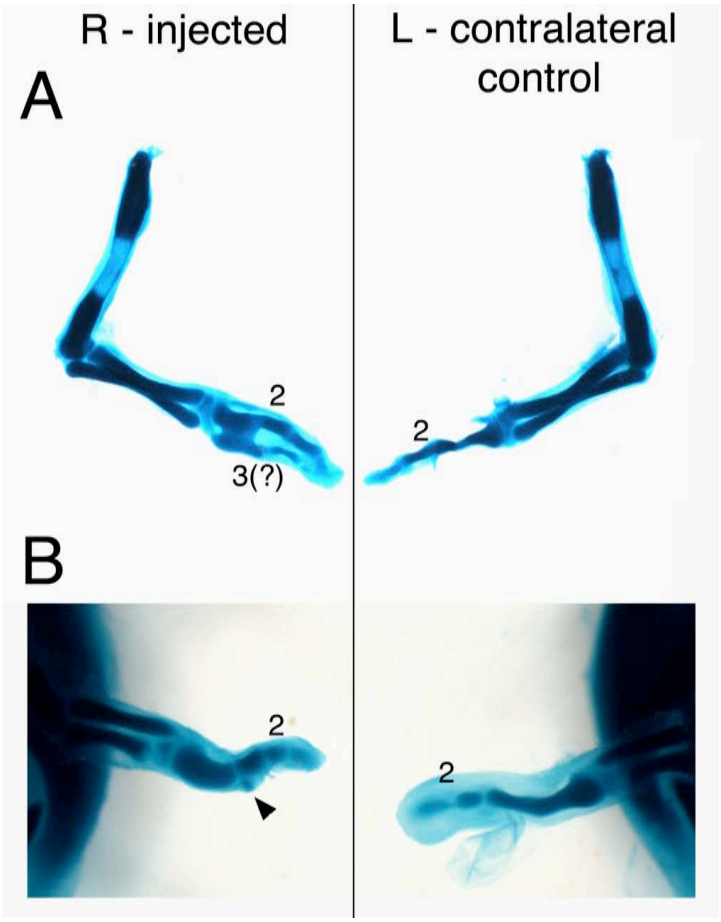

Figure 33. Precocious expression of *Tbx5* in the emu LPM can rescue digit loss.

Alcian blue/alizarin red staining of emu forelimbs. **A**,**B**, Day 23 RCAS injected emus showing the contralateral control left wing with a single digit 2, while in the right injected wing, an additional digit is present, (**A,** 3?) or a single additional condensation forms (**B,** arrowhead).

Taken together, these results suggest that the forelimbs and sternum are functionally linked, and that changes in *Tbx5* expression may enable adaptations in these features. In birds, the size of the sternal keel determines the surface area available for the attachment of the pectoral and supracoracoideus muscles. I have shown that sternum size is correlated with the use of the wings in locomotion across a range of bird species. Flightless birds do not require powerful flight muscles, and have been shown to form the smallest sterna relative to their size. Using the emu as a model flightless bird, I show that the delay in the emergence of the forelimb bud may result in a failure to maintain all but one digit in the wing. I was able to rescue the formation of an additional digit in the emu wing by the introduction of precocious *Tbx5* into pre-limb bud stage embryos. This indicates that the delay in emu *Tbx5* expression may underlie the reduction in the size of the forelimb and sternum.

Chapter Six:

Discussion

Chapter Six: Discussion

6.1 The Sternum and Forelimbs are Developmentally Linked

I have uncovered an embryological link between the forelimbs and sternum, through their common embryological origin and their shared requirement for *Tbx5*. The precursor cells of the sternum originate in the somatic LPM adjacent to the forelimb bud, which places the sternum as a component of the appendicular skeleton, along with the bones of the forelimb and the pectoral girdle. The sternum therefore resides axially within the skeleton but shares an embryological origin with the more laterally residing forelimbs. The *Tbx5* gene expression domain encompasses the progenitors of both the forelimbs and sternum, which provides an explanation for why both elements are affected in *Tbx5* conditional mutants. In *Tbx5* conditional mutant embryos the sternum precursor cells appear to be specified but do not form the sternal bands. Therefore I propose a role for *Tbx5* in the migration of the sternal precursors.

6.1.1 Fate Mapping the Sternum Precursor Cells

The embryological origin of the clavicle, scapula and the bones of the limbs have been well characterised (Huang *et al.* 2000; Valasek *et al.* 2010; Shearman *et al.* 2011). However, the origin of the sternum and the path of sternal precursor cell migration to the midline is not understood. In Chapter 3, I showed that the sternum precursor cells originate in a region of the LPM that is distinct from the forelimb bud and lies adjacent to somites 14 to 21 (Figure 5, Figure 6, Figure 8). This supports the conclusions of early grafting experiments that demonstrated that the cells making up

the sternum do not originate in the somites (Chevallier *et al.* 1977). Early explanting work also suggested that regions of the LPM grown in culture could generate 'sternal band-like' condensations (Fell 1939; Chen 1952; Murillo-Ferrol 1963), but no formal evidence was presented to determine whether these condensations correspond to the sternal tissue. My fate mapping data suggests that the sternum precursor cells would have been present within these cultures, so the condensations formed may indeed correspond to the sternal bands.

Early observational work in the mouse claims the sternal rudiments migrate ahead of the distal tips of the ribs, at the leading edge of the ventral body wall (Chen 1952). However no labelling or lineage tracing was used in this study, and inferences were made based solely on histological observations. I have now shown by DiI labelling that the sternum precursor cells reside at the medial most edge of the body wall as it closes up, moving ahead of the rib progenitors (Figure 9, Figure 16). Initially the cells move directly medially from their origin in the LPM, but from HH30 onwards, they also move rostrally and caudally to form bands at the leading edge of the ventral body wall (Figure 9). The sternum precursor cells appear to mix along the rostro-caudal axis of the sternal bands as they move across the thorax, as each DiI labelling site leads to the distribution of DiI positive cells along most of the length of the sternum (Figure 5, Table 2, Figure 9). Labelling cells in the most rostral region of the sternal precursor population resulted in a rostral bias to the distribution of DiI positive cells seen within the sternum. Conversely, labelling cells in the most caudal region resulted in a caudal bias, and cells in the medial region lead to no bias in the DiI contribution to the sternum. Therefore mixing of the cells along the sternal bands

is not complete, although all regions of the sternal precursor population within the LPM appear to be equally potent in contributing to the sternum.

Sectioning DiI labelled embryos reveals that labelled cells within the sternum do not cross the sternal midline (Figure 6). This result is in agreement with the position of *LacZ* positive cells within the sternum of *Tbx5Intron2lacZ* mouse embryos, which appear as two distinct populations, not mixing at the midline (Figure 15, Figure 16). The mechanism of sternal band fusion is not yet understood, and the behaviour of the cells at the boundary between the left and right sternal bands is not clear. The process of sternal band fusion could be investigated further by labelling the left and right sternal bands with different lineage tracing dyes and incubating embryos to a stage after initial band fusion. This could confirm whether cell mixing occurs at the sternal midline.

6.1.2 How does *Tbx5* Function in Sternum Development?

Tbx5 plays a crucial role in the initiation of forelimb outgrowth, and I have demonstrated that it is also essential in sternum formation. Skeletal preparations show that *Tbx5* conditional mutant embryos completely fail to form both forelimbs and a sternum (Figure 11), and *Tbx5* is expressed throughout the region encompassing the sternal precursors (Figure 13, Figure 14). *Runx1* expression was used as a marker of the sternal bands in mouse embryos, demonstrating that in the absence of *Tbx5*, the bands fail to form (Figure 19). Instead, clusters of *Runx1* positive cells are visible in the most rostral region of either side of the thorax in *Tbx5* conditional mutants. This suggests that *Tbx5* is required early in sternum

development, as the sternal defect is already apparent by E12.5. This is supported by results using a tamoxifen inducible *Prx1CreErt2* transgenic to delete *Tbx5* in the LPM at different times during embryogenesis (Hasson, Logan unpublished). Deletion prior to E10.5 leads to sternal defects, however deletion at E11.5 and onwards leads to the formation of a normal sternum, indicating that *Tbx5* is required prior to E11.5. This time-frame would fit with the hypothesis that *Tbx5* is required for sternum precursor migration to form the sternal bands.

I was unable to directly assess whether or not the requirement for *Tbx5* in sternum development is autonomous to the sternal precursors. Using the *Prx1Cre* line, I generated embryos lacking *Tbx5* in all LPM derived tissues, including the sternal precursors as well as the surrounding connective tissue. The presence of *Runx1* expressing cells in *Tbx5* mutant mice suggests that (at least some) sternal precursors are initially specified in the absence of *Tbx5*. This could indicate a non-autonomous role for *Tbx5* in instructing or laying down a path for the migrating sternal precursors. I have not been able to determine whether the sternal precursors themselves express *Tbx5*, but the expression of the *Tbx5Intron2lacZ* reporter gene within the sternum suggests that this is likely (Figure 16). Chick and mouse *in situ* hybridisation analysis also shows that the *Tbx5* expression domain encompasses the sternal precursor population (Figure 13, Figure 14). To formally demonstrate whether the sternal precursors express *Tbx5*, section *in situ* hybridisations could be carried out for *Runx1* and *Tbx5*, looking for co-expression of the two genes. However, it is important to note that *Tbx5* may be expressed in the sternal precursors, but instead (or additionally) may be required in the surrounding cells. In line with this, a role for *Tbx5* in the muscle connective tissue of the limb has previously been

described (Hasson *et al.* 2010). Connective tissue organisation becomes disrupted in the absence of *Tbx5*, leading to secondary mispatterning of the muscles and tendons. Therefore it is possible that *Tbx5* is required in the abaxial thoracic connective tissue, perhaps instructing or laying down a path for the migrating sternal precursors.

6.1.3 Downstream Targets of *Tbx5* in Sternum Development

In the limb, *Tbx5* directly activates the expression of *Fgf10*, which establishes an FGF-signalling positive feedback loop that drives limb outgrowth (Sekine *et al.* 1999; Ng *et al.* 2002; Rallis *et al.* 2003; Harvey *et al.* 2006). However, *Fgf10* does not appear to play a role in sternum development. In the *Fgf10* null mouse the sternum forms normally, and *Runx1* expression in the sternal bands also appears to be the same in mice lacking *Fgf10* as in control mice (Figure 11 and Figure 19). The expression domain of *Fgf10* does not extend beyond the limb buds and so does not encompass the sternum precursor cells (Figure 13, Figure 14). This rules out *Fgf10* as a crucial target of *Tbx5* in sternum development.

Another potential downstream target of *Tbx5* during sternum formation is *Cx40*. It has been suggested that *Tbx5* may regulate the patterning of the sternum via *Cx40*, and that Holt-Oram syndrome defects occur as a result of reduced *Cx40* levels (Pizard *et al.* 2005). *Cx40* and *Tbx5* have also been shown to be co-expressed in the migrating sternal bands. However, I only found *Cx40* expression in the sternal bands from E13.5 onwards (Figure 20). This suggests that any alteration in *Cx40* expression would arise too late to explain the defects seen in *Tbx5* conditional mutant mice. It is also unlikely therefore that *Cx40* deficiency underlies the sternal

defects observed in Holt-Oram syndrome. I was unable to identify any further candidate genes as targets for *Tbx5* in the sternum, so the direct downstream target(s) of *Tbx5* in sternum development remain to be identified.

6.1.4 *Tbx5* is not Required for Ventral Body Wall Closure

Ventral body wall closure involves a number of different tissues moving medially across the thorax en masse, and meeting at the ventral midline. Little is known about the mechanisms driving the closure of the ventral body wall, or which tissues are necessary or sufficient for the process to be successfully completed. It has been shown that the ribs are not required for body wall closure, as a rib-less mutant mouse in which *Hoxa10* is misexpressed throughout the entire presomitic mesoderm is still able to form a ventral body wall with fused sternal bands (Carapuco *et al.* 2005).

In *Tbx5* conditional mutant embryos, the sternum is completely absent and the ribcage does not close over completely (Figure 11). Many of these embryos show herniation of the internal organs and the ventral body wall remains open (Figure 18F), but in some of these embryos the ventral body wall is able to close normally (Figure 11B). Therefore *Tbx5* is not essential for body wall closure, but it is likely that the disruption caused by the lack of a sternum and the failure of ribcage closure leads to secondary problems in body wall closure in some embryos.

6.1.5 The Sternum is Situated at the Lateral Somitic Frontier

The vertebrate mesoderm can be divided into two separate domains based on environments of tissue patterning. The primaxial domain is made up of musculoskeletal structures that have differentiated in a somite derived connective tissue environment, while the abaxial domain includes all musculoskeletal structures that differentiate in an environment surrounded by connective tissue derived from the LPM (Burke *et al.* 2003). The sternum precursor cells are surrounded by LPM derived connective tissue, placing the sternum within the abaxial patterning domain, along with the pectoral muscle, sternal ribs and limbs (Durland *et al.* 2008). However, the intercostal muscles and proximal ribs belong to the primaxial patterning domain, having differentiated within the somitic compartment (with the exception of the first rib) (Durland *et al.* 2008). Many gene regulatory mechanisms and interactions have been observed to have a different effect in the abaxial and primaxial domains (Burke *et al.* 2003; Winslow *et al.* 2007). For example, in *Hoxb6* and *Hoxb9* deficient mice the sternum and sternal ribs are mispatterned, but the proximal ribs and vertebrae instead show normal patterning but undergo homeotic transformations. (McIntyre *et al.* 2007; Shearman *et al.* 2009). This indicates that the lateral somitic frontier enables adaptations to be made to one domain but not the other (Shearman *et al.* 2009). This could have implications for the occurrence of evolutionary modifications, for example enabling adaptations to be made to the limb skeleton and sternum without affecting the axial skeleton or musculature.

6.1.6 The Segmentation of the Sternum

Mammals form a segmented sternum, with cartilaginous sterno-costal junctions separating ossified sternebrae. These segments are maintained throughout life in most species, although in humans the sterno-costal junctions ossify during puberty and the sternebrae fuse completely (McCormick *et al.* 1981). The avian sternum is not segmented at any stage of development and instead ossifies uniformly along its entire length including at the sites of attachment of the ribs. The mechanism underlying sternum segmentation is not understood, but it has been suggested that the distal ribs may inhibit ossification of the sternum at the sterno-costal junctions (Bryson 1945). This is in agreement with the absence of segmentation in rib-less *Hoxa10* mutant mice (Carapuco *et al.* 2005). Additionally, de-regulation of *Hoxc8* expression results in the formation of one additional pair of ribs, causing the formation of one additional sternebra (Juan *et al.* 2006). These results suggest that rib attachment to the sternum is necessary and sufficient for sternum segmentation, and that the segmentation pattern is determined after sternal band fusion.

I have shown that *Tbx5* expression forms a segmented, ladder-like pattern in the ventral body wall of the mouse from E11.5-E13.5 (Figure 14) and there are also signs of segmentation in the expression of *Runx1* at E13.5 (Figure 19). It is not clear what this ladder-like pattern corresponds to, but it is possible that *Runx1* and *Tbx5* expression reveal a 'pre-pattern' in the sternal bands, delineating the regions of the sternal bands that will go on to form the sternebrae. Chick *Tbx5* expression in the ventral body wall appears as one continuous band, with no signs of segmentation (Figure 13), which fits with the absence of segmentation in the chick sternum. These

results appear at odds with evidence suggesting that segmentation of the sternum occurs after rib attachment. Fate mapping experiments in the chick also reveal that the sternum precursor cells mix along the length of the sternal bands as they migrate (Figure 5, Figure 9), which also seems to conflict with the idea of 'pre-patterning' within the sternal bands. Alternatively, it is possible that the sternal precursors may behave differently within the sternal bands in the chick and in the mouse.

6.1.7 Insights into Holt-Oram Syndrome Aetiology and other Sternal Defects

Holt-Oram syndrome is caused by mutations in *Tbx5* and is known to affect the upper limbs and sternum (Newbury-Ecob *et al.* 1996; Basson *et al.* 1997). The role of *Tbx5* in the forelimbs has been well studied, but here for the first time I present evidence of an essential role for *Tbx5* in the formation of the sternum. This has clinical relevance in explaining the aetiology of sternal defects in Holt-Oram syndrome. An estimated 40% of Holt-Oram patients exhibit pectus excavatum, where the sternum becomes sunken into the chest (Newbury-Ecob *et al.* 1996). I have found that *Tbx5* is required at the earliest stages of sternum development, as there is a failure of sternal band formation prior to E12.5 in $Tbx5^{lox/lox}$*;Prx1Cre* mouse embryos (Figure 19) and conditional deletion after E11.5 does not produce sternum defects (Hasson, Logan unpublished). My data indicates that sternum abnormalities arising in the absence of *Tbx5* are caused by disrupted migration of sternal precursors, rather from disruption of sternal band fusion, or a failure to specify this population of cells. Therefore I suggest that in Holt-Oram syndrome patients, pectus excavatum arises as a result or aberrant sternal precursor cell

migration. This work could also provide the basis of a framework for understanding the origins of other sternum abnormalities in humans. With a clearer knowledge of the process of sternum formation, it is easier to dissect what developmental problems may underlie sternum defects.

6.2 An Evolutionary Link between the Sternum and Forelimbs

I have generated evidence to suggest that the sternum and forelimbs adapt in concert in different tetrapod lineages. Focusing on avians, I have shown that sternum size is correlated with the use of the forelimbs in both flying and diving species (Figure 21, Figure 22). For example, flightless birds do not use their wings for locomotion, and have a small sterna with a short keel. Flightless species also tend to have much smaller wings than flighted species (King *et al.* 1975; McCall *et al.* 1998) As species have less use for the wings, the cost of maintaining a high mass of pectoral muscle becomes less beneficial. The pectoral muscle can often make up one quarter of the weight of the bird (King *et al.* 1975), and places high demands on the metabolism, so flightless species tend to display a reduced pectoral muscle mass (McNab 1994). A similar correlative relationship has been observed between avian flight style and the shape of the furcula (Hui 2002). A V-shaped furcula, which creates less drag, is seen in sub-aqueous species such as penguins, while a more U-shaped furcula, generating more drag, is observed in aerial soaring birds. This demonstrates that the morphology of more axially located features should be considered in addition to elements of the wing when examining flight ability and adaptations.

6.2.1 Outgrowth of the Sternal Keel

I have demonstrated that sternal keel height is quantitatively related to differences in flight requirements (Figure 21). However, very little is known about the process of keel outgrowth. In birds the fusion of the two sternal bands is followed immediately by the development of the keel, which forms along the line of fusion of the two sternal plates (Fell 1939). Explants of ventral body wall tissue have indicated that the keel is still able to grow out following removal of the pectoral muscle and rib rudiments, and also that sternal band fusion may not be required for keel outgrowth (Fell 1939). It is possible that the sternal keel may be a highly adapted bone ridge. Bone ridges provide anchoring points for the attachment of muscles (Blitz *et al.* 2009). For example the deltoid tuberosity is a bone ridge formed in the middle of the humerus where the deltoid muscle attach. The formation of bone ridges is regulated by tendon attachment (Blitz *et al.* 2009), and therefore if a chick lacking pectoral muscle or tendons could be generated, sternal keel formation could be examined to determine whether the keel is indeed a bone ridge.

6.2.2 Temporal Adaptations in *Tbx5* expression underlie Forelimb and Sternum Adaptation in the Emu

I investigated the genetic mechanisms underlying the reduction in wing and sternum size in flightless birds, uncovering a role for *Tbx5* in this process. Modulation at the level of *Tbx5* expression enables adaptations of these features specifically, without affecting other skeletal elements. I demonstrate that *Tbx5* expression is temporally delayed in the emu LPM (Figure 31), causing a delay in the initiation of emu forelimb outgrowth. This delay means that the emu hindlimb emerges ahead of the

forelimb, in a reversal of the heterochrony in limb formation observed in the chick (Figure 31; Bellairs *et al.* 2005).

I propose that the delay in *Tbx5* expression results in the recruitment of a smaller pool of forelimb and sternum progenitor cells and a delay in the emergence of the forelimb bud. There is evidence to suggest that limb initiation usually occurs during an optimal temporal window. Undifferentiated cells within the LPM are able to respond to *Tbx5* for a limited time, but later are exposed to other cues that may cause them to differentiate into other cell types. The introduction of a FGF-soaked bead into the chick LPM is able to induce the outgrowth of an ectopic limb, but if this bead is applied at a later developmental time, no limb is able to form (Cohn *et al.* 1995). The recruitment of a smaller pool of progenitor cells may explain why the emu forelimb is not able to support the maintenance of three mature digits, despite all three being specified (Figure 24). However, it is also possible that a different mechanism underlies the reduction in digit number, such as an early silencing of *Sonic Hedgehog* (*Shh*) signalling in the forelimb, as observed in the Australian skink (Shapiro *et al.* 2003).

Limb heterochrony is observed in many other tetrapod species. For example marsupials form preccocial forelimbs which help them to climb to the teat after birth. An acceleration in the marsupial forelimb developmental program has been demonstrated, including an acceleration in the activation of *Tbx5* in the LPM (Keyte *et al.* 2010). Flightless bird species have arisen in multiple different avian families, and new phylogenetic evidence also suggests that flight has been lost multiple times

independently within the ratite family (Harshman *et al.* 2008). Therefore it would be interesting to investigate whether other ratite species show limb heterochrony and/or a delay in *Tbx5* expression accompanying forelimb and sternum reduction. Alternatively, the reduction in forelimb and sternum size in other avian species may have evolved through entirely different adaptation mechanisms.

6.2.3 *Tbx5* acts as a Regulatory Node in the Development of the Forelimbs and Sternum

My work suggests that modulation of *Tbx5* expression allows changes to be made specifically to the forelimb and sternum developmental programs, without affecting the hindlimbs or other LPM derived structures. Previous work has also suggested *Tbx5* modulation as a mechanism to generate limb-type specific morphological changes on an evolutionary scale (Duboc *et al.* 2009). The downstream targets of *Tbx5* differ in sternum and forelimb development, but by modulating expression at the level of *Tbx5*, adaptations can be made to both structures. Additionally, modulations in *Tbx5* affect only the forelimbs, and leave the hindlimbs unaffected. I propose that modulation at the level of *Tbx5* could explain the concerted adaptation of the sternum and forelimbs in other tetrapod lineages.

6.3 Summary

The fin-to-limb transition and acquisition of sterna were critical steps in the evolution of tetrapods. The sternum is essential for tetrapod locomotion, acting as an attachment site for the pectoral muscles, which, in quadrupeds, help lift the body

from the ground. However, despite the importance of the sternum in enabling tetrapod locomotion and avian flight, the acquisition and adaptation of the sternum have been overlooked in previous studies. Additionally, little is known about the genetic regulation of sternum development or the origins of sternum defects.

Here I demonstrate that *Tbx5* is essential for the formation of both the forelimbs and sternum. I reveal the shared embryological origins of the forelimbs and sternum, and demonstrate a common *Tbx5* gene expression domain encompassing the forelimb and sternum progenitors, providing a mechanistic explanation for how these structures have adapted in concert in different tetrapod lineages. Developing these links further, I demonstrate a quantitative correlation between sternum dimensions and forelimb use across avian species. Using the emu as an example of a flightless bird, I show that *Tbx5* acts as a regulatory node for the adaptation of derivatives of the forelimb skeleton and I suggest that other tetrapod locomotor adaptations may also involve modulation of *Tbx5* expression.

References

Abdala, V. and R. Diogo (2010). Comparative anatomy, homologies and evolution of the pectoral and forelimb musculature of tetrapods with special attention to extant limbed amphibians and reptiles. *Journal of Anatomy* **217**(5): 536-573.

Ahlberg, P. E., J. A. Clack and H. Blom (2005). The axial skeleton of the Devonian tetrapod Ichthyostega. *Nature* **437**(7055): 137-140.

Akiyama, H., M. C. Chaboissier, J. F. Martin, A. Schedl and B. de Crombrugghe (2002). The transcription factor Sox9 has essential roles in successive steps of the chondrocyte differentiation pathway and is required for expression of Sox5 and Sox6. *Genes & Development* **16**(21): 2813-2828.

Baffi, M. O., M. A. Moran and R. Serra (2006). Tgfbr2 regulates the maintenance of boundaries in the axial skeleton. *Developmental Biology* **296**(2): 363-374.

Baier, D. B., S. M. Gatesy and F. A. Jenkins (2007). A critical ligamentous mechanism in the evolution of avian flight. *Nature* **445**(7125): 307-310.

Bamshad, M., R. C. Lin, D. J. Law, W. C. Watkins, P. A. Krakowiak, M. E. Moore, P. Franceschini, R. Lala, L. B. Holmes, T. C. Gebuhr, B. G. Bruneau, A. Schinzel, J. G. Seidman, C. E. Seidman and L. B. Jorde (1997). Mutations in human TBX3 alter limb, apocrine and genital development in ulnar-mammary syndrome. *Nat Genet* **16**(3): 311-315.

Basson, C. T., D. R. Bachinsky, R. C. Lin, T. Levi, J. A. Elkins, J. Soults, D. Grayzel, E. Kroumpouzou, T. A. Traill, J. LeblancStraceski, B. Renault, R. Kucherlapati, J. G. Seidman and C. E. Seidman (1997). Mutations in human TBX5 cause limb and cardiac malformation in Holt-Oram syndrome. *Nature Genetics* **15**(1): 30-35.

Basson, C. T., T. Huang, R. C. Lin, D. R. Bachinsky, S. Weremowicz, A. Vaglio, R. Bruzzone, R. Quadrelli, M. Lerone, G. Romeo, M. Silengo, A. Pereira, J. Krieger, S. F. Mesquita, M. Kamisago, C. C. Morton, M. E. Pierpont, C. W. Muller, J. G. Seidman and C. E. Seidman (1999). Different TBX5 interactions in heart and limb defined by Holt-Oram syndrome mutations. *Proc Natl Acad Sci U S A* **96**(6): 2919-2924.

Bellairs, R. and M. Osmond (2005). The Atlas of Chick Development. London, Academic Press.

Belting, H. G., C. S. Shashikant and F. H. Ruddle (1998). Multiple phases of expression and regulation of mouse Hoxc8 during early embryogenesis. *Journal of Experimental Zoology* **282**(1-2): 196-222.

Blitz, E., S. Viukov, A. Sharir, Y. Shwartz, J. L. Galloway, B. A. Pryce, R. L. Johnson, C. J. Tabin, R. Schweitzer and E. Zelzer (2009). Bone Ridge Patterning during Musculoskeletal Assembly Is Mediated through SCX Regulation of Bmp4 at the Tendon-Skeleton Junction. *Developmental Cell* **17**(6): 861-873.

Bruneau, B. G., G. Nemer, J. P. Schmitt, F. Charron, L. Robitaille, S. Caron, D. A. Conner, M. Gessler, M. Nemer, C. E. Seidman and J. G. Seidman (2001). A murine model of Holt-Oram syndrome defines roles of the T-box transcription factor Tbx5 in cardiogenesis and disease. *Cell* **106**(6): 709-721.

Bryson, V. (1945). Development of the sternum in screw tail mice. *The Anatomical Record* **91**(2): 119-141.

Burke, A. C. and J. L. Nowicki (2003). A new view of patterning domains in the vertebrate mesoderm. *Developmental Cell* **4**(2): 159-165.

Carapuco, M., A. Novoa, N. Bobola and M. Mallo (2005). Hox genes specify vertebral types in the presomitic mesoderm. *Genes & Development* **19**(18): 2116-2121.

Chen, J. M. (1952). Studies on the Morphogeneesis of the Mouse Sternum I. Normal Embryonic Development. *Journal of Anatomy* **86**(4): 373-386.

Chen, J. M. (1952). Studies on the Morphogenesis of the Mouse Sternum II. Experimens on the Origin of the Sternum and its Capacity for Differentiation *in vitro*. *Journal of Anatomy* **86**(4): 387-401.

Chen, J. M. (1953). Studies on the Morphogenesis of the Mouse Sternum III. Experiments on the Closure and Segmentation of the Sternal Bands. *Journal of Anatomy* **87**(2): 130-149.

Chevallier, A. (1975). Role of Somitic Mesoderm in Development of Rib Cage of Bird Embryos.1. Origin of Sternal Component and Conditions for Development of Ribs. *Journal of Embryology and Experimental Morphology* **33**(Apr): 291-311.

Chevallier, A., M. Kieny, A. Mauger and P. Sengel (1977). Developmental fate of the somitic mesoderm in the chick embryo. Vertebrate limb and somite morphogenesis. D. A. Ede, J. R. Hinchcliffe and M. Balls. Cambridge, Cambridge University Press.

Clack, J. A. (2002). Gaining Ground: The Origin and Evolution of Tetrapods. Bloomington, Indiana, Indiana University Press.

Clack, J. A. (2005). Getting a leg up on land. *Scientific American* **293**(6): 100-107.

Clarke, J. A., Z. H. Zhou and F. C. Zhang (2006). Insight into the evolution of avian flight from a new clade of Early Cretaceous ornithurines from China and the morphology of Yixianornis grabaui. *Journal of Anatomy* **208**(3): 287-308.

Cohn, M. J., J. C. Izpisua-Belmonte, H. Abud, J. K. Heath and C. Tickle (1995). Fibroblast growth factors induce additional limb development from the flank of chick embryos. *Cell* **80**(5): 739-746.

Compagni, A., M. Logan, R. Klein and R. H. Adams (2003). Control of skeletal patterning by ephrinB1-EphB interactions. *Developmental Cell* **5**(2): 217-230.

Deeming, D. C. (1997). Ratite Egg Incubation. Buckinghamshire, Ratite Conference Books.

Dietrich, S. and P. Gruss (1995). Undulated Phenotypes Suggest a Role of Pax-1 for the Development of Vertebral and Extravertebral Structures. *Developmental Biology* **167**(2): 529-548.

Duboc, V. and M. P. O. Logan (2009). Building limb morphology through integration of signalling modules. *Current Opinion in Genetics & Development* **19**(5): 497-503.

Dunker, N. and K. Krieglstein (2002). Tgfbeta2 -/- Tgfbeta3 -/- double knockout mice display severe midline fusion defects and early embryonic lethality. *Anatomy and Embryology (Berlin)* **206**(1-2): 73-83.

Durland, J. L., M. Sferlazzo, M. Logan and A. C. Burke (2008). Visualizing the lateral somitic frontier in the Prx1Cre transgenic mouse. *Journal of Anatomy* **212**(5): 590-602.

Elzanowski, A. (1988). Ontogeny and Evolution of the Ratites. *Acta XIX Congress Internationalis Ornithologici* **2**: 2037-2046.

Eng, S. R., J. Lanier, N. Fedtsova and E. E. Turner (2004). Coordinated regulation of gene expression by Brn3a in developing sensory ganglia. *Development* **131**(16): 3859-3870.

Engum, S. A. (2008). Embryology, sternal clefts, ectopia cordis, and cantrell's pentalogy. *Seminars in Pediatric Surgery* **17**(3): 154-160.

Fell, H. B. (1939). The Origin and Developmental Mechanics of the Avian Sternum. *Philosophical Transactions of the Royal Society B: Biological Sciences* **229**(563): 407-463.

Gibson-Brown, J. J., S. I. Agulnik, D. L. Chapman, M. Alexiou, N. Garvey, L. M. Silver and V. E. Papaioannou (1996). Evidence of a role for T-box genes in the evolution of limb morphogenesis and the specification of forelimb/hindlimb identity. *Mechanisms of Development* **56**(1-2): 93-101.

Gilbert, S. F., G. A. Loredo, A. Brukman and A. C. Burke (2001). Morphogenesis of the turtle shell: the development of a novel structure in tetrapod evolution. *Evolution & Development* **3**(2): 47-58.

Gladstone, R. J. and C. G. Wakely (1932). The Morphology of the Sternum and its Relation to the Ribs. *Journal of Anatomy* **66**: 508-564.

Gordon, C. T., F. A. Rodda and P. G. Farlie (2009). The RCAS Retroviral Expression System in the Study of Skeletal Development. *Developmental Dynamics* **238**(4): 797-811.

Hall, B. K. (2001). Development of the clavicles in birds and mammals. *Journal of Experimental Zoology* **289**(3): 153-161.

Hamburger, V. and H. L. Hamilton (1951). A Series of Normal Stages in the Development of the Chick Embryo. *Journal of Morphology* **88**(1): 49-92.

Harshman, J., E. L. Braun, M. J. Braun, C. J. Huddleston, R. C. Bowie, J. L. Chojnowski, S. J. Hackett, K. L. Han, R. T. Kimball, B. D. Marks, K. J. Miglia, W. S. Moore, S. Reddy, F. H. Sheldon, D. W. Steadman, S. J. Steppan, C. C. Witt and T. Yuri (2008). Phylogenomic evidence for multiple losses of flight in ratite birds. *Proceedings of the National Academy of Sciences of the United States of America* **105**(36): 13462-13467.

Harvey, S. A. and M. P. O. Logan (2006). Sall4 acts downstream of Tbx5 and is required for pectoral fin outgrowth. *Development* **133**(6): 1165-1173.

Hasson, P., J. Del Buono and M. P. O. Logan (2007). Tbx5 is dispensable for forelimb outgrowth. *Development* **134**(1): 85-92.

Hasson, P., A. DeLaurier, M. Bennett, E. Grigorieva, L. A. Naiche, V. E. Papaioannou, T. J. Mohun and M. P. O. Logan (2010). Tbx4 and Tbx5 Acting in Connective Tissue Are Required for Limb Muscle and Tendon Patterning. *Developmental Cell* **18**(1): 148-156.

Hasty, P., A. Bradley, J. H. Morris, D. G. Edmondson, J. M. Venuti, E. N. Olson and W. H. Klein (1993). Muscle Deficiency and Neonatal Death in Mice with a Targeted Mutation in the Myogenin Gene. *Nature* **364**(6437): 501-506.

Havelkova, P. and Z. Rocek (2006). Transformation of the pectoral girdle in the evolutionary origin of frogs: insights from the primitive anuran Discoglossus. *Journal of Anatomy* **209**(1): 1-11.

Huang, R., Q. Zhi, K. Patel, J. Wilting and B. Christ (2000). Dual origin and segmental organisation of the avian scapula. *Development* **127**(17): 3789-3794.

Hui, C. A. (2002). Avian furcula morphology may indicate relationships of flight requirements among birds. *Journal of Morphology* **251**(3): 284-293.

Hume, J. P. and L. Steel (2013). Fight club: a unique weapon in the wing of the solitaire, *Pezophaps solitaria* (Aves: Columbidae), an extinct flightless bird from Rodrigues, Mascarene Islands. *Biological Journal of the Linnean Society*.

Janis, C. M. and J. C. Keller (2001). Modes of ventilation in early tetrapods: Costal aspiration as a key feature of amniotes. *Acta Palaeontologica Polonica* **46**(2): 137-170.

Juan, A. H., H. Y. Lei, P. Bhargava, M. Lebrun and F. H. Ruddle (2006). Multiple roles of Hoxc8 in skeletal development. *Skeletal Development and Remodeling in Health, Disease, and Aging* **1068**: 87-94.

Kaiser, G. W. (2007). The Inner Bird: Anatomy and Evolution. Vancouver, University Washington Press.

Kardong, K., V. (1998). Vertebrates: comparative Anatomy, Function, Evolution, McGraw Hill.

Kaufman, M. H. (1992). The Atlas of Mouse Development. London, Academic Press.

Kelly, R. E. (2008). Pectus excavatum: historical background, clinical picture, preoperative evaluation and criteria for operation. *Seminars in Pediatric Surgery* **17**(3): 181-193.

Keyte, A. L. and K. K. Smith (2010). Developmental origins of precocial forelimbs in marsupial neonates. *Development* **137**(24): 4283-4294.

Kimura, A., H. Inose, F. Yano, K. Fujita, T. Ikeda, S. Sato, M. Iwasaki, T. Jinno, K. Ae, S. Fukumoto, Y. Takeuchi, H. Itoh, T. Imamura, H. Kawaguchi, U. Chung, J. F. Martin, S. Iseki, K. Shinomiya and S. Takeda (2010). Runx1 and Runx2 cooperate during sternal morphogenesis. *Development* **137**(7): 1159-1167.

King, A. S. and J. McLelland (1975). Outlines of Avian Anatomy. London, Bailliere Tindall.

Komori, T., H. Yagi, S. Nomura, A. Yamaguchi, K. Sasaki, K. Deguchi, Y. Shimizu, R. T. Bronson, Y. H. Gao, M. Inada, M. Sato, R. Okamoto, Y. Kitamura, S. Yoshiki and T. Kishimoto (1997). Targeted disruption of Cbfa1 results in a complete lack of bone formation owing to maturational arrest of osteoblasts. *Cell* **89**(5): 755-764.

Kotzot, D. and A. H. Schwabegger (2009). Etiology of chest wall deformities -a genetic review for the treating physician. *Journal of Pediatric Surgery* **44**(10): 2004-2011.

Kriss, V. M. (1999). Down Syndrome: Imaging of multiorgan involvement. *Clinical Pediatrics* **38**(8): 441-449.

Laclef, C., G. Hamard, J. Demignon, E. Souil, C. Houbron and P. Maire (2003). Altered myogenesis in Six1-deficient mice. *Development* **130**(10): 2239-2252.

Levanon, D. and Y. Groner (2004). Structure and regulated expression of mammalian RUNX genes. *Oncogene* **23**(24): 4211-4219.

Li, Q. Y., R. A. Newbury-Ecob, J. A. Terrett, D. I. Wilson, A. R. Curtis, C. H. Yi, T. Gebuhr, P. J. Bullen, S. C. Robson, T. Strachan, D. Bonnet, S. Lyonnet, I. D. Young, J. A. Raeburn, A. J. Buckler, D. J. Law and J. D. Brook (1997). Holt-Oram syndrome is caused by mutations in TBX5, a member of the Brachyury (T) gene family. *Nature Genetics* **15**(1): 21-29.

Liakhovitskaia, A., E. Lana-Elola, E. Stamateris, D. P. Rice, R. J. van't Hof and A. Medvinsky (2010). The essential requirement for Runx1 in the development of the sternum. *Developmental Biology* **340**(2): 539-546.

Lian, J. B., G. S. Stein, A. Javed, A. J. van Wijnen, J. L. Stein, M. Montecino, M. Q. Hassan, T. Gaur, C. J. Lengner and D. W. Young (2006). Networks and hubs for the transcriptional control of osteoblastogenesis. *Reviews in Endocrine and Metabolic Disorders* **7**(1-2): 1-16.

Liu, K. J., J. R. Arron, K. Stankunas, G. R. Crabtree and M. T. Longaker (2007). Chemical rescue of cleft palate and midline defects in conditional GSK-3 beta mice. *Nature* **446**(7131): 79-82.

Livezey, B. C. (1992). Morphological Corollaries and Ecological Implications of Flightlessness in the Kakapo (Psittaciformes, Strigops-Habroptilus). *Journal of Morphology* **213**(1): 105-145.

Logan, M., J. F. Martin, A. Nagy, C. Lobe, E. N. Olson and C. J. Tabin (2002). Expression of Cre Recombinase in the developing mouse limb bud driven by a Prxl enhancer. *Genesis* **33**(2): 77-80.

Logan, M., H. G. Simon and C. Tabin (1998). Differential regulation of T-box and homeobox transcription factors suggests roles in controlling chick limb-type identity. *Development* **125**(15): 2825-2835.

Logan, M. and C. Tabin (1998). Targeted gene misexpression in chick limb buds using avian replication-competent retroviruses. *Methods-a Companion to Methods in Enzymology* **14**(4): 407-420.

Logan, M. and C. J. Tabin (1999). Role of Pitx1 upstream of Tbx4 in specification of hindlimb identity. *Science* **283**(5408): 1736-1739.

Manley, N. R., J. R. Barrow, T. Zhang and M. R. Capecchi (2001). Hoxb2 and Hoxb4 act together to specify ventral body wall formation. *Developmental Biology* **237**(1): 130-144.

Mathes, S. J., A. E. Seyfer and E. P. Miranda (2011). Congenital Abnormalities of the Chest Wall. Congenital Thoracic Wall Deformities. A. H. Schwabegger. Wien, Springer-Verlag.

Mathew, S. J., J. M. Hansen, A. J. Merrell, M. M. Murphy, J. A. Lawson, D. A. Hutcheson, M. S. Hansen, M. Angus-Hill and G. Kardon (2011). Connective tissue fibroblasts and Tcf4 regulate myogenesis. *Development* **138**(2): 371-384.

Maxwell, E. E. and H. C. E. Larsson (2007). Osteology and myology of the wing of the Emu (Dromaius novaehollandiae), and its bearing on the evolution of vestigial structures. *Journal of Morphology* **268**(5): 423-441.

McCall, R. A., S. Nee and P. H. Harvey (1998). The role of wing length in the evolution of avian flightlessness. *Evolutionary Ecology* **12**(5): 569-580.

McCormick, W. F. and M. M. Nichols (1981). Formation and Maturation of the Human Sternum. 1. Fetal Period. *American Journal of Forensic Medicine and Pathology* **2**(4): 323-328.

McGrew, M. J., A. Sherman, F. M. Ellard, S. G. Lillico, H. J. Gilhooley, A. J. Kingsman, K. A. Mitrophanous and H. Sang (2004). Efficient production of germline transgenic chickens using lentiviral vectors. *Embo Reports* **5**(7): 728-733.

McIntyre, D. C., S. Rakshit, A. R. Yallowitz, L. Loken, L. Jeannotte, M. R. Capecchi and D. M. Wellik (2007). Hox patterning of the vertebrate rib cage. *Development* **134**(16): 2981-2989.

McNab, B. K. (1994). Energy-Conservation and the Evolution of Flightlessness in Birds. *American Naturalist* **144**(4): 628-642.

Mehta, A. V., B. Chidambaram, A. A. Suchedina and A. R. Garrett (1993). Radiologic Abnormalities of the Sternum in Turners-Syndrome. *Chest* **104**(6): 1795-1799.

Minguillon, C. and M. Logan (2003). The comparative genomics of T-box genes. *Brief Funct Genomic Proteomic* **2**(3): 224-233.

Minguillon, C., S. Nishimoto, S. Wood, E. Vendrell, J. J. Gibson-Brown and M. P. Logan (2012). Hox genes regulate the onset of Tbx5 expression in the forelimb. *Development* **139**(17): 3180-3188.

Miyajima, D., T. Hayata, T. Suzuki, H. Hemmi, T. Nakamoto, T. Notomi, T. Amagasa, R. T. Bottcher, M. Costell, R. Fassler, Y. Ezura and M. Noda (2012). Profilin1 Regulates Sternum Development and Endochondral Bone Formation. *Journal of Biological Chemistry* **287**(40): 33545-33553.

Murillo-Ferrol, N. L. (1963). About the forming material of the ribs and sternum. An experimental analysis in the chick embryo. *Anales del desarollo*.

Nagai, H., S. S. Mak, W. Weng, Y. Nakaya, R. Ladher and G. J. Sheng (2011). Embryonic Development of the Emu, *Dromaius novaehollandiae*. *Developmental Dynamics* **240**(1): 162-175.

Newbury-Ecob, R. A., R. Leanage, J. A. Raeburn and I. D. Young (1996). Holt-Oram syndrome: a clinical genetic study. *Journal of Medical Genetics* **33**(4): 300-307.

Ng, J. K., Y. Kawakami, D. Buscher, A. Raya, T. Itoh, C. M. Koth, C. Rodriguez Esteban, J. Rodriguez-Leon, D. M. Garrity, M. C. Fishman and J. C. Izpisua Belmonte (2002). The limb identity gene Tbx5 promotes limb initiation by interacting with Wnt2b and Fgf10. *Development* **129**(22): 5161-5170.

Ohuchi, H., T. Nakagawa, A. Yamamoto, A. Araga, T. Ohata, Y. Ishimaru, H. Yoshioka, T. Kuwana, T. Nohno, M. Yamasaki, N. Itoh and S. Noji (1997). The mesenchymal factor, FGF10, initiates and maintains the outgrowth of the chick limb bud through interaction with FGF8, an apical ectodermal factor. *Development* **124**(11): 2235-2244.

Okuda, T., J. van Deursen, S. W. Hiebert, G. Grosveld and J. R. Downing (1996). AML1, the target of multiple chromosomal translocations in human leukemia, is essential for normal fetal liver hematopoiesis. *Cell* **84**(2): 321-330.

Olk, S., G. Zoidl and R. Dermietzel (2009). Connexins, Cell Motility, and the Cytoskeleton. *Cell Motility and the Cytoskeleton* **66**(11): 1000-1016.

Olson, S. L. and A. Feduccia (1979). Flight Capability and the Pectoral Girdle of Archaeopteryx. *Nature* **278**(5701): 247-248.

Ostrom, J. H. (1970). Archaeopteryx - Notice of a New Specimen. *Science* **170**(3957): 537.

Otto, F., A. P. Thornell, T. Crompton, A. Denzel, K. C. Gilmour, I. R. Rosewell, G. W. Stamp, R. S. Beddington, S. Mundlos, B. R. Olsen, P. B. Selby and M. J. Owen (1997). Cbfa1, a candidate gene for cleidocranial dysplasia syndrome, is essential for osteoblast differentiation and bone development. *Cell* **89**(5): 765-771.

Parker, T. J. (1891). On the presence of a sternum in *Notidanus indicus*. *Nature* **43**: 142.

Patterson, A. M. (1900). The sternum; its early development and ossification in man and mammals. *Journal of Anatomy and Physiology* **35**(1).

Pierce, S. E., P. E. Ahlberg, J. R. Hutchinson, J. L. Molnar, S. Sanchez, P. Tafforeau and J. A. Clack (2013). Vertebral architecture in the earliest stem tetrapods. *Nature* **494**(7436): 226-229.

Pizard, A., P. G. Burgon, D. L. Paul, B. G. Bruneau, C. E. Seidman and J. G. Seidman (2005). Connexin 40, a target of the transcription factor Tbx5, patterns wrist, digits, and sternum. *Mol Cell Biol* **25**(12): 5073-5083.

Poore, S. O., A. SanchezHaiman and G. E. Goslow (1997). Wing upstroke and the evolution of flapping flight. *Nature* **387**(6635): 799-802.

Rallis, C., B. G. Bruneau, J. Del Buono, C. E. Seidman, J. G. Seidman, S. Nissim, C. J. Tabin and M. P. Logan (2003). Tbx5 is required for forelimb bud formation and continued outgrowth. *Development* **130**(12): 2741-2751.

Riddle, R. D., R. L. Johnson, E. Laufer and C. Tabin (1993). Sonic hedgehog mediates the polarizing activity of the ZPA. *Cell* **75**(7): 1401-1416.

Romer, A., S. and T. Parsons, S. (1978). The Vertebrate Body. Piladelphia, W. B. Saunders Company.

Ruge, G. (1880). About the Development of the Sternum (Uber die Entwickelung des Sternum). *Morphological Jahrbuch* **6**.

Scambler, P. J., A. H. Carey, R. K. Wyse, S. Roach, J. P. Dumanski, M. Nordenskjold and R. Williamson (1991). Microdeletions within 22q11 associated with sporadic and familial DiGeorge syndrome. *Genomics* **10**(1): 201-206.

Sekine, K., H. Ohuchi, M. Fujiwara, M. Yamasaki, T. Yoshizawa, T. Sato, N. Yagishita, D. Matsui, Y. Koga, N. Itoh and S. Kato (1999). Fgf10 is essential for limb and lung formation. *Nature Genetics* **21**(1): 138-141.

Seno, T. (1961). The Origin and Evolution of the Sternum. *Anatomischer Anzeiger* **110**: 97-101.

Shapiro, M. D., J. Hanken and N. Rosenthal (2003). Developmental basis of evolutionary digit loss in the Australian lizard Hemiergis. *Journal of Experimental Zoology Part B-Molecular and Developmental Evolution* **297B**(1): 48-56.

Shearman, R. M. and C. Burke (2009). The Lateral Somitic Frontier in Ontogeny and Phylogeny. *Journal of Experimental Zoology Part B-Molecular and Developmental Evolution* **312B**(6): 603-612.

Shearman, R. M., F. J. Tulenko and A. C. Burke (2011). 3D reconstructions of quail-chick chimeras provide a new fate map of the avian scapula. *Developmental Biology* **355**(1): 1-11.

Shubin, N. H., E. B. Daeschler and F. A. Jenkins (2006). The pectoral fin of *Tiktaalik roseae* and the origin of the tetrapod limb. *Nature* **440**(7085): 764-771.

Smigiel, R., A. Jakubiak, M. P. Lombardi, W. Jaworski, R. Slezak, D. Patkowski and R. C. Hennekam (2011). Co-occurrence of Severe Goltz-Gorlin Syndrome and Pentalogy of Cantrell - Case Report and Review of the Literature. *American Journal of Medical Genetics Part A* **155A**(5): 1102-1105.

Smith, N., Y. Dong, J. B. Lian, J. Pratap, P. D. Kingsley, A. J. van Wijnen, J. L. Stein, E. M. Schwarz, R. J. O'Keefe, G. S. Stein and M. H. Drissi (2005). Overlapping expression of Runx1(Cbfa2) and Runx2(Cbfa1) transcription factors supports cooperative induction of skeletal development. *J Cell Physiol* **203**(1): 133-143.

Soriano, P. (1999). Generalized lacZ expression with the ROSA26 Cre reporter strain. *Nature Genetics* **21**(1): 70-71.

Strickland, H. E. and A. G. Melville (1848). The Dodo and Its Kindred; or the History, Affinities and Osteology of the Dodo, Solitaire, and Other Extinct Birds of the Islands Mauritius, Rodriguez, and Bourbon. London, Benham and Reeve.

Sylva, M., V. S. W. Li, A. A. A. Buffing, J. H. van Es, M. van den Born, S. van der Velden, Q. Gunst, J. H. Koolstra, A. F. M. Moorman, H. Clevers and M. J. B. van den Hoff (2011). The BMP Antagonist Follistatin-Like 1 Is Required for Skeletal and Lung Organogenesis. *Plos One* **6**(8).

Takagi, T., H. Moribe, H. Kondoh and Y. Higashi (1998). DeltaEF1, a zinc finger and homeodomain transcription factor, is required for skeleton patterning in multiple lineages. *Development* **125**(1): 21-31.

Tucker, M. E., H. J. Garringer and D. D. Weaver (2007). Phenotypic spectrum of mosaic trisomy 18: Two new patients, a literature review, and counseling issues. *American Journal of Medical Genetics Part A* **143A**(5): 505-517.

Valasek, P., S. Theis, A. DeLaurier, Y. Hinits, G. N. Luke, A. M. Otto, J. Minchin, L. He, B. Christ, G. Brooks, H. Sang, D. J. Evans, M. Logan, R. Huang and K. Patel (2011). Cellular and molecular investigations into the development of the pectoral girdle. *Developmental Biology* **357**(1): 108-116.

Valasek, P., S. Theis, E. Krejci, M. Grim, F. Maina, Y. Shwartz, A. Otto, R. J. Huang and K. Patel (2010). Somitic origin of the medial border of the mammalian scapula and its homology to the avian scapula blade. *Journal of Anatomy* **216**(4): 482-488.

van der Merwe, A. E., D. A. Weston, R. J. OOstra and M. G. J. R. (2013). A review of the embryological development and associated developmental abnormalities of the sternum in the light of a rare palaeopathological case of sternal clefting. *Journal of Comparative Human Biology* **64**: 129-141.

Vickaryous, M. K. and B. K. Hall (2006). Homology of the reptilian coracoid and a reappraisal of the evolution and development of the amniote pectoral apparatus. *Journal of Anatomy* **208**(3): 263-285.

Videler, J. J. (2005). Avian Flight. Oxford, Oxford University Press.

Vivian, J. L., L. Gan, E. N. Olson and W. H. Klein (1999). A hypomorphic Myogenin allele reveals distinct Myogenin expression levels required for viability, skeletal muscle development, and sternum formation. *Developmental Biology* **210**(2): 513-513.

Wang, Q., T. Stacy, M. Binder, M. Marin-Padilla, A. H. Sharpe and N. A. Speck (1996). Disruption of the Cbfa2 gene causes necrosis and hemorrhaging in the central nervous system and blocks definitive hematopoiesis. *Proceedings of the National Academy of Sciences of the United States of America* **93**(8): 3444-3449.

Wang, Y., R. M. Belflower, Y. F. Dong, E. M. Schwarz, R. J. O'Keefe and H. Drissi (2005). Runx1/AML1/Cbfa2 mediates onset of mesenchymal cell differentiation toward chondrogenesis. *Journal of Bone and Mineral Research* **20**(9): 1624-1636.

Warrick, D., T. Hedrick, M. J. Fernandez, B. Tobalske and A. Biewener (2012). Hummingbird flight. *Current Biology* **22**(12): R472-477.

Weatherbee, S. D., L. A. Niswander and K. V. Anderson (2009). A mouse model for Meckel syndrome reveals Mks1 is required for ciliogenesis and Hedgehog signaling. *Human Molecular Genetics* **18**(23): 4565-4575.

Wilm, B., E. Dahl, H. Peters, R. Balling and K. Imai (1998). Targeted disruption of Pax1 defines its null phenotype and proves haploinsufficiency. *Proceedings of the National Academy of Sciences of the United States of America* **95**(15): 8692-8697.

Winslow, B. B., R. Takimoto-Kimura and A. C. Burke (2007). Global patterning of the vertebrate mesoderm. *Developmental Dynamics* **236**(9): 2371-2381.

Xu, X. and S. Mackem (2013). Tracing the evolution of avian wing digits. *Curr Biol* **23**(12): R538-544.

Yamashiro, T., X. P. Wang, Z. Li, S. Oya, T. Aberg, T. Fukunaga, H. Kamioka, N. A. Speck, T. Takano-Yamamoto and I. Thesleff (2004). Possible roles of Runx1 and Sox9 in incipient intramembranous ossification. *Journal of Bone and Mineral Research* **19**(10): 1671-1677.